ASSESSMENT OF INTEGRATING SOLAR ENERGY TECHNOLOGY WITH COMBINED CYCLE POWER PLANTS

by

Ahmad Abd Elmahmoud Mohmed Abd Elrahman

A Thesis Presented to the Faculty of the
American University of Sharjah
College of Engineering
in Partial Fulfillment
of the Requirements
for the degree of

Master of Science in
Mechanical Engineering

Sharjah, United Arab Emirates

June 2014

Approval Signatures

We, the undersigned, approve the Master's Thesis of Ahmad Abd Elmahmoud Mohmed Abd Elrahman.

Thesis Title: Assessment of Integrating Solar Energy Technology with Combined Cycle Power Plants

Signature **Date of Signature** (dd/mm/yyyy)

_____ _____

Dr. Mohamed Gadalla
Professor, Department of Mechanical Engineering
Thesis Advisor

_____ _____

Dr. Andreas Poullikkas
Visiting Associate Professor, Department of Mechanical Engineering
Thesis Co-Advisor

_____ _____

Dr. Mehmet Fatih Orhan
Assistant Professor, Department of Mechanical Engineering
Thesis Committee Member

_____ _____

Dr. Naif Darwish
Professor, Department of Chemical Engineering
Thesis Committee Member

_____ _____

Dr. Essam Wahba
Head, Department of Mechanical Engineering

_____ _____

Dr. Mohamed El Tarhuni
Associate Dean, College of Engineering

_____ _____

Dr. Leland Blank
Dean, College of Engineering

_____ _____

Dr. Khaled Assaleh
Director of Graduate Studies

Acknowledgements

First of all, thanks to Allah - Subhanahu Wa Ta'ala - for the blessing and opportunity for me to finish my thesis. I could never have done this without the faith I have in you, the Almighty.

Secondly, my special thanks for my advisor, Professor Mohamed Gadalla and co-advisor Dr. Andreas Poullikkas for guiding me in my thesis, and for their expertise, kindness, and continuous support. I am very thankful to them for encouraging and guiding me during the preparation of this work. My thanks and appreciation also go to my thesis committee members, Professor Naif Darwish, and Dr. Mehmet Fatih Orhan for their time, insightful comments and for providing me with valuable feedback.

At the end I would like to express my heartfelt gratitude to my beloved mother, father and sister for their unconditional love, encouragement and care. Special thanks also to the newest addition to my family, Yasmine, for the untold joy and happiness she brought to our lives. I would like also to thank my beloved uncle Dr. Zein Mirghani for his support and advice throughout my time here; without their constant support I would not have been able to carry out this work.

Abstract

The integration of solar energy technology with the conventional combined cycle is considered as a promising technology to produce electricity due to its valuable and unique benefits. Also, adding thermal energy storage (TES) is a key issue in the development of solar thermal power plants (STPP) in the future.In order to select the suitable working heat transfer fluid (HTF), a comparative study was carried out using the system advisor model (SAM) software on six different HTFs: Nitrate Solar Salt, Caloria HT 43, Therminol VP-1, Hitec, Dowtherm Q and Dowtherm RP. Therminol VP-1, which is a synthetic heat transfer fluid designed to meet the demanding requirements of vapor and liquid phase systems, was selected as the suitable HTF for the parabolic trough system and Hitec Solar Salt was selected as the storage medium. In this study, a technical, economic and environmental analysis for two proposed power plant designs was carried out to find out which integration option has the best technical performance and economic benefits in terms of levelized cost of electricity (LCOE) value, carbon footprint and fuel savings. Detailed energy and exergy analyses were carried out and the efficiency values were obtained based on the average and maximum values of monthly global beam irradiance. The results showed that the ISCC with 12.5 hours storage capacity had the lowest LCOE after the conventional combined cycle with a LCOE value ranging from 3.46 Cents/kWh to 4.76 Cents/kWh, which makes it the least cost feasible choice among the proposed integration options. Finally, it was found that utilizing thermal energy storage with maximum storage capacity of 12.5 hours led to more greenhouse gas reduction potential while reducing the amount of fossil fuels consumed by the power plant.

Search Terms: Renewable energy; solar energy; thermal storage; parabolic trough; hybridization; combined cycle; heat transfer fluid

Table of Contents

List of Figures

Figure Page

List of Tables

Table Page

Abbreviations

A	Aperture area, m^2
c	cost per exergy unit, $\$.kWh^{-1}$
C_p	Specific heat, $J.(kg.K)^{-1}$
$\dot{C}$	Cost rate, $\$.h^{-1}$
D	Diameter, m
$\dot{E}$	Exergy rate, MW
f	Annuity Factor
F	Faraday's constant
G	Solar radiation, $kW.m^{-2}$
Gr	Grashof number
H	Operation Period, h
$\bar{h}_f$	Enthalpy of formation, $kJ.kg^{-1}$
h_a	Heat transfer, $W.(m^2.K)^{-1}$
I_k	Investment Cost, $
k	Thermal conductivity, $W.(m.K)^{-1}$
L	Length, m
$\dot{m}$	Mass flow rate, $kg.s^{-1}$
n	Number
Nu	Nusselt number
P	Pressure, bar
Pr	Prandtl number
q	Energy, J
$\dot{Q}$	Heat, MW
R	Gas constant
Re	Reynolds number
$\bar{s}$	Entropy, J/kg.K
T	Temperature, K
u	Wind speed, $m.s^{-1}$
U_L	Conductance, $W.(m^2.K)^{-1}$
$\dot{W}$	Power, MW

Subscripts

a	Ambient

ap	Aperture
ar	Aperture-to-receiver
ave	Average
del	Delivered
e	Exit
f, i	Inlet fuel
f, o	Outlet fuel
i	Inlet
r	Receiver
s	Steam
w	Water

Greek Letters

γ	Ratio of specific heat
Δ	Change
ε	Emissivity
η	Efficiency
μ	Dynamic viscosity, $N.s.m^{-2}$
ν	Kinematic viscosity, $m^2.s^{-1}$
π	Pi value
ρ	Density $kg.m^{-3}$
σ	Stefan-Boltzmann constant
φ	Maintenance Factor

Acronyms

BD	Blow Down Factor
CC	Combined Cycle
CCPP	Combined Cycle Power Plants
CHP	Combined Heat and Power
CR	Concentration Ratio
CRS	Central Receiver System
CSP	Concentrated Solar Power
DNI	Direct Normal Irradiance
DSG	Direct Steam Generation
EERE	Energy Efficiency & Renewable Energy
EES	Engineering Equations Solver
EIA	Energy Information Administration

EOT	Equation of Time
GCC	Gulf Cooperation Council
GDP	Gross Domestic Product
GHG	Greenhouse Gas
GHI	Global Horizontal Irradiations
HCE	Heat Collection Element
HRSG	Heat Recovery Steam Generator
HTF	Heat Transfer Fluid
IEA	International Energy Agency
IGCC	Integrates Gasification Combined Cycle
IPP	Independent Power Producers
IRENA	International Renewable Energy Agency
ISCC	Integrated Solar Combined Cycle
LCOE	Levelized Cost of Electricity
LFRS	Linear Fresnel Reflector System
LHS	Latent Heat Storage
LHV	Lower Heating Value
LOTHECO	Low Temperature Heat Combined Cycle
NREL	National Renewable Energy Laboratory
PCM	Phase Change Materials
PDRS	Parabolic Dish Reflector System
PTC	Parabolic Trough Collector
PV	Photovoltaic
RES	Renewable Energy Source
SAM	System Advisor Model
SAPCAP	Solar Assisted Post Combustion Capture
SCA	Solar Collector Assembly
SFC	Specific Fuel Consumption
SHS	Sensible Heat Storage
SSG	Solar Steam Generator
STPP	Solar Thermal Power Plants
TES	Thermal Energy Storage
UAE	United Arab Emirates

Chapter 1: Introduction

The steady increase in demand for energy in the United Arab Emirates (UAE) driven by a quickly growing population, expanding economy and large infrastructure projects, has encouraged the UAE to focus on developing a balanced energy mix that includes fossil fuels, hydrocarbons, nuclear and renewable energy to meet its rising power demand. The objective from this interest of developing clean energy sources is to promote sustainable development to position the UAE as one of the pioneers in sustainability in the region. Consequently, the main focus of this study is to achieve the goal of sustainable development by providing tools for the evaluation of renewable energy technologies by focusing on solar energy technology and the benefits of adding thermal energy storage (TES).

1.1 Background and Motivation

Due to the growing demand for electricity in the UAE in recent years and the expected future shortages in the national reserves that may not be sufficient to meet consumers need for electricity in the future, the UAE leadership is supporting initiatives that call for sustainable development approaches that encourage exploring alternative renewable sources to supply a clean, reliable and a low energy footprint. Current global efforts are looking for the most cost effective possibility for power generation through the use of renewable energy sources in existing plants such as combined cycle power plants (CCPP), which have proven widely successful in operation in the last forty years. The construction of new hybrid plants is also considered as an appealing option. CCPP has the potential to add solar energy to the *Rankine Cycle* of a combined cycle unit. This is a promising new technology in power generation that has been introduced recently in Egypt, Algeria, Morocco and Spain. The integration of solar energy technology with conventional power plants is a very suitable option for the UAE due to the fact that vast natural gas reserves and locations with excellent direct normal irradiance (DNI) are considerable. Using thermal energy storage provides the potential to maximize the solar energy contribution with advantages of fuel savings and flexible operation during peak demand periods.

The motivation for this study can be summarized by the following:

i. Promote the use of renewable energy sources
ii. Supply a clean, reliable and affordable energy source (sustainability)
iii. Raise environmental awareness and identify effective solutions to the problems of global warming
iv. Shed light on different CSP technologies and integration options

1.2 Problem Statement

The use of renewable energy sources (RES) for power generation can help the UAE reach its sustainable development target through the production of clean, reliable and affordable energy. The UAE is paying particular attention to diversifying its sources of energy to comply with the national policies towards sustainable development. This vision led to the construction of the first solar power plant in the UAE (Shams 1) that uses CSP technology [1]. Other projects are underway and are planned to launch soon. Recent reports suggest that the UAE will be able to meet about 25% of its global energy demand by the end of this decade by relying on non-conventional energy sources [2],[3]. The UAE strategic target is to achieve around 7% of renewable energy power generation capacity by 2020. The UAE is also tracking its strategy of reducing carbon emissions and conserving natural resources [4],[5].Some basic energy trends for the GCC countries are shown in Figure 1.

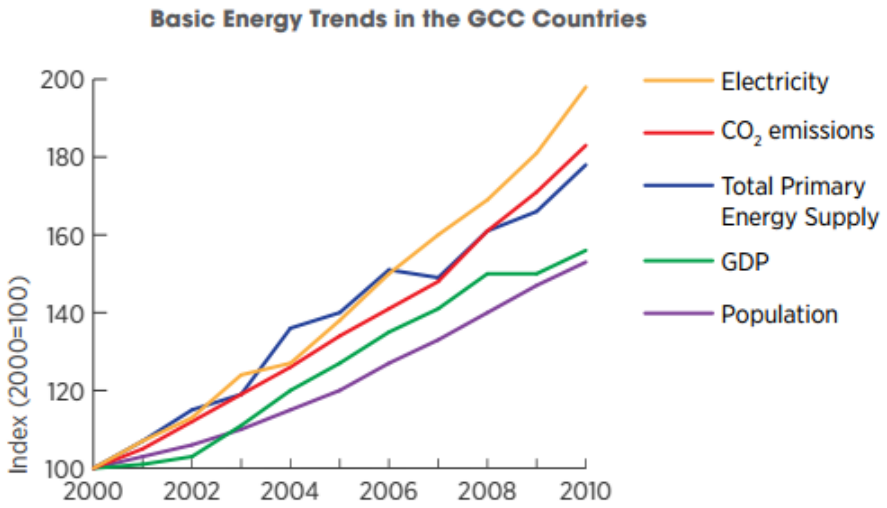

Figure 1: Basic energy trends in GCC Countries [6].

Some renewable energy projects have already been launched in the UAE. Among these projects was the investment of Masdar City in Abu Dhabi which is contributing to the diversification of the UAEs energy mix and spreading the vision of clean, reliable and sustainable energy [7].

Solar technology has very low variable costs and is considered very competitive in the market place with other power generation technologies such as nuclear energy and coal-fired plants. The hybridization of renewable energy sources with conventional power plants is discussed and different configuration options are compared later. This study will be an attempt to contribute to finding attractive solutions for providing a new clean energy by combining the traditional energy sources with renewables to provide a sustainable production with the objective of reducing harm to the environment and minimizing the use of the UAE's exhaustible resources.

1.3 Research Objectives

i. To carry out a technical, economic and environmental analysis on the integration of conventional power plants with solar energy technology.
ii. Investigate the integration of thermal energy storage with ISCC plants.
iii. Perform a comparison between the two proposed configurations to find the most suitable system for the UAE's conditions.

1.4 Scope

Renewable power generation can help countries meet their sustainable development goals through provision of access to clean, secure, reliable and affordable energy. Using hybridization of solar energy with the traditional combined cycle power plants to contribute to fuel saving and reduce CO_2 emissions has been investigated in this study. Another option that will be covered this study is the integration of a thermal energy storage system that will store the required thermal energy for later use to provide dispatchable power generation. In addition, a preliminary study on the selection of the heat transfer fluid for each loop is conducted.

1.5 Methodology

In order to evaluate the benefits of developing combined cycle power plants to be ISCC plants with/without thermal energy storage, data taken from a real existing

traditional plant is developed to the ISCC scheme. Each component of the proposed design for the ISCC is investigated and the integration of a thermal energy storage system with the plant is discussed. The objectives of this research are accomplished through the following phases.

Phase 1: Technical Analysis

Assessment of the technical performance of integrating solar energy technology with a conventional power plant based on a thermodynamic analysis (energy and exergy analysis).

Phase 2: Economic and Environmental Analysis

An economic analysis for the two proposed designs of different capacities is carried out. Fuel savings prevent carbon dioxide emissions to the atmosphere and are considered an important factor for the economic effectiveness of the proposed designs. Some assumptions are made to predict the levelized cost of electricity (LCOE) and the annual generated CO_2 emissions.

Phase 3: Comparative Analysis

The integrated solar combined cycle (ISCC) plant with and without thermal energy storage is analyzed to find the most suitable system to be used in the UAE.

1.6 Thesis Organization

This chapter introduced the background and motivation of this thesis. In addition, the problem statement, research objectives and scope of the study have been also clarified.

Chapter 2 consists of the literature review and background that is required in conducting the study. The current technologies of concentrated solar power (CSP) and thermal energy storage hold great potential for this region. The focus of this chapter is to shed light on the different power generation technologies with a focus on solar energy technology and the combined cycle. Background on some thermal energy storage technologies for integrated solar combined cycle power plants are also presented in this chapter.

Chapter 3 gives a detailed description of the two proposed systems with a focus on the unique design considerations that are essential for developing the performance model and analyzing the work done in later chapters.

Chapter 4 discusses the performance model for analyzing the two proposed designs using thermodynamic, economic, environmental and comparative analysis. This is carried out using data from real-world systems.

In Chapter 5, a summary of the most significant results including all the analyses conducted for the two proposed designs is presented, along with a discussion of these results.

Finally, Chapter 6gives a general conclusion and recommendations for further development of the current work.

Chapter 2: Literature Review

2.1 Introduction

The UAE is an oil producing country which is ranked seventh among the largest oil reserve countries in the world. The UAE is located in the southwest part of Asia bordering the Arabian Gulf and Gulf of Oman. The total area of the UAE is 83,600 km^2 with a growing population of 9.206 million mostly living on the coast.

The UAE is situated between the 22°30' and 26°10' north latitude and between the 51° and 56°25′ east longitude. Due to this geographical location in the Sun Belt, the UAE is blessed with high amounts of solar radiation with a yearly average daily energy input of 18.48 MJ/m^2/day [7].

The power sector of the UAE relies on steam and gas turbine units to produce electricity. Most of the generating power plants are located along the coast as they use water to create high pressure steam to drive the steam turbine. Another advantage is processing sea water into drinking water through desalination plants. Figure 2 shows the UAE Interconnectedpower grid.

Some challenges are facing the UAE due to the varied annual demand curves during the summer and winter seasons. As the demand during summer days can exceed more than 92% of the total installed generation capacity while the demand drops during winter to around 33% only. Further, the UAE plans to host EXPO 2020 has set new heights for upgrading the power and water infrastructure in the county. The UAE government is seeking also to implement efficiency measures that will lead to significant reduction in the overall demand by 2030. Energy projects such as Masdar and the UAE engagement with nuclear energy are examples for means of economic diversification away from fossil fuels. These efforts will improve the reliability of the existing energy systems as well as saving billions dirhams in electricity cost.

The establishment of the GCC power grid will bring many benefits to the UAE by importing and exporting power through the common grid. During power shortages, considerable savings can occur in addition to reductions in the generating capacity in each system as a result of sharing power reserves. This will allow expanding the use of renewable energy sources in the common grid and reducing the capital cost per megawatt of the installed capacity.

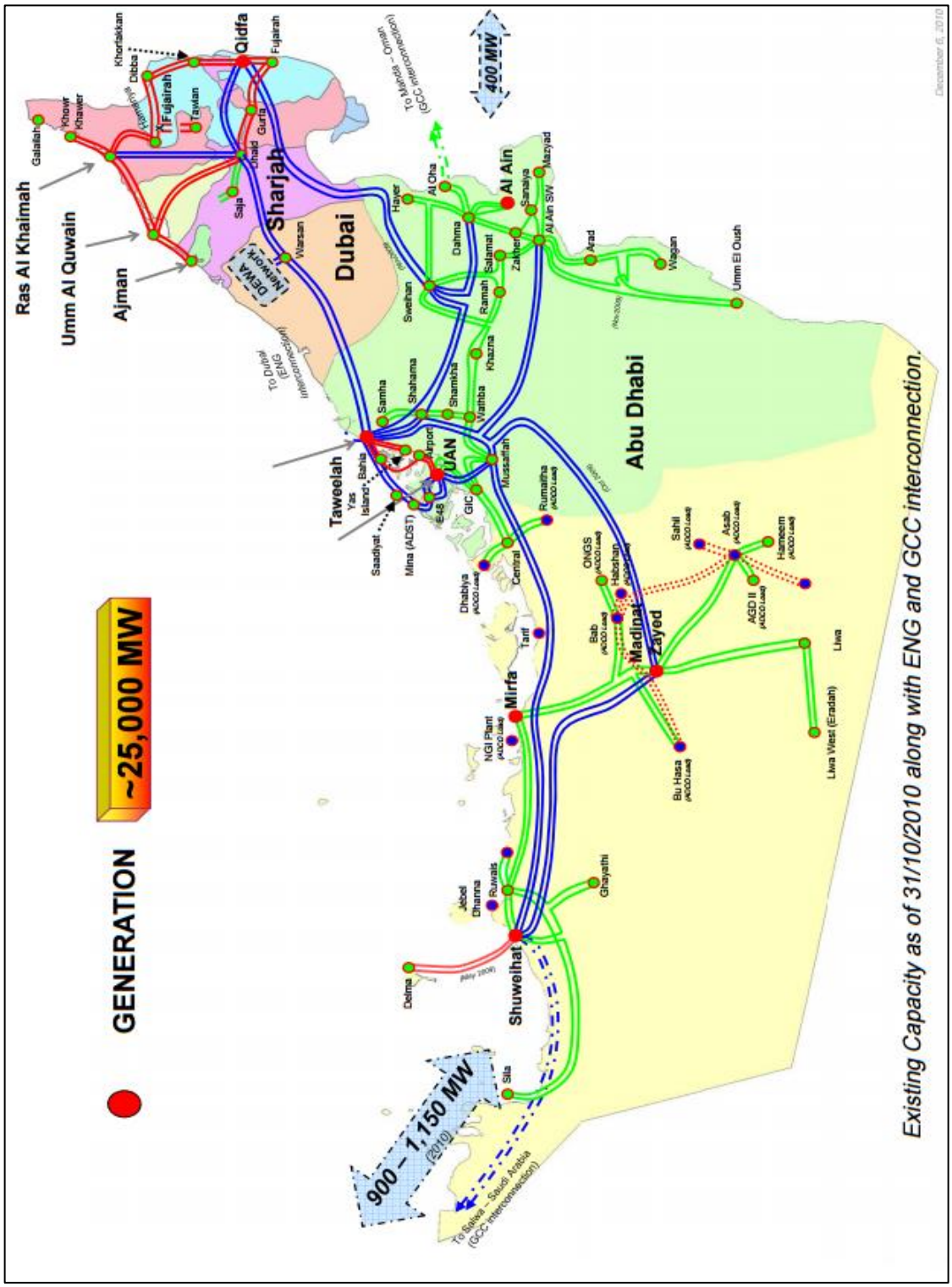

Figure 2: UAE Electricity Grid [8]

Table 1 lists the power plants in the country with their outputs, intensity and capacity.

Table 1 :UAE Power Plants List [9]

Plant	***Output (MWh)***	***CO_2 (kTon)***	***Intensity (KgMWh)***	***Name Plate Capacity (MW)***
Jebel Ali	15,300,000	5,695.96	371.04	4,772
Shuweihat	5,901,490	2,075.8	351.53	1,500
Umm Al Nar Apc	5,462,700	1,825.71	334.3	1,706
Al Taweelah A1	3,008,840	975.15	324.32	1,502
Al Taweelah A2	2,742,180	1,032.6	376.48	710
Qidfa Union	2,471,750	902.65	365.14	893
Al Taweelah B1	2,403,590	962.81	400.52	1,075
Dubai Smelter	2,298,430	986.36	429.1	2,350
Jebel Ali L I	2,295,870	748.71	326.13	969
Umm Al Nar West	1,581,130	743.54	470.38	790
Ruwais Refinery	1,268,450	594.68	469.02	680
Umm Al Nar East	1,120,000	540.11	482.17	250
Al Ain	450,567	211.59	469.47	428
Al Taweelah A	386,312	201.34	521.18	286.5
Mirfa	229,086	124.04	541.59	192
Dubai Gt	228,881	123.93	541.59	
Madinat Zayed	146,684	82.5	562.46	118
Adnoc Gt	108,952	56.85	521.63	
Fujairah	16,895	11.06	654.99	760
Al Taweelah B2	0	0	0	1,050
Al Taweelah Smelter	0	0	0	1,730
Jebel Ali M	0	0	0	2,060

Large investments in alternative energy sources are expected to change the UAEs energy mix in upcoming years. The number of power generating plants classified per fuel type is shown in Figure 3. The UAE has ideal opportunities for combining natural gas resources with the abundant solar energy by integrating CSP into natural gas combined cycles. The availability of an exceptional solar resource (DNI) makes the UAE a high contender for the implementation of solar technologies.

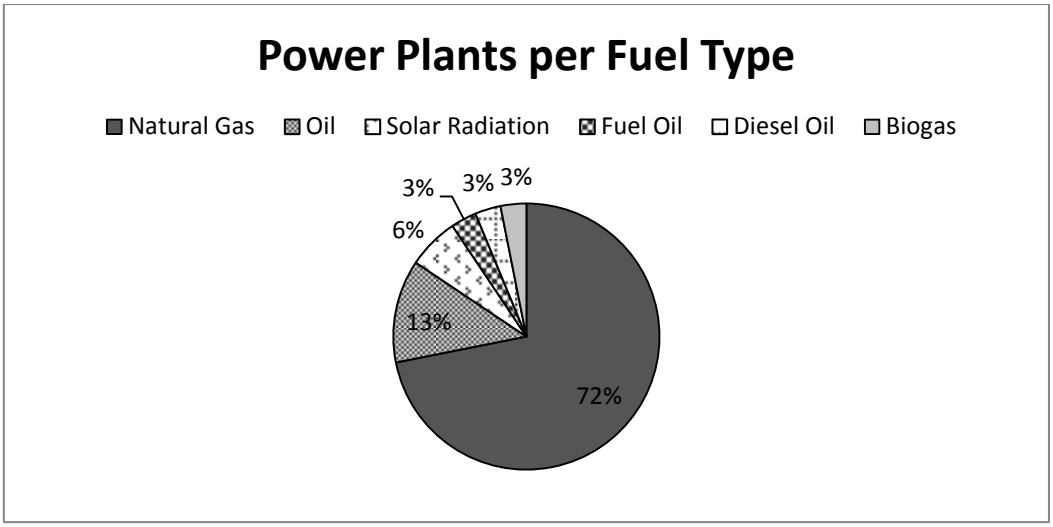

Figure 3: Number of power plants per fuel type in the UAE [9]

As mentioned before, the UAE is a Sun-Belt country where its location, meteorological, climate conditions, and precipitation rate create great potential for using solar energy for power generation [10],[11]. Figure 4 shows the average daylight hours and temperatures for Abu Dhabi, the capitol of the UAE.

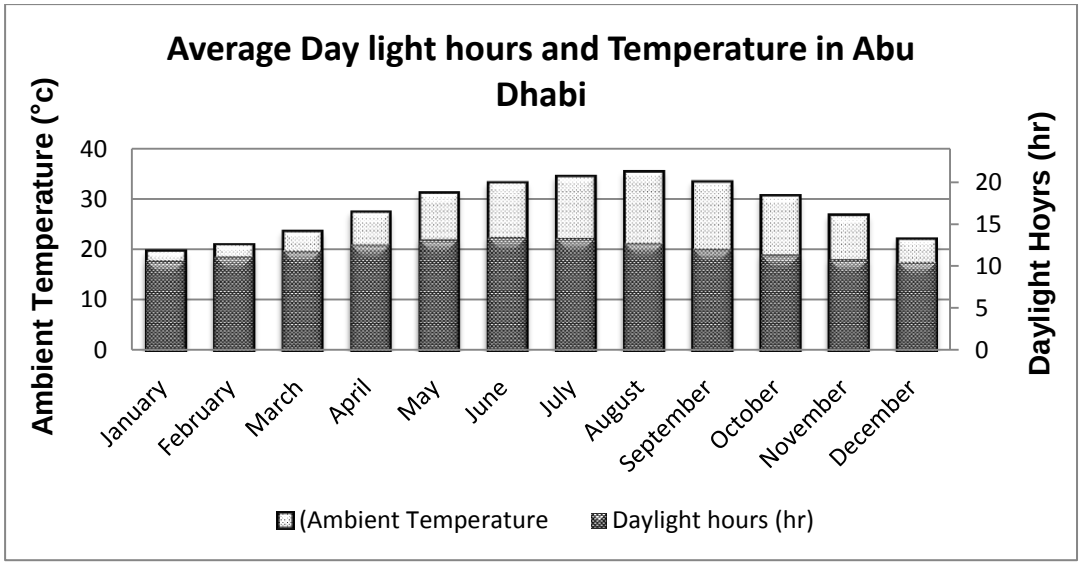

Figure 4: Average daylight hours and temperatures in Abu Dhabi [12]

2.2 Power Generation Technologies

This literature review covers information available about current power generation technologies. Nowadays, there is still a lack of accurate, reliable and comparable data about the performance and costs of power generation technologies. According to a

World Bank report, electricity production from natural gas sources in the UAE reached 98.21% in 2009 [13]. Several reports specified that the volumes of natural gas used to produce electricity will not be sufficient to meet future demand for power generation. Based on other recent reports, the peak demand for electricity is expected to increase to more than 40,000 MW by 2020 [14], while natural gas resources are expected to provide a power generation capacity (ranging between 20,000 – 25,000 MW) only until 2020. Thus, the need to develop new energy sources to meet future demand is of major concern for the UAE government.

The evaluation of alternative energy sources such as solar, wind and nuclear suggests that they have a high potential to be deployed in the UAE. These energy sources could make significant contributions towards developing a diverse portfolio and securing energy demands for the future.

Despite the high costs, the UAE government has supported renewable energy to help achieve its strategy of reducing dependence on fossil fuels and to be a leader in the global energy market. This was reinforced by the founding of Masdar Institute in 2006 with a vision towards sustainable economic development and diversification. Also, the UAE has engaged with leading international partners such as the International Renewable Energy Agency (IRENA) and agreed to grant permanent headquarters in Abu Dhabi to the agency. This collaborative partnership with organizations and governments abroad will benefit not only the people of the UAE but all communities in the Middle East region and the world as a whole.

Alnaser and Alnaser [6] studied the current state and future of renewable energy technologies in the GCC countries. It was reported that electricity consumption had increased by a fast rate of 3.5% annually in the period between 2005 and 2009. Furthermore, the average electricity consumption rate in the GCC countries was measured as 1149W per person which is considered a high rate compared to the world electricity consumption average of (297W per person) [15]. Figure 5 shows the peak load demand forecast in the UAE from 2009 to 2019. In conclusion, the policy makers in the GCC countries are looking at energy for sustainable development taking into consideration the economic, social and environmental issues. Major investments in renewable fuels are planned to diversify their energy mix. Investments in alternative sources of energy such as solar and nuclear power are on the rise. As the GCC population is forecasted to reach 53.5 million by 2020 with a growing real GDP

of 56% in the same period, the conservation of hydrocarbon resources has become an important requirement to maintain the finite resources and to achieve economic diversification.

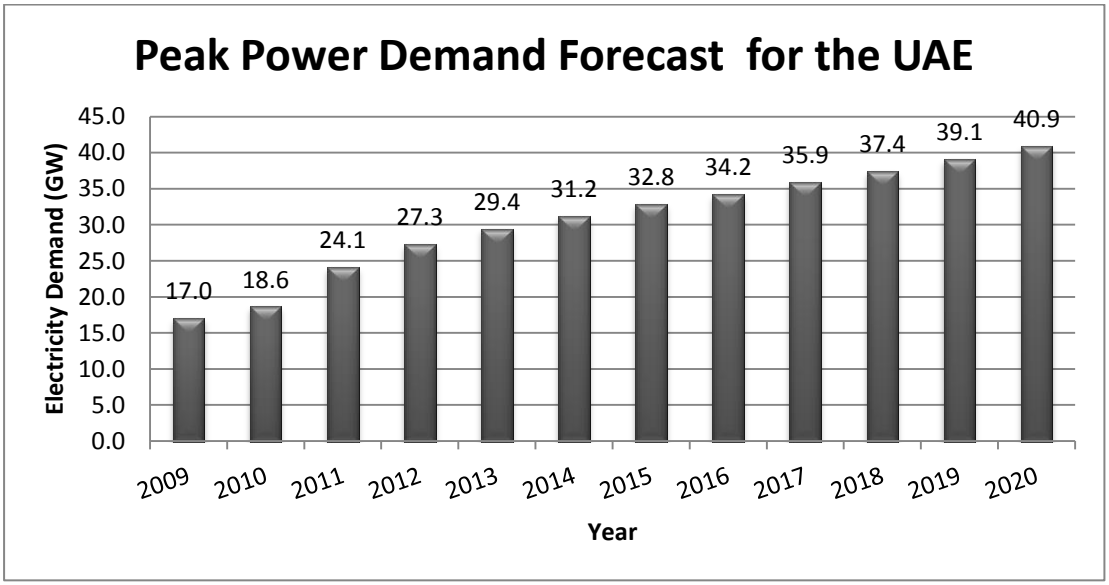

Figure 5: Peak load demand forecast in the UAE

The various forms of power generation technologies available for potential development are discussed next. The appropriate hybrid options for the GCC countries energy situation are also proposed.

Generally, the most common types of plants used to provide large amounts of steady power are thermal plants and kinetic plants. Figure 6 shows a schematic diagram of the different types of power generating plants.

2.2.1 Thermal Generating Plants. Thermal generating plants are plants that generate electricity using the energy of heat. Water is vaporized in the boiler to produce steam at saturated temperature. This steam can be used immediately to produce power through a turbine and alternator.

2.2.1.1 Fossil-fueled plants

Fossil fuels are formed from the remains of dead plants and animals that were exposed to heat and high pressure for millions of years. Fossil fuels have a high content of carbon and include coal, oil and natural gas. Fossil fuels are not renewable because they can take up to millions of years to form and they are expected to run out in the future.

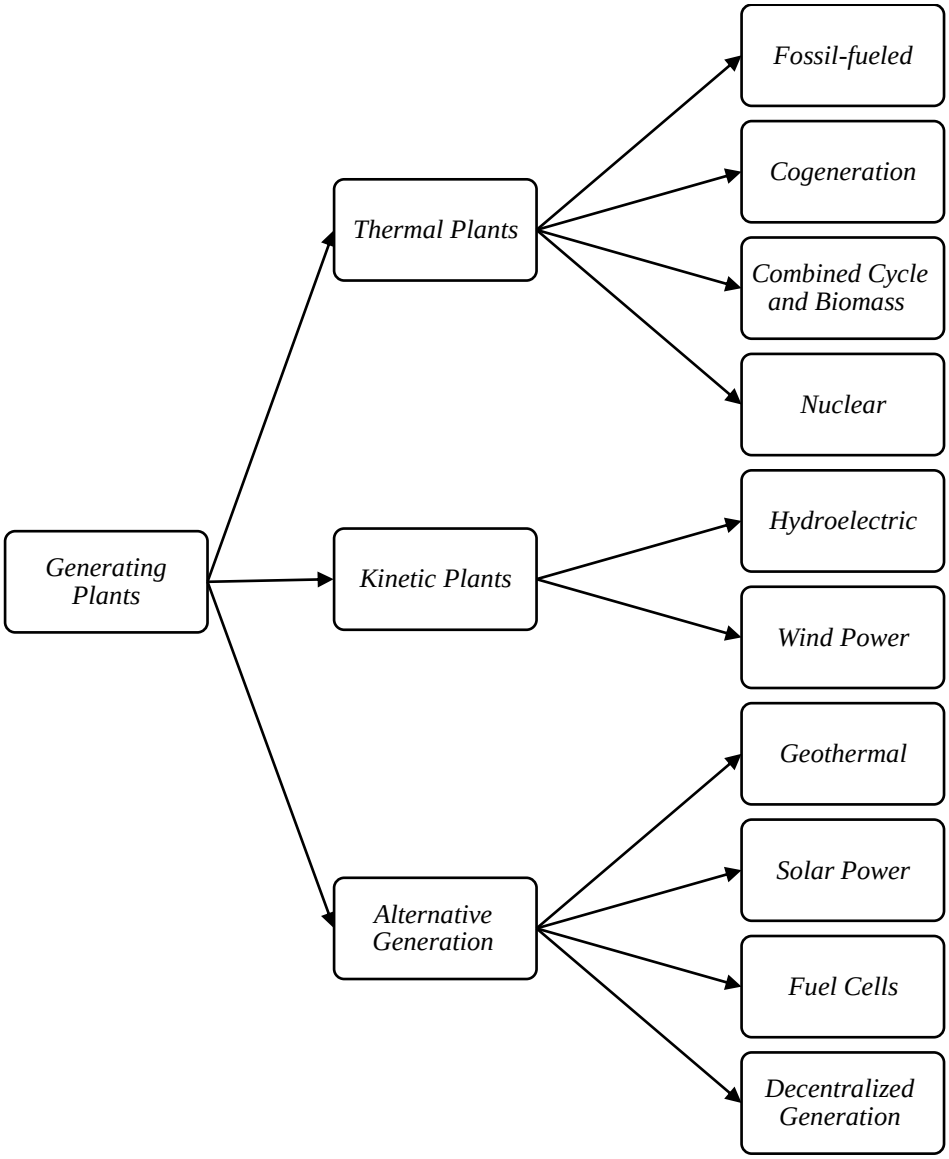

Figure 6: Schematic diagram for the types of power generating plants

Many environmental problems result from the use of fossil fuels such as air pollution and carbon dioxide emissions which have the ability to absorb infrared radiation that emits from earth and re-radiate it back which can cause an increase in the average temperature of the earth. The increasing concentrations of CO_2 emissions cause what is known as the "greenhouse effect" leading to global warming [16]. So, alternatives to overcome these environmental problems are currently being investigated. Many researchers point to the advantages of hybridization of renewable energy sources such as solar energy with conventional and non-conventional power plants.

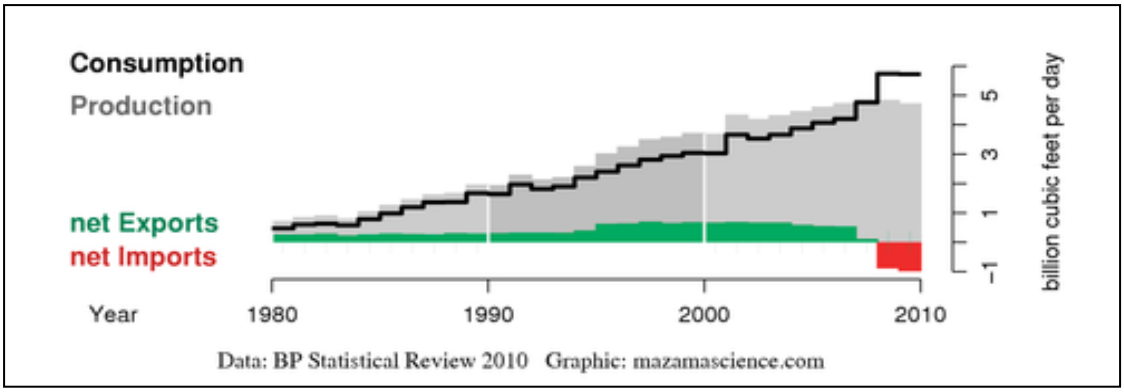

Figure 7: Natural gas flow in the UAE (billion cubic feet per day) [17]

A new approach was suggested to overcome challenges arising from the high costs of using solar thermal energy for power generation compared with conventional power plants [18]. Many different configurations for hybridization of both solar energy and fossil fuels were proposed. It was found that hybrid power plants have technical and economic advantages over solar only plants. Helal and Al-Malek have designed a hybrid system for a diesel-solar power plant using mechanical vapor compression technology to provide fresh water to remote areas in the UAE [19].

2.2.1.2 Cogeneration

Cogeneration which is often called combined heat and power (CHP) is the combined production of two forms of energy: *electrical* and *useful thermal* energy in one process. Cogeneration is a proven and promising option to solve pressing energy problems by reducing the consumption of fossil fuels, which in turn means lower greenhouse gas (GHG) emissions [20]. There are two types of cogeneration: *topping cycle* and *bottoming cycle*. The *topping cycle* is more commonly used to generate electricity as a portion of the waste heat is used to provide thermal energy. In general, cogeneration systems are categorized according to their prime movers or technology types as either gas turbines, steam turbines, reciprocating engines, micro turbines or fuel cells.

Raj et al. reported that only cost-effective alternative energy sources will be capable of meeting the growing demand for electricity in commercial and industrial sectors. The authors argued that cogeneration systems are ideal to implement in different utility sectors. A review of the latest cogeneration technologies with theoretical and experimental analysis including the design, analysis, modeling and

simulation, and environmental and economic effects for different renewable energy sources was carried out in the same study[20]

2.2.1.3 Combined Cycle Power Plants

Combined cycle systems (CC) are becoming a popular electricity generation method in many countries. The principle of such systems is to use the exhaust of one heat engine as the heat source for another. The system is a combination of two or more thermodynamic cycles to improve the overall efficiency. Among the widely used combinations is a gas turbine operating by the *Brayton cycle* and a steam power plant operating by the *Rankine cycle*. The heat of the gas turbine exhaust is used to generate steam by passing through a heat recovery steam generator (HRSG) transferring energy from one cycle to another. The thermal efficiency of the combined cycle can reach up to 60%, while unit thermal efficiencies of the gas turbine and the steam turbine are between 30 - 40% [21]. Different hybrid configurations of the combined cycle were presented such as the integrated gasification combined cycle (IGCC) technology, a power generation process that integrates a gasification system with a combined cycle power plant. Another similar integration option is discussed later in this study. Figure 8 below shows a snapshot of the flow diagram for the process of a combined cycle system using Aspen HYSYS. The steam turbines in most large power plants are divided into two sections: the *High Pressure Section* (HP) and the *Low Pressure Section* (LP). The efficiency of the steam section in many of these plants varies from 30-40%.To ensure that the steam turbine is operating efficiently, the gas turbine exhaust temperature is maintained over a wide range of operating conditions. This enables the HRSG to maintain a high degree of effectiveness over this wide range of operation. Poullikkas et al. investigated the use of the Low Temperature Heat Combined Cycle (LOTHECO Cycle) for electric power generation [22],[23]. They noted that in a combined cycle plant, high steam pressures do not necessarily imply a high thermal efficiency. Expanding the steam at higher pressure could causes an increase in the moisture content at the exit of the steam turbine. This moisture content can create major erosion and corrosion problems in the later stages of the turbine.

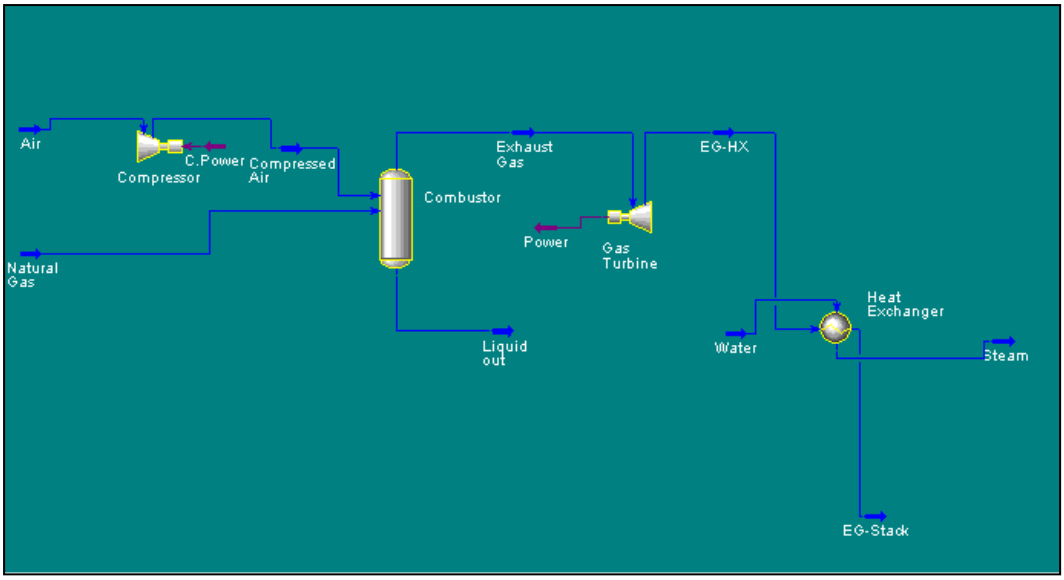

Figure 8: Combined Cycle System(Snapshot from Aspen HYSYS)

2.2.1.4 Nuclear Plants

Nuclear power stations are thermal plants that use a nuclear reactor as the source of heat. This heat resulting from an atomic fission is used to produce steam to generate electricity. Nuclear plants have high capital costs but low direct fuel costs. The cost estimates take into account the nuclear waste storage which could remain dangerous for thousands of years [24]. Thus, high concerns over safety, economic and environmental issues have been raised by the public leading nuclear engineers to develop safer plant designs with technical fixes of common problems [25].

2.2.2 Kinetic Plants. Kinetic plants use the energy of motion instead of the energy of heat to produce electricity. Some examples of kinetic plants are wind mills and hydro-electric plants. The source of energy used is clean and renewable as there is no air pollution. The mechanism of these plants is using the flow of water or wind to spin the blades of the turbine and therefore spin the rotor part of the generator. However, some problems exist even with these technologies as detailed below.

2.2.2.1 Hydro-Electric Plants

Hydro-electric plants uses hydropower to generate electricity. This is performed by taking advantage of the gravitational force of falling or flowing water. These plants

are widely used for power generation and have a long economic life. Hydroelectric dams can reduce carbon dioxide emissions since there are no fossil fuels to be burned.

The power costs of hydro-electric plants are relatively low as there is no fuel used. However, the construction of large dams could harm local ecosystems and destroy the wild-life habitat. Another major problem for hydropower projects is the need to relocate people living near the planned reservoirs area. The most common used plants in practice are the *run-of-river plants* and *pumped storage plants* [26].

2.2.2.2 Wind Power

The kinetic energy of the wind is converted into electricity using wind turbines. The size of the wind turbines depends on their application. Small wind turbines may be used in applications such as to power traffic warning signs whilst slightly larger turbines can supply domestic power [27]. Wind farms may consist of several hundreds of individual small turbines with almost the same design. However, large wind farms could have high construction costs and may be suited for only limited locations. The environmental impact of wind power is relatively minor compared to other traditional energy sources in terms of air pollution, but it was reported that wind power could endanger certain bird species [28].

2.2.3 Alternative Generation. Other alternative energy technologies have been under development to stop the reliance on fossil fuels. Common types of alternative energy sources are solar and geothermal energy, fuel cells and decentralized generating plants.

2.2.3.1 Solar Energy

Solar energy is the energy generated by the sun which is converted into useful energy for heating or electricity generation. Every year the sun supplies four times more energy than we can consume, so its potential is almost unlimited [29].

Many historians believe that Archimedes used the shields of the soldiers, arranged in a large parabola, for focusing the sun rays to a common point on a ship. Although this was a military experiment, it proved that solar radiation could be a powerful source of energy [30]. Solar energy is not available around the clock and the intensity of the available energy at a defined point of the Earth depends on the day of the year, the hour and the latitude. The quantity of energy that can be obtained depends also on

the orientation of the receiver mechanism. Several solar energy technologies that are used for different applications are shown in Figure 9 below.

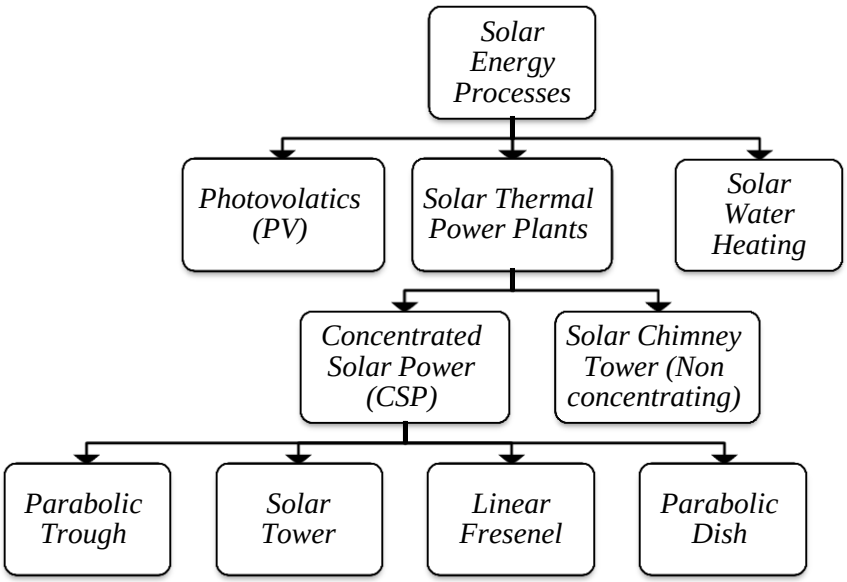

Figure 9: Classification of Solar Energy Processes

2.2.3.2 Geothermal

Geothermal plants use the thermal energy stored in the Earth. This geothermal power is considered sustainable, reliable and environmentally friendly. However, the thermal efficiency of geothermal plants is relatively low because the geothermal fluid does not reach high temperatures compared to fossil-fueled plants.

Geothermal energy could be used for heating as well as electricity generation. Some environmental effects of geothermal energy are the mixture of gases drawn with the geothermal fluid. This mixture of gases contains pollutants that could cause environmental damage and could contribute to global warming. A comparison between geothermal with solar and wind power generation was carried out by Li [28].

2.2.3.3 Fuel Cells

Fuel cells are used to produce electricity by using a source of fuel that reacts chemically with oxygen or air. Hydrogen is the most common fuel used in fuel cells [31],[32]. However, fuel cells are different from batteries. They are powered by a constant flow of fuel. Most fuel cells consist of an anode, cathode and an electrolyte. Electrons move from the anode to the cathode through an external circuit producing a direct current.

2.2.3.4 Decentralized Generation

Decentralized Generation - also known as Distributed Generation -depends on small energy sources to produce power typically in the range between 3 KW to 10 KW [33]. One main concern about this power generation technology is its high cost. The power generated on site is preferred to using central power stations, since on-site power eliminates the need for transmission and distribution. Solar panels are one of the popular distributed generation options.

2.3 Concentrated Solar Power Technology

Concentrated solar power technology, more commonly referred to as CSP, is used to provide energy by converting solar thermal energy into high-temperature heat using various mirror configurations which concentrate the rays of the sun. For reaching this, it is essential to have a high amount of direct solar radiation. This is more the case in countries that lie within the Sun Belt which is located between the 35th northern and 35th southern latitudes. The UAE latitude and longitude is 24° 00' N and 54° 00' E.

Islam et.al.[34] measured the global solar radiation and surface temperature average values in the UAE over one year. Other meteorological data was also analyzed in order to evaluate the solar energy potential in Abu Dhabi. The results showed that the highest daily average solar radiation value was calculated to be 369 W/m^2 recorded in 2007 whilst the maximum daily solar radiation was 1041 W/m^2 measured on February the 8th. The author analyzed the data and compared it with other corresponding data to make sure that the data considered was presentable. The maximum average temperature was found to be 36.2°C whilst the highest daily temperature was 50.94°C. Figure 10 below depicts the solar radiation in Abu Dhabi. Concentrating solar power plants consist of two parts: one part, the solar field collects solar energy and converts it to heat, and another part, the power island, converts heat energy to electricity. The power gained from sunlight can be increased if the light is gathered and concentrated on a single point and the heat is then channeled through a conventional generator.

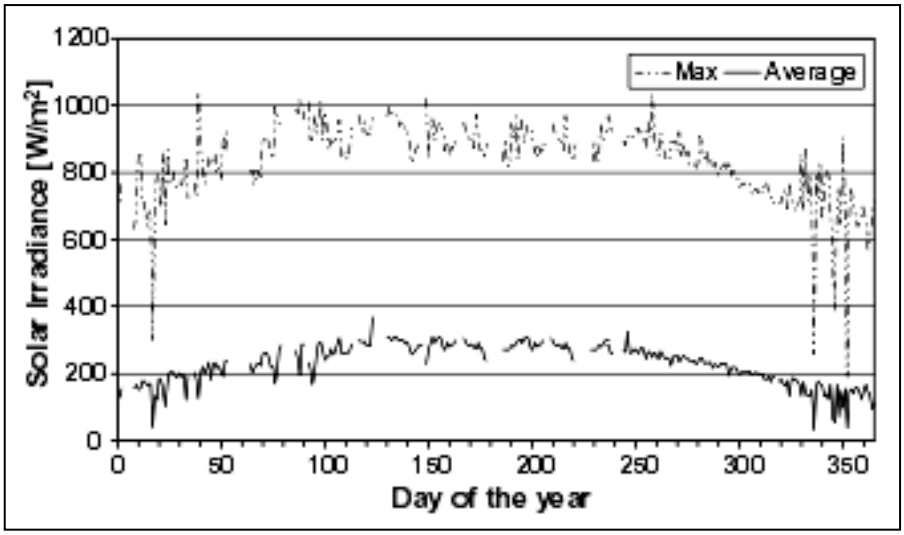

Figure 10: Daily Global Solar Radiation in Abu Dhabi [35]

For concentrating the sun rays there are two possibilities: concentrating the radiation at a fixed point (here the concentrators have to follow the sun by moving along two axes) or using linear concentrators that only need to move along one axis in order to follow the sun.

CSP technology is used mostly for power generation. However, it can be used in many industrial applications. The operating temperature is an important factor for choosing the most suitable technique for any proposed application.

Figure 11 shows different CSP applications depending on the operating temperature. The power cycle of a conventional concentrated solar power plant is based on a Rankine cycle. It is known that steam turbines used in solar plants are typically smaller than those used in current fossil fueled plants. Furthermore, most CSP power plants used nowadays have lower steam temperatures (up to 380°C compared to around 600°C in fossil fuel power plants). This is due to issues with the HTF stability. The high pressure steam is expanded through the turbine converting the thermal energy of steam to mechanical work which drives a generator to produce electricity. The pressure drop across the unit could affect the turbine's efficiency. This pressure drop is a function of the "cold sink" temperature which is the temperature at which the thermal energy is rejected from the system through cooling.

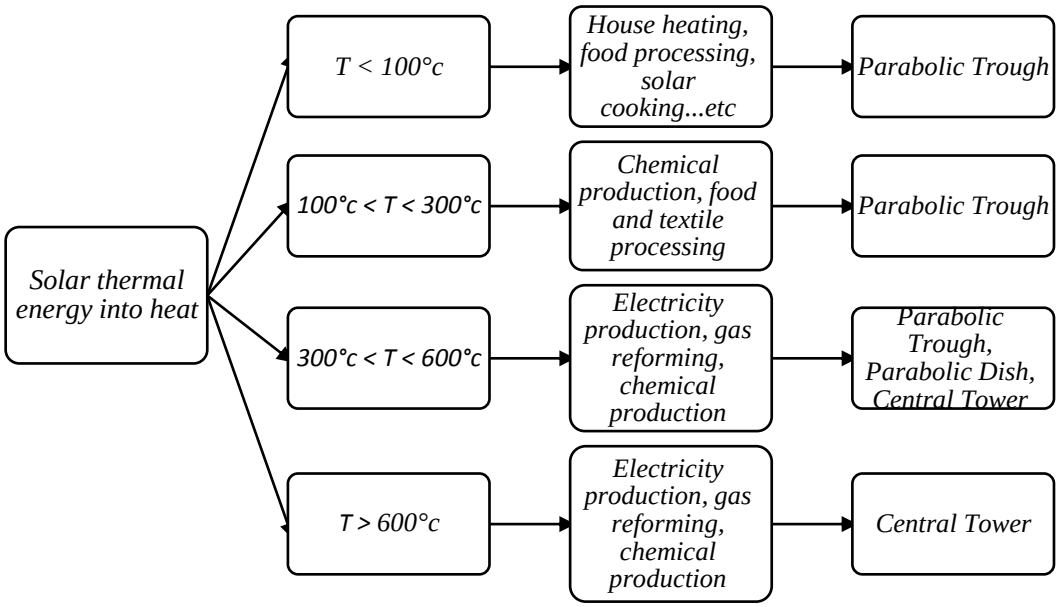

Figure 11: Concentrated Solar Power Applications [36]

In order to concentrate the direct solar radiation onto the small receiver area, a tracking system can be used. Different types of tracking systems have been introduced. In general, concentrating collectors can be divided into two basic types. The first types are collectors that focus the radiation along a line. The second type focuses the radiation at a point. *Point focus* collectors can achieve much higher concentration ratios than *linear collectors* [37]. This enables higher temperatures and the possibility to improve the efficiency of conversion of solar thermal energy into electricity. Concentrating collectors can be divided into four categories that will be discussed next:

1. Parabolic Trough Collectors
2. Solar Towers
3. Linear Fresnel Collectors
4. Parabolic Dish Reflectors

2.3.1 Parabolic Trough Collectors (PTC). Parabolic trough collectors (PTC) are the most proven and widely deployed CSP technology in solar thermal power plant (STPP) applications. They are made by forming a parabolic shape reflector that concentrates the incoming sunlight onto a central tubular receiver. The collected thermal energy in the tubular receiver is absorbed by the heat transfer fluid (HTF). Water and synthetic oils are commonly used as heat transfer fluids. A single-axis tracking where the collectors are aligned on the north-south axis can be used to orient toward the sun as shown in Figure 12 below.

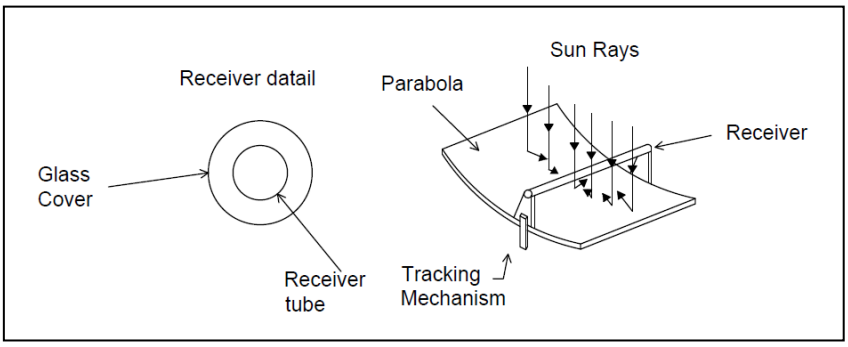

Figure 12: Diagram of a Parabolic Trough

2.3.2 Central Receiver System (CRS). The solar tower power system, also known as a central receiver system, uses a ground-based field of heliostat reflectors to focus solar radiation onto a receiver mounted high on a central tower. A tracking mechanism for the sun position is used to direct the sunlight to the receiver. The concentrated solar energy is absorbed by the HTF in the receiver. The central receiver system uses small concentrator mirrors called heliostats. The heliostat focuses the rays of the sun onto a common point situated on a central tower, where the receiver collects the heat.

The receiver is mounted on top of a standard wind turbine shaft. Water can be directly evaporated and superheated to approximately 440°C without the use of heat exchangers. Large central receiver systems (CRS) with thousands of heliostats, each with 100 m^2 of reflecting surface, require towers 100-200 m high and can collect several hundred MWs of solar radiation power [38]. A diagrammatic representation of the system is shown below. Storing heat energy is almost impossible, however, without having high amounts of heat losses. Therefore, solar power plants are based

on saturated steam at moderate temperatures and pressures to avoid these problems. Another possibility is the use of alkali-metal salts as heat transfer mediums. They have two advantages: good heat transfer properties and the possibility of storage at low pressures in tanks. Yet, the high melting point makes electrical heating of the pipes necessary to avoid freezing out of the salts which results in pipe blockage.

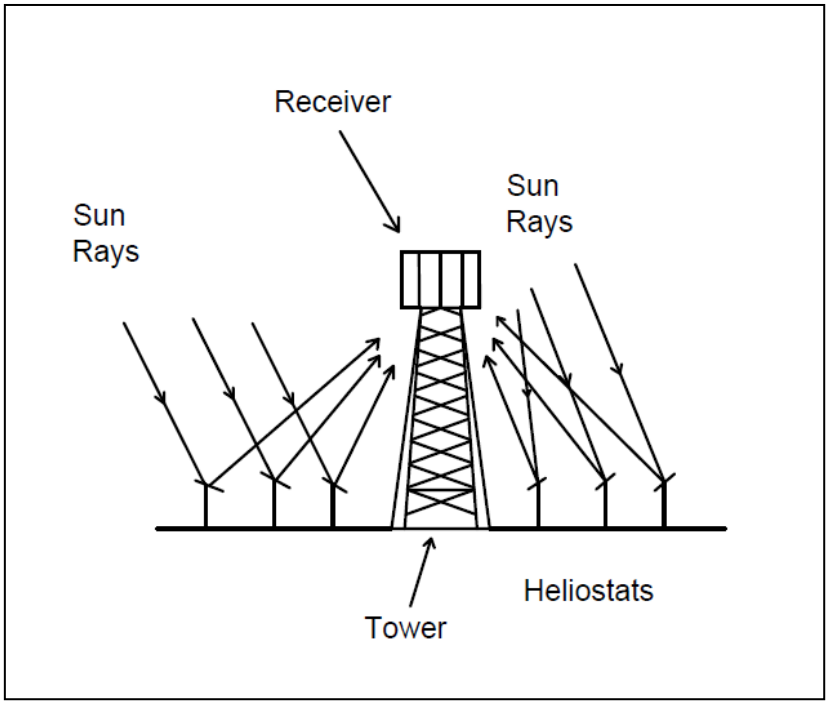

Figure 13: Diagram of a Solar Power Tower

Solar towers allow high concentration ratios and are well suited to large scale implementation for utility power generation. A wide range of applications such as gas turbines, combined cycles, CHP and some industrial processes using solar towers for more efficient electricity generation are readily available. Two commercial solar power plants are now operating in Spain where water is heated to superheated steam at about 300°C. The design parameters are conservative, ensuring a successful demonstration, and it is widely accepted that future plants will achieve greater energy conversion efficiencies utilizing higher steam temperatures. A third plant, commissioned in early 2011, uses molten salt to increase steam temperatures to around 550ºC.

2.3.3 Linear Fresnel Reflectors (LFRS). The linear fresnel reflector system (LFRS) consists of a field of long linear mirror reflectors to concentrate light on a fixed absorber receiver. The mirrors used are flat or elastically curved and are mounted on a steel structure. The reflector mirrors rotates around the receiver axis to track the sun. Some proto types were built and are in operation for applications ranging from medium-temperature steam production for power stations to solar thermal cooling. Another advantage of linear fresnel plants is that they require less capital costs than parabolic trough plants due to reduced structural requirements; see Figure 14 for a diagrammatic illustration.

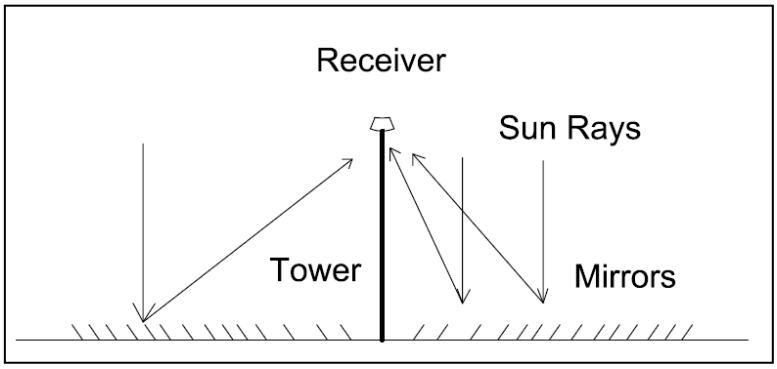

Figure 14: Diagram of a Linear Fresnel

2.3.4 Parabolic Dish Reflectors (PDRC). A parabolic dish reflector collector (PDRC) consists of a parabola shaped frame that supports curved mirrors to concentrate solar radiation onto a receiver at the focal point where the sun is tracked using two axes. The parabolic dish has one of the highest efficiencies compared to other concentrated solar power technologies. The concentration of energy onto a single point yields a very high concentration ratio and hence very high temperatures. The solar radiation energy is absorbed in the receiver and converted to thermal energy stored in the heat transfer fluid. The parabolic dish technology is suitable for decentralized generation and remote areas. This technology could be used in many applications such as steam generation, ammonia dissociation, Brayton Cycles, sterling engines and concentrating Photovoltaics – Figure 15.

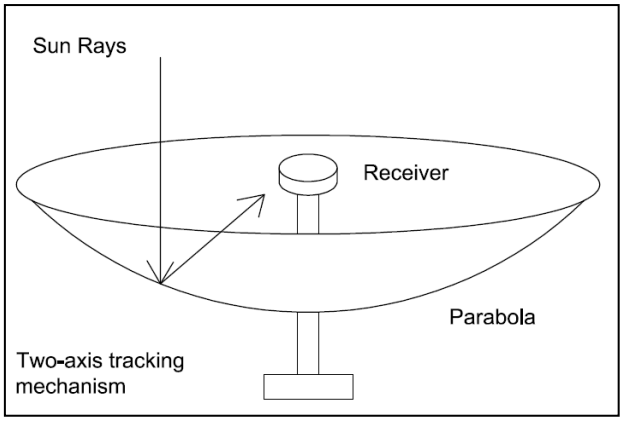

Figure 15: Diagram of a Parabolic Dish

In Table 2, a comparison between four different CSP technologies is presented.

Table 2: Comparison between different CSP technologies [39]

CSP Technology	***Parabolic trough***	***Central receiver***	***Linear Fresnel***	***Dish***
Solar collector	Line focus	Point focus	Line focus	Point focus
Solar receiver	Mobile	Fixed	Fixed	Mobile
Power conversion cycle	RC,CC	RC,BC,CC	RC	RC,SC
Concentration ratio	70-80	> 1000	> 60	> 1300
Working Temperature ©	Medium	Higher	Relatively lower	Highest
Typical capacity (MW)	10-300	10-200	10-200	0.01-0.025
Storage System	Indirect 2-tank molten salt or Direct 2-tank molten salt	Direct 2-tank molten salt	Short-term pressurized steam storage	No storage, chemical storage under development
Development status	Commercial proven	Commercial	Pilot project	Demonstration stage

Py et al. have presented the history of different concentrating solar power (CSP) technologies that were developed over the last 30 years. Major technical and policy issues were discussed in his research [40]. They concluded that optimization of several components of the CSP power plant is possible to enhance its performance. The authors also discussed major technical issues related to the solar field, receiver, HTF side, thermal energy storage (TES), water consumption, energy transport and distribution.

Table 3: Heat Transfer Fluids used in CSP Plants

HTF	***Max Temp. (°C)***	***Drawbacks***	***Advantages***
Mineral Oil	< 400	Inflammable	Good Performance
Synthetic Oil (Therminol VP1)	390	Inflammable Highly Toxic Expensive	Good Performance
Water/Steam (250°C 40 bar)	-	High T leads to High P and cost	Cheap Environmentally friendly
Molten Salts (Nitrates)	600	Corrosion Freezing Point	Heat transfer and storage media
Air (700°C)	-	Low Performance	Cheap

Many researches argue that the use of water as a HTF will improve the steam properties as specific heat, temperature and pressure so that the steam turbine performance will be more efficient. Also, converting to direct steam in CSP technologies instead of synthetic oils will reduce the environmental impacts associated with CSP and lower the investment, operation and maintenance costs.

Fernandez-Garcia et al. [41]reviewed different types of solar concentrating systems that have been developed and their wide range of applications including electricity generation, space heating, air conditioning and refrigeration, domestic hot water, pumping irrigation water and desalination.

Rovira et al. [42]investigated the effect of using different configuration assessments based on exergy analysis to find the best performance. A comparison was performed for Direct Steam Generation (DSG) and Heat Transfer Fluid (HTF) technologies to find the irreversibility sources that affect the performance of the subsystems. The authors proposed four different layouts and three different comparison techniques. The study revealed that the only-evaporative DSG configuration is the best choice in terms of its thermal efficiency and low irreversibility at the steam generator.

Reddy et al. [43]also carried out an energy and exergy analysis for a parabolic trough solar thermal power plant in two different locations in India. The results showed that the maximum energy heat loss was found in the heat engine circuit in the condenser while the most exergetic losses were found in the solar collector field. The

operating pressure was increased from 90 bar to 105 bar which led to improvements in the energetic and exergetic efficiencies by 1.49% and 1.51%, respectively.

Behar et al. [44] investigated existing central receiver solar thermal power plants. The basic concept, design, experiment and enhancement of different components in central receiver systems were discussed. The authors reviewed the main components of the central receiver system which are the heliostat, the receiver and the power block. Central receiver systems (CRS) were classified into three categories which are *particle receivers*, *cavity receivers* and *volumetric receivers*.

Detailed techniques and thermodynamic analysis were used to assess performance of the subsystems. Other studies were conducted on power conversion systems including the main concept, design, experiment and enhancement of the three most used thermodynamic cycles: the *Rankine Cycle*, *Brayton Cycle* and the *Combined Cycle*, respectively.

Pihl et al. conducted a study on the types and amount of materials required to build two power plants using different CSP technologies [45]. The two cases in this study are a parabolic trough and a central tower with receiver. Pihl stated that the need for nitrate salts, steel and silver alloys can be significant for CSP projects in the future and that the focus on extracting those materials can eliminate fears of material restrictions in CSP power plants.

Allani et al. proposed a thermodynamic optimization approach to be utilized in a hybrid solar combined cycle power plant in Tunisia. The design of this integrated system with maximum power outputs of 88 MW during the day and 58 MW at night was discussed. To prove the advantage of this hybrid model against other conventional power plants, a comparison was made with two other steam turbines with a steam cycle configuration of outputs 67.5 MW and 51.5 MW respectively [46]. For each configuration a quasi-stationary approach was used that proposed two different strategies depending either on the maximum power output or the global efficiency of the hybrid system.

The results showed that the most economic configuration was the plant with the smallest solar field and longest operating hours. In addition, the results obtained show the high potential of CO_2 mitigation at significantly lower costs than other technologies based on renewable energy sources. The percentage of annual

CO_2mitigation varied between 13% and 17% and can be increased to over 25% by shutting off the power plant operation at off peak hours during the night.

Derbal-Mokrane et al. described a mathematical model for the basic components of a combined cycle power plant integrated with parabolic trough technology. A simulation program was used to determine the performance of a typical parabolic trough configuration through the year. The output power produced from the solar collector was 30MW in addition to 120MW produced from the combined cycle. The simulation shows that an efficiency of 52% is obtained for the configuration [47]. In Figure 16, a simple description of the conversion processes occurring in the solar power plant is shown. Nezammahalleh et. al. performed a techno-economic assessment on three different configurations, a concentrated solar power system (CSP), an integrated solar combined cycle with HTF and an integrated solar combined cycle with DSG [48].

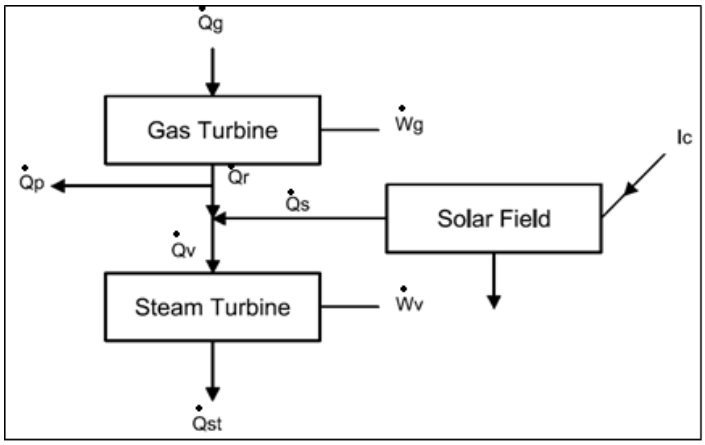

Figure 16: Energy balance of a solar-thermal power plant

The solar capacity factor, fuel cost, fuel consumption, operation and maintenance costs were included in the calculations to obtain the levelized electricity cost (LEC). It was found that a power plant with the DSG technology had the lowest LEC and highest nominal power (451.46 MW) amongst the other two power plants (444.8 MW and 67 MW) respectively. Horn et al. studied the potential of implementing an integrated solar combined cycle technology in Egypt. Three technologies were proposed for large-scale applications: a solar tower with air receiver, parabolic trough collector with HTF and a solar tower power plant with molten salt technology (MST).

The economic assessment yielded the incremental solar cost, net present value (NPV) and LEC for the various systems. The LEC for the parabolic trough collector with heat transfer fluid was slightly lower than for the solar air tower. However, both options were considered economically feasible and attractive for power generation using renewable energy sources.

Baghernejad and Yaghoubi conducted a comprehensive energy and exergy analysis to assess the performance of an integrated solar combined cycle in Iran [49]. The exergy destruction in all components of the plant was calculated and presented in an exergy flow diagram. The results showed that the energy and exergy efficiencies in the power plant were 46.14% and 45.16% respectively. The highest exergy lost occurred in the combustor (29.62%) followed by the solar collector field (9%), and pump, turbine and compressor losses (8%). The least exergy loss was stack and heat exchanger losses with 7.78% of the total exergy input.

Behar et al. [44] assessed the performance of the Hassi R'Mel integrated solar combined cycle power plant in Algeria. Each component of the system was evaluated and the overall performance of the plant was based on thermal efficiency, electricity production and the net solar electricity produced. The results showed that an amount of 134MW can be produced for a conventional CC system with an efficiency of 57.7% at night. The author stated that the solar net electricity could reach 15% during the daytime. Integrating solar energy increased the plant capacity to 157 MW and the thermal efficiency to 67%. As a result, the overall performance of the plant improved. Ordorica-Garcia et al. evaluated the techno-economic performance for three different solar-fossil hybrid configurations. The configurations were an integrated solar combined cycle, a solar assisted post combustion capture (SAPCAP) and a solar gasification with CO_2 capture [50]. It was stated that these concepts have big potential benefits to achieve maximum greenhouse gas mitigation and lower carbon emission. When there is no sunlight or during bad weather the use of an energy storage system can improve the economic and environmental aspects for the power plant and will provide sustainable and continuous production.

Using molten salts for storage is considered an attractive solution due to their excellent transport and thermal properties [51],[52]. Boukelia and Mecibah reviewed the principles and economic viability of CSP plants with parabolic trough technology [53]. The authors believe that CSP power plants have a great potential in Algeria due

to the high quality Direct Normal Insolation (DNI), sufficient water resources and appropriate land. The solar radiation levels are between 4.66 kWh/m^2 and 7.26 kWh/m^2 making Algeria one of the countries with the highest levels of solar radiation in the world and with an ideal opportunity for integrating solar power into conventional combined cycles. Montes et al. assessed the performance of two different configurations: a parabolic trough collector coupled to a Rankine cycle (solar only) and a combined cycle gas turbine (CCGT) [54]. A power plant featuring direct steam generation technology (DSG) was proposed. A technical and economic analysis was carried out on two well-known solar thermal power plants in Almeria (Spain) and Las Vegas (USA). The results showed that the system performed better in Las Vegas due to high solar radiation and high temperatures and the annual efficiency of the ISCC system was greater in Almeria (52.18%) than in Las Vegas (51.90%). The levelized cost of energy (LEC) values were nearly similar because the solar hybridization in the two configurations was very small, although it was lower in Las Vegas (79.65 €/MWh) than in Almeria (156.64 €/MWh). Cau et al. proposed the use of CO_2 as a heat transfer fluid in a parabolic trough configuration which can lead to improvements in the solar to electricity conversion efficiency [55]. The results showed that a maximum temperature of 550°C for CO_2 can yield a solar to electricity conversion efficiency between 23% and 25%. It was reported that using a steam generator with an evaporating part will only increase the conversion efficiency slightly. The cost analysis showed that the electricity production cost for a solar thermal power plant is greater than for the conventional combined cycle due to the installation of a solar field. In the case of a conventional combined cycle operating with natural gas, the LEC increased from 6.79 €/KWh to around 6.91 €/KWh for the solar thermal configuration. Hosseini et al. evaluated the technical and economic performance of the first solar thermal power plant located in Yazd (Iran) [56]. The study shows that an integrated solar combined cycle with a solar field capacity of 67 MW can save up to 59 million USD in fuel consumption and that an amount of 2.4 million tons of CO_2 emissions can be reduced over a period of 30 years. Hosseini reported that the annual net efficiency can be improved from 49.3% for a CC power plant to approximately 51.6% in the case of the hybrid configuration. Finally, the LEC of the proposed system was found to be 2.035 Cents/KWh which is much lower than for a typical CC that has an LEC of 2.263Cents/KWh. Therefore, the use of renewable energy sources was necessary to meet the growing demand for electricity. The study

highlights major renewable energy projects in the region which are expected to generate an electricity output of 10 GW by 2022.

Barigozzi et al. proposed a modeling and simulation method to predict the performance of a solar hybrid gas turbine and then compared the results with a conventional gas turbine at ISO conditions to illustrate the benefits of hybridization [57]. The results showed that during summer the hybrid system can reach an output of 33.1 MW and 28.5 MW for the standard gas turbine. The net electric efficiencies of the gas turbine were found to be 37.8% and 36.6% respectively. The influence of the pressure losses in the compressor was analyzed due to its important role in determining the performance of the hybrid system. The Darcy Equation was used to calculate the pressure drop in the pipes. It was found that the pressure drop in piping to the combustor was 70% higher than in piping to the receiver during sunny hours. A formula was suggested to choose the proper piping size to reduce pressure losses. Spelling et al. developed a dynamic model to determine the thermodynamic and economic performance of a solar tower integrated with a combined cycle power plant.

Several layouts were evaluated and the model was then optimized in terms of its cost and technical performance using a population-based evolutionary algorithm. The objective was to minimize the levelized cost of energy (LCOE) and investment costs. The results showed that the system can reach an efficiency of 18% to 24% and that the LCOE is in the range between 12 Cents/KWh and 24 Cents/KWh. Dersch et al. stated the advantages and disadvantages of using hybrid systems over CSP plants and conventional CC power plants at the same operating conditions [58]. The technical assessment was based on a 270,320 m^2 solar field using parabolic trough collectors. A thermal energy storage system was proposed to reduce fuel consumption during non-solar hours which increased the investment costs but provided a higher solar share. Dersch et. al. found that a solar share of approximately 10% can be reached. Also, carbon dioxide emissions were found to be lower in hybrid systems than in the traditional CC power plant. For CSP plants with thermal energy storage, fossil fuels can be used only for start-up and warming purposes with small amounts. The net electric efficiencies for the proposed configurations of CC and CSP without energy storage was measured as 56.5% and 34.7% whereas with energy storage it was 56.5% and 32.6% respectively. The use of thermal energy storage was better in the sense that the LEC value with energy storage was 10% to 15% lower than the LEC

value without energy storage [58]. Poullikkas proposed an optimization algorithm that can be used by independent power producers (IPPs) to calculate the unit cost of electricity in order to help them in evaluating several power generation technologies. The algorithm was used in this study to evaluate different integration options in terms of electricity unit cost and the amount of generated CO_2 emissions for each system [59]. In conclusion, this literature review illustrated the potential and benefits of renewable energy technologies. Significant developments have been made in renewable energy technology performance and environmental considerations. Major improvements have occurred in terms of reducing CO_2 emissions and enhancing fuel savings.

2.4 Thermal Energy Storage (TES)

Energy storage is another important consideration for CSP plants where the energy demand can be balanced between day time and night time. Nowadays, the trend for plants is to provide hours of storage so that less impact is caused by variations in solar radiation through the day.

Thermal energy storage comprises different technologies that store thermal energy in energy storage reservoirs for later use. Several concepts for storing thermal energy for use in solar thermal power plants have been proposed. Until very recently, thermal energy storage was only limited to prototypes or demonstration projects. The benefits of integrating thermal energy storage include not only extending utilization and dispatchabilty for the power block but also shaping the output to better match the consumer need for electricity [60].

During sunlight hours in the morning, the solar field starts delivering heat to the thermal cycle by concentrating the sun's energy using mirrors. This energy is used then to heat up the medium in the thermal storage system which will deliver the required heat when the sun is not shining or at night time. Although, thermal energy storage has high initial capital costs due to the need for extra solar collectors, a larger receiver system, and of course the storage system and medium itself, these costs are less compared with other storage technologies, mechanical or chemical [61], [62].

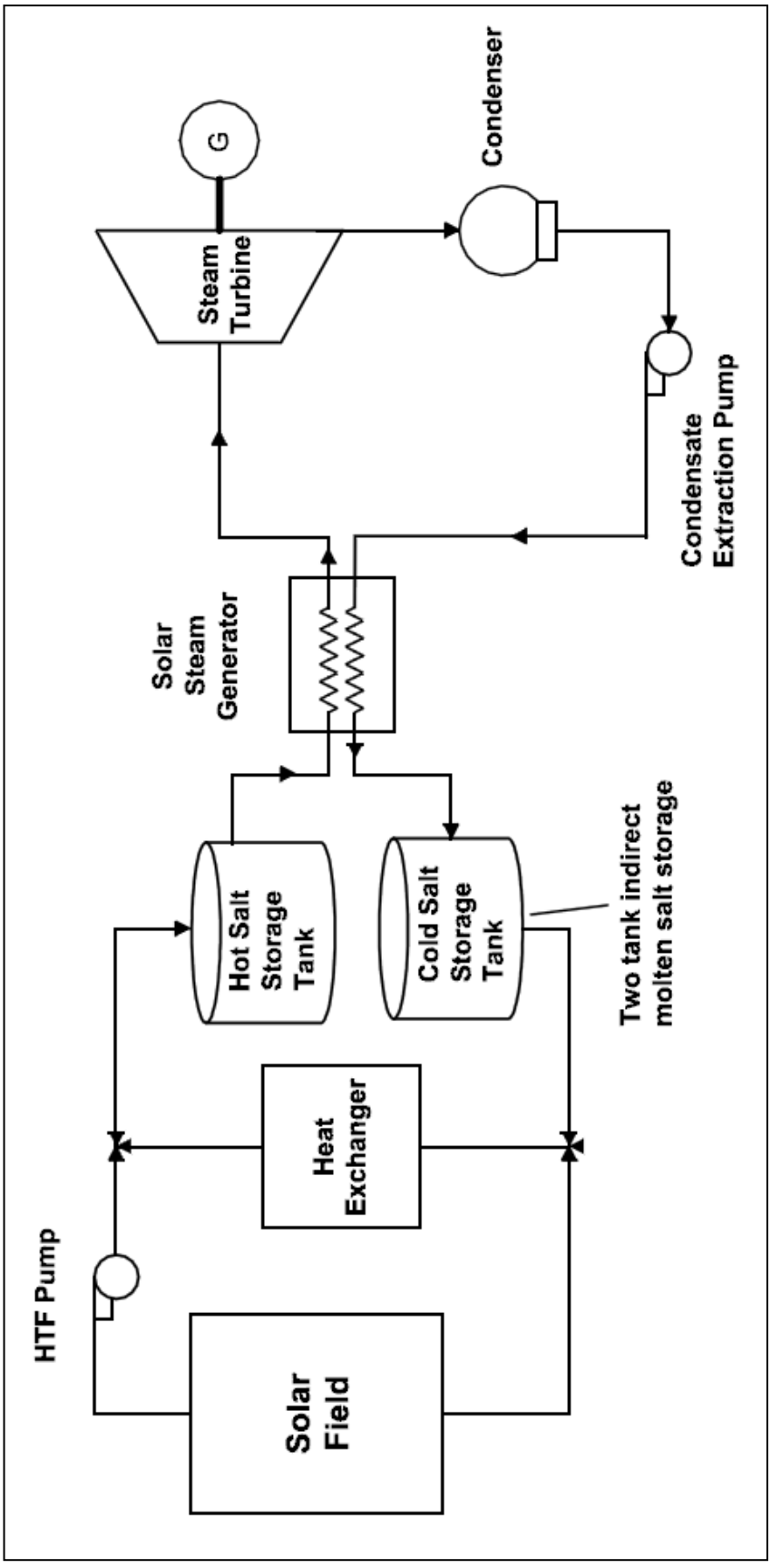

Figure 17: CSP power plant using molten salt storage

The current practice is to use molten salts which are a mixture of sodium and potassium nitrate that melts at around 220°C and is stable to about 590°C [63], although, there is considerable research into new materials to extend the upper temperature limit. Fath reviewed the major developments in TES systems and the parameters that effect the selection and performance of these systems [64].

Several studies were conducted on the materials used in *latent* and *sensible* heat storage systems and the main problems associated with them. The corrosion effect, insulation, melting temperature and heat transfer characteristics are critical factors in the selection of the storage materials.

Thermal energy storage can be classified as either direct or indirect depending on the role of the storage medium in the TES system.

a) Direct Storage

i. Thermal oil storage in tank

ii. Steam accumulation in pressure vessel

b) Indirect Storage

i. Sensible Storage

- *Molten salt tanks*
- *Sand, with rocks for solar tower with receiver*
- *Room temperature ionic*
- *Concrete*

ii. Latent Storage

iii. Chemical Storage

Figure 18 shows the full organization of thermal energy storage with the suitable concentrated solar power technology and the available commercial storage methods.

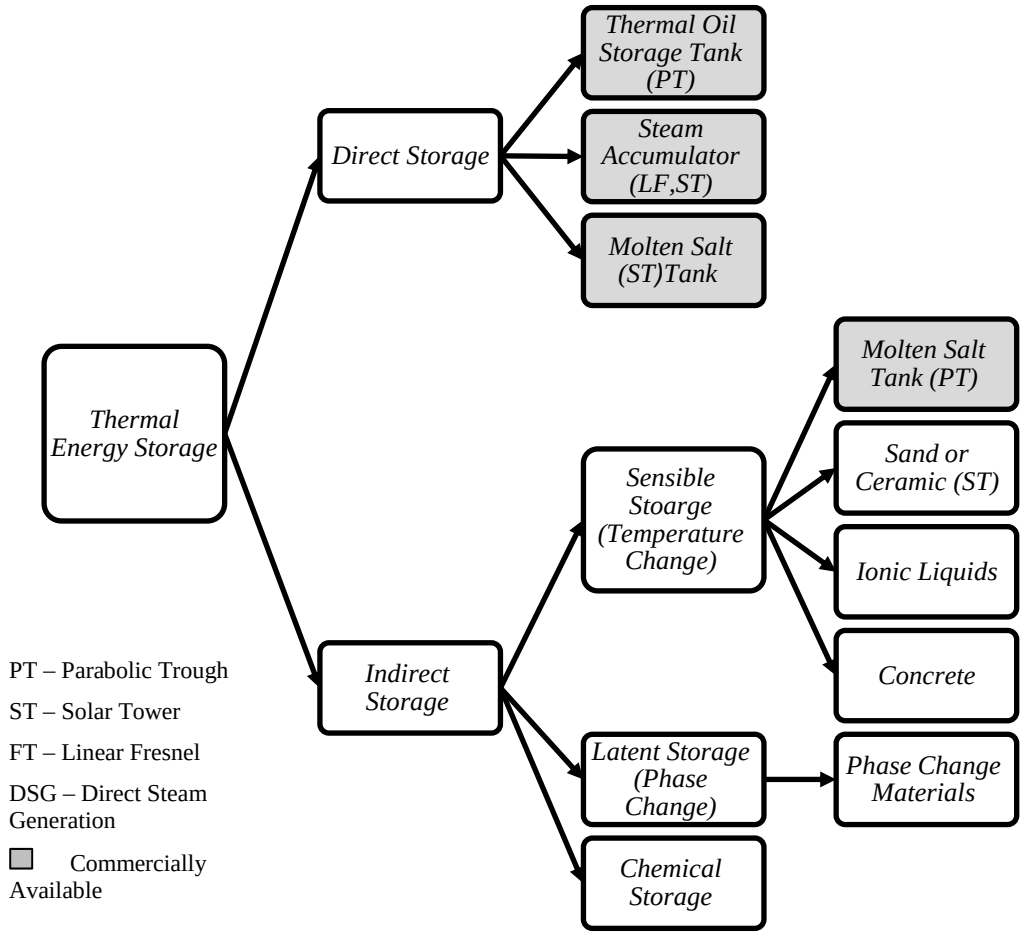

Figure 18: Organization of Thermal Energy Storage

Kuravi et al. reviewed different TES design methodologies [65]. The authors suggested that the design of thermal energy storage systems depends on some considerations related to the CSP plant type, size and design. The criterion used depends on the following:

a) *Maximum load*
b) *Operation strategy*
c) *Integration into the plant*
d) *Nominal temperature and specific enthalpy drop in the load*

For a practical design of the CSP plant integrated with a TES system, a hierarchy of the system with emphasis on the plant, components and system levels is presented in Figure 19.

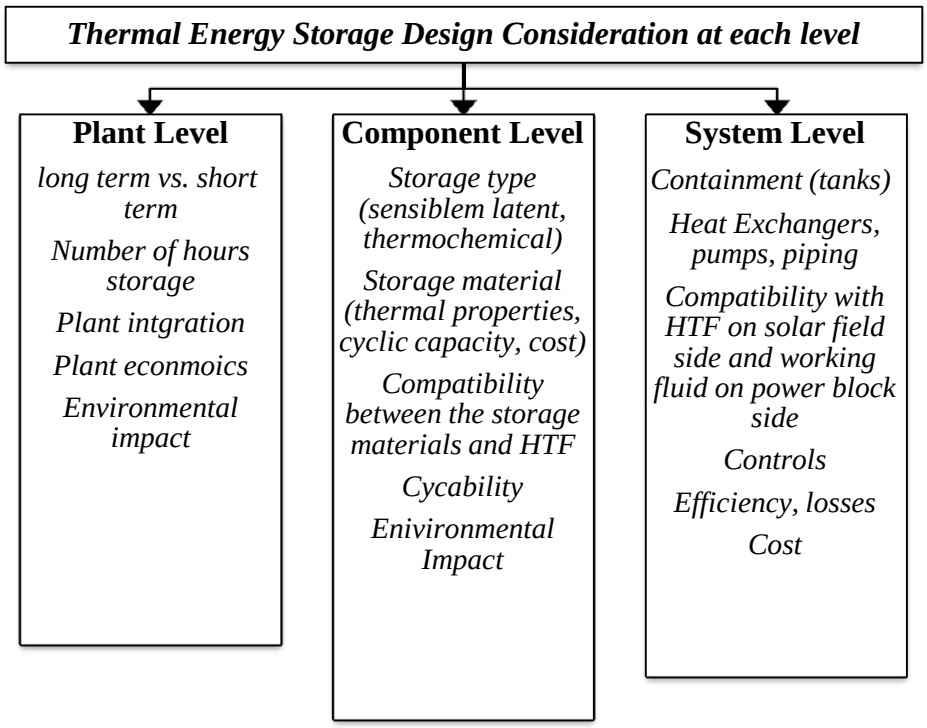

Figure 19: Design Considerations for TES

Furthermore, there are several requirements that have to be considered for optimum storage which are:

1. *Good heat transfer between the storage medium and the HTF*
2. *Chemical stability and compatibility*
3. *High energy density*
4. *Low thermal losses*
5. *Low environmental impact*
6. *Low cost*

2.5 Material Selection

The selection of the storage medium materials must take into consideration the cost, material properties, thermal losses and chemical stability. These factors are essential to develop a robust system that will withstand thousands of thermal cycles. There are a number of important thermo-physical properties including availability, specific heat capacity, thermal expansion, density, thermal conductivity, cost and production methods. In the case of sensible heat storage (SHS), a rise in temperature of the storage medium occurs during the storage process. The heat capacity of the storage material has a direct influence on the amount of heat released or extracted

from the storage material. Some of the potential sensible heat storage materials are shown in Table 4 along with their thermo-physical properties.

Table 4: Sensible Heat Storage materials

Material	T_{cold} *(°c)*	T_{hot} *(°c)*	*Thermal Conductivity (W/m.k)*	*Density (kg/m^3)*	*Average Specific heat Cp (kj/kg k)*	*Type of medium*
Sand-rock-oil	200	300	1	1,700	1.3	Solid
Cast iron	200	400	37	7,200	0.56	Solid
NaCl	200	500	7	2,160	0.85	Solid
Cast steel	200	700	40	7,800	0.6	Solid
Synthetic oil	250	350	0.11	900	2.3	Liquid
Nitrate salts	250	450	0.57	1,825	1.5	Liquid
Lithium liquid salt	180	1,300	38.1	510	4.19	Liquid
Therminol 66	0	345	-	750	2.1	Liquid

Another method for storing thermal energy is using latent heat storage (LHS). The enthalpy of phase change and the specific heat of the material are the two main factors for this type of storage. Some of the potential latent storage materials are presented in Table 5 below. Tian and Zhao reviewed different types of thermal energy storage systems [66]. The study was carried out based on design method, material selection and HTF used. In this study, three types of solar collectors were evaluated: parabolic dish, heliostat field and parabolic trough collectors. The authors compared the three systems to determine which materials are most suitable for thermal storage at high temperatures.

Table 5: Latent Heat Storage materials

Material	T_{melt} *(°c)*	*Thermal Conductivity (W/m.k)*	*Latent heat of fusion (J/g)*
$NaNO_3$	307	0.5	177
KNO3	335	0.5	88
KOH	380	0.5	149.7
48 wt% NaCl – 52% $MgCl_2$	450	0.95	430
36 wt% KCl – 64% $MgCl_2$	470	0.83	388
LiBr	550	-	203

The authors stated that the thermal storage capacity must be high to increase the system efficiency and that the heat transfer material should be chemically stable and cost-effective. According to Tian and his colleague, molten salts were ideal materials to be used as heat transfer mediums due to their excellent properties. A comparison between molten salts and different high temperature oils was investigated in his study. Table 6 shows the factors that influence the selection of the thermal storage system.

Table 6: Influencing factors for Thermal Energy Storage Systems

Criteria	***Influencing factors***
Technical Criteria	1. High thermal energy storage capacity 2. Efficient heat transfer rate between HTF and storage material 3. Good mechanical and chemical stability 4. Compatibility between HTF, heat exchanger and storage material 5. Complete reversibility of a large number of charging and discharging cycles 6. Low thermal losses and ease of control
Cost-effectiveness Criteria	1. The cost of thermal energy storage materials 2. The cost of the heat exchanger 3. The cost of the space and/or enclosure for the thermal energy storage
Environmental Criteria	1. Operation strategy 2. Maximum load 3. Nominal temperature and specific enthalpy drop in load 4. Integration to the power plant

Bai and Xu presented a thermal analysis on a thermal energy storage system composed of a high temperature stage using concrete and a low temperature stage using a steam accumulator [67]. It was reported that the conductivity of concrete and the distance between the piping can greatly affect the system performance. The concrete storage unit is connected to the discharge of the steam accumulator where the steam is heated until it is in the superheated state and can be fed to the steam turbine to generate power. Some assumptions were made for the steam properties (e.g. temperature, pressure, flow rate, etc.) to formulate the model and solve the discharge problem of the steam accumulator. The results showed that the exit temperature of steam from the concrete storage unit and steam accumulator is decreasing during time and that the higher conductivity of concrete will increase the steam temperature in the

piping therefore increasing the thermal efficiency of the system. The study concluded that a two stage TES system is ideal for use in solar thermal power plants.

Kolb et al. examined the economic potential of different hybrid configurations with molten salt towers and solar only power plants [68]. The case of a solar power boosting a combined cycle had economic potential and the CO_2 avoidance costs were more competitive than other methods of reducing CO_2 from other natural gas-fired or coal fired power plants. Xu et al. [67] have presented an energy and exergy analysis for a solar tower with receiver using molting salt technology. Exergy and energy losses were calculated for each component of the system and it was reported that the maximum exergy losses appeared in the solar receiver system (44.2%), followed by the heliostats (33.1%). The results showed that the DNI values had affected the exergy and energy efficiencies. Likewise, the concentration ratio and aperture area size were important factors to reduce heat losses and increase total system efficiency. Birnbaum et. al demonstrated that the integration of thermal energy storage will increase the complexity of the power plant. He suggested the use of phase change materials (PCM) as a storage medium [69],[70]. Zalba et al. discussed the use of PCM in TES systems. A list of available materials with their thermo physical properties was presented. The authors classified the materials according to their availability in the market and whether they were organic or inorganic. The melting temperature, density, heat of fusion and thermal conductivity value was presented to find the potential of using these materials as PCM for energy storage [71]. The authors found that corrosions and poor stability were major problems for phase change storage materials and several studies were conducted on molten salts melting at high temperatures to find the corrosion effect. The different applications of TES were categorized as either storage or thermal protection.

2.6 Molten Salt Technology (MST)

Most of the currently integrated thermal energy storage systems in solar thermal power plants use sensible heat storage. These state-of-the-art plants employ molten salts in an indirect two tank design. Sodium-nitrate salts and potassium-nitrate salts are cheap materials for storage systems. They have a high transmission coefficient and can be stored in big salt tanks. The problem is their high melting point which requires electrical heating of the piping to avoid blockage during system start

up and operation. The system is predicted to have an annual efficiency of about 99%, (a reference to the energy lost by storing heat before turning it into electricity) [72]. The salt melts at 131°C. It is kept liquid at 288°C in an insulated cold storage tank. The liquid salt is pumped through panels in a solar collector where the focused sun heats it to 566°C. It is then sent to a hot storage tank. This is so well insulated that the thermal energy can be usefully stored for up to a week. When electricity is needed, the hot salt is pumped to a conventional solar steam generator (SSG) to produce superheated steam for a turbine/generator [73],[74].

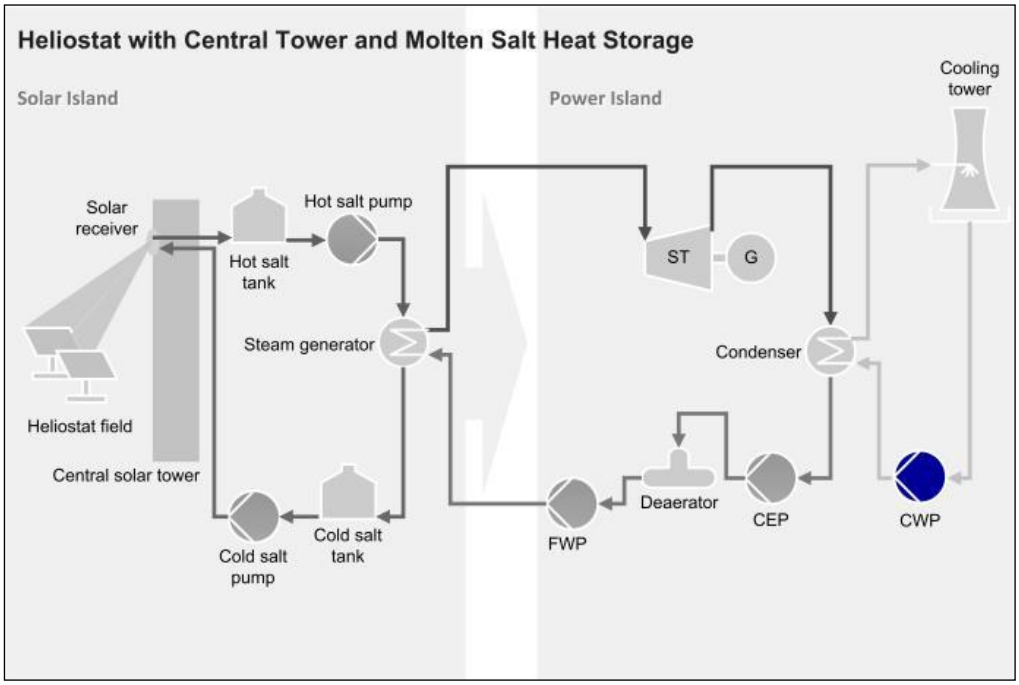

Figure 20: Schematic diagram of Molten Salt power tower system [75]

Chapter 3: Configurations of Integrated Systems

In this chapter, schematic diagrams of two proposed integrated designs are provided and the principle of operation is explained for each system.

3.1 Design 1: Integrated Solar Combined Cycle (ISCC)

The first design proposed in this study is the integrated solar combined cycle. This system is composed of two main components which are the Solar Field and the Power Block. The power cycle used for this design is a conventional combined cycle operating on natural gas. This configuration is attractive because it draws the environmental benefits from using solar energy with the operational advantages of the conventional combined cycle.

When the sun is not shining, the combined cycle power plant can be used as a backup for solar power. By integrating solar energy, the reduction of natural gas consumption is possible (fuel saver mode). At periods of peak demand, the solar steam can boost the electricity production of the power plant (solar boost mode).

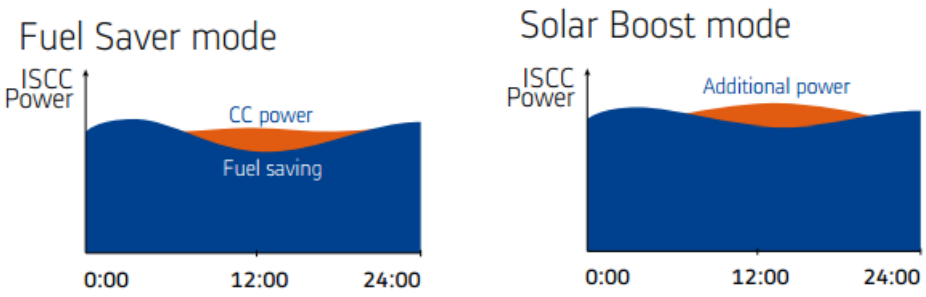

Figure 21: ISCC operation modes

In this configuration, the selected heat transfer fluid (Therminol VP-1) enters the loop with an inlet temperature of 293°C where it is circulated through the receiver and heated to an outlet temperature of 391°C. Afterwards, the HTF runs through a steam generator to generate high pressure steam. The generated steam passes then through the heat recovery steam generator (HRSG) which is a series of heat exchangers. The steam gains input heat energy from the high temperature exhaust gases from the gas turbine unit. The generated superheated steam produced thus can be used to drive the steam turbine. The steam turbine delivers the energy to the

generator drive shaft. The generator converts this energy into electricity and the discharged steam from the steam turbine is condensed into water that will be pumped back to a steam generator. The design and operating parameters for the integrated solar combined cycle are presented in Table 7. The schematic diagram of the integrated solar combined cycle power plant is shown in Figure 22.

Table 7: Design and operating parameters for the ISCC configuration

Parameter	***Symbol***	***Unit***	***Value***
Ambient temperature	T_{amb}	K	300.1
Compression Ratio	rp	-	6
Isentropic efficiency for compressor	ζ_c	%	85
Isentropic efficiency for turbine	ζ_t	%	90
Mechanical efficiency for compressor	ζ_m	%	95
Gas turbine inlet temperature	T_3	K	1023
Low Heating Value	LHV	GJ/T	50
Specific heat of fuel	Cp_f	kj/kg.k	2.34
Fuel Temperature	T_f	K	853
Gas flow rate	$\dot{m}_g$	kg/s	150
Pinch Point	T_{pp}	K	288
Approach Point	T_{ap}	K	281
Ratio of specific heat for air	γ_a	-	1.4
Ratio of specific heat for gas	γ_g	-	1.33

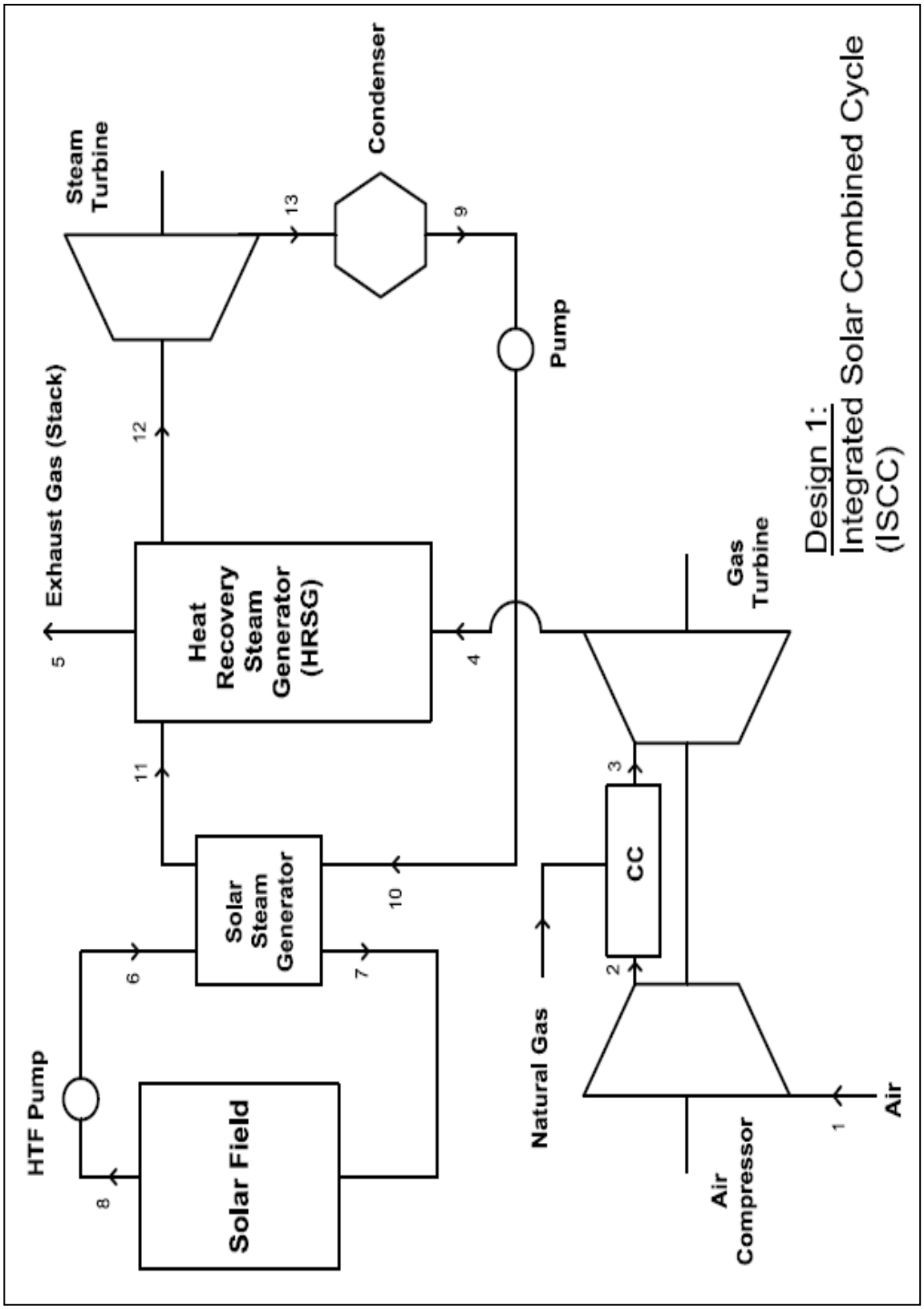

Figure 22: Schematic diagram of ISCC power plant

The power cycle in this proposed system is a conventional combined cycle. The operation parameters of the power cycle are shown in Table 8 as follows:

Table 8: Operation parameters of the power cycle

Power Block	
Turbine capacity (gross)	150 MW
Turbine capacity (net)	150 MW
Output type	Steam Rankine
Gas Turbine	
Number of units	1
Type: GE	Frame 6FA
Fuel	Natural Gas
Heat Recovery Steam Generator	
Number of units	1
Type	Modular HRSG
Pressure levels	1
Specific feature	Solar heat as energy source
Steam Turbine	
Steam flow (kg/s)	39.4
Steam Pressure (bar)	95
Steam Temperature (°C)	500-560

The mathematical analysis for each component of the integrated solar combined cycle is carried out. The model is developed for the following eight components:

i. Air Compressor
ii. Combustion Chamber
iii. Gas Turbine
iv. Heat Recovery Steam Generator
v. Solar Steam Generator
vi. Steam Turbine
vii. Condenser
viii. Pump

i. Air Compressor

First, air is forced through the compressor with a compression ratio r_p

$$r_p = \frac{P_2}{P_1} \tag{3.1}$$

The inlet air temperature ($T_1 = T_{ambient}$) and isentropic efficiency of the compressor (ζ_c) are known. The isentropic efficiency for compressors and turbines are in the range of (85% - 90%) and can be calculated from the following equation:

$$\zeta_c = \frac{T_{2s} - T_1}{T_2 - T_1} \tag{3.2}$$

The exit temperature T_2 of the compressor is:

$$T_2 = T_1 \left(1 + \frac{r_p^{\frac{\gamma_a - 1}{\gamma_a}}}{\zeta_c} \right) \tag{3.3}$$

where γ_a is the ratio of specific heat for air.

The work of the compressor $\dot{W}_c$ can be given from the following relation:

$$\dot{W}_c = \frac{C_{pa}.T_1 \left(r_p^{\frac{\gamma_a - 1}{\gamma_a}} - 1 \right)}{\zeta_m.\zeta_c} \tag{3.4}$$

where:

C_{pa} is the specific heat of air (J/kg.k)

ζ_m is the mechanical efficiency of the compressor and turbine

ii. Combustion Chamber

The energy balance equation for the combustion chamber is:

$$\dot{m}_a C_{pa}.T_2 + \dot{m}_f.LHV + \dot{m}_f.C_{pf}.T_f = (\dot{m}_a + \dot{m}_f) C_{pg}.T_3 \tag{3.5}$$

where:

$\dot{m}_a$ is air mass flow rate (kg/s)

$\dot{m}_f$ fuel mass flow rate (kg/s)

LHV the low heating value of the fuel (kj/kg)

C_{pf} specific heat of fuel (J/kg.k)

T_f temperature of the fuel (Kelvin)

T_3 gas turbine inlet temperature (Kelvin)

C_{pg} specific heat of flue gas that was given by Naradasu as:

$$C_{pg} = 1.8083 - 2.3127x10^{-3}T + 4.045x10^{-6}T^2 - 1.7363x10^{-9}T^3 \quad (3.6)$$

The fuel-air ratio f can be expressed as:

$$f = \frac{\dot{m}_f}{\dot{m}_a} = \frac{C_{pg}.T_3 - C_{pa}.T_1\left(1 + R_{pg}\right)}{LHV + C_{pf}.T_f - C_{pg}.T_3} \quad (3.7)$$

where:

$$R_{pg} = 1 - \frac{1}{r_p^{\frac{\gamma_g - 1}{\gamma_g}}} \quad (3.8)$$

The ratios of specific heat of air γ_a and gas γ_g can be taken as 1.4 and 1.33 respectively.

iii. Gas Turbine

The exhaust gas temperature from the gas turbine is given by:

$$T_4 = T_3\left(1 - \zeta_t.\left(1 - \frac{1}{r_p^{\frac{\gamma_g - 1}{\gamma_g}}}\right)\right) \quad (3.9)$$

The exhaust gas temperature from the gas turbine T_4 is equal to the inlet gas temperature T_{g1} to the HRSG ($T_4 = T_{g1}$).The shaft work of the turbine $\dot{W}_t$ is given by:

$$\dot{W}_t = \frac{C_{pg}.T_3.\zeta_t.R_{pg}}{\zeta_m} \quad (3.10)$$

The net work of the gas turbine is calculated from the difference of the turbine work and the compressor work as:

$$\dot{W}_{Gnet} = \dot{W}_t - \dot{W}_c \tag{3.11}$$

The output power from the gas turbine P is:

$$P = \dot{m}_a . \dot{W}_{Gnet} \tag{3.12}$$

The specific fuel consumption SFC is determined from:

$$SFC = \frac{3600 . \dot{m}_f}{\dot{W}_{Gnet}} \tag{3.13}$$

The heat supplied is expressed as:

$$\dot{Q}_{add} = \frac{\dot{m}_f . LHV}{\dot{W}_{Gnet}} \tag{3.14}$$

The gas turbine efficiency is given by:

$$\zeta_{GT} = \frac{\dot{W}_{Gnet}}{\dot{Q}_{add}} \tag{3.15}$$

iv. Heat Recovery Steam Generator

The HRSG consists of three main parts which are the economizer, the evaporator and the superheater. This single pressure model is a common type for the combined cycle power plant. The energy balance equations are shown next.

The gas temperature and water properties are calculated using pinch analysis. The actual processes in the HRSG are represented in Figure 23. Using pinch technology, the thermal analysis for the HRSG is carried out. The designed pinch point T_{pp} and approach point T_{ap} is shown in Figure 23.

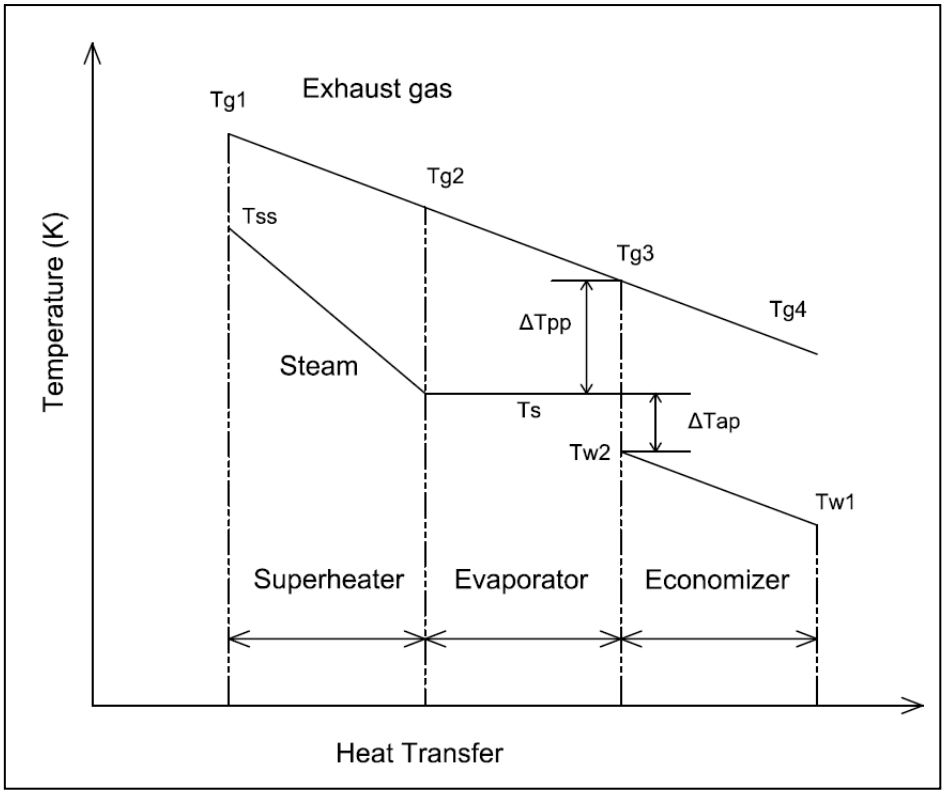

Figure 23: Temperature profile in Heat Recovery Steam Generator

The temperature of gas leaving the evaporator T_{g3} is:

$$T_{g3} = T_s + T_{pp} \tag{3.16}$$

where:

T_s is the saturation steam temperature.

The inlet water temperature T_{w2} to the evaporator is given by:

$$T_{w2} = T_s - T_{ap} \tag{3.17}$$

The available heat from the gas turbine exhaust can be expressed as:

$$\dot{Q}_{av} = \dot{m}_g . C_{pg} . \left(T_{g1} - T_{g3}\right) . h_{1f} \tag{3.18}$$

where:

$\dot{m}_g$ gas flow rate (kg/s)

h_{1f} the heat loss factor which is in the range of (0.98-0.99)

The steam flow rate $\dot{m}_s$ is found from the relation:

$$\dot{m}_s = \frac{\dot{Q}_{av}}{(h_{sh} - h_s) + BD.(h_s - h_{w2f})} \tag{3.19}$$

where:

BD the blow down factor

The gas temperature entering the evaporator T_{g2} is:

$$T_{g2} = T_{g1} - \frac{\dot{m}_s.(h_{sh} - h_s)}{h_{1f}.\dot{m}_g.C_{pg}} \tag{3.20}$$

The duty of the superheater can be obtained from the following equation:

$$\dot{Q}_{sh} = \dot{m}_s.(h_{sh} - h_s) = \dot{m}_g.C_{pg}.(T_{g1} - T_{g2}).h_{1f} \tag{3.21}$$

The water flow rate $\dot{m}_w$ is given by:

$$\dot{m}_w = \dot{m}_s.BD \tag{3.22}$$

Finally, the stacks exhaust temperature T_{g4} leaving the HRSG is:

$$T_{g4} = T_{g1} - \frac{\dot{m}_s.BD.(h_{w2f} - h_{w1f})}{\dot{m}_g.C_{pg}} \tag{3.23}$$

v. Solar Steam Generator

The solar steam generator is used to raise the temperature of the feeding water in the steam cycle by exchanging heat with the thermal energy of the heat transfer fluid from the solar concentrator. The energy balance equation of the solar steam generator is:

$$\dot{m}_{HTF}.C_{pHTF}(T_6 - T_7) = \dot{m}_w.(h_{11} - h_{10}) \tag{3.24}$$

vi. Steam Turbine

The superheated steam with high pressure obtained from the HRSG is then expanded through the steam turbine where the steam turbine work $\dot{W}_s$ can be given as:

$$\dot{W}_s = \dot{m}_s.(h_{12} - h_{13}) \quad (3.25)$$

vii. Condenser

The heat rejected from the condenser $\dot{Q}_{cond}$ is given from:

$$\dot{Q}_{cond} = \dot{m}_w.(h_{13} - h_9) \quad (3.26)$$

viii. Pump

The pump work $\dot{W}_P$ from extracting the condensate water to the economizer is:

$$\dot{W}_P = \dot{m}_w.(h_{10} - h_9) \quad (3.27)$$

Therefore, the net work of the steam turbine W_{snet} is calculated from:

$$\dot{W}_{snet} = \dot{W}_s - \dot{W}_P \quad (3.28)$$

The efficiency of the steam turbine unit is:

$$\zeta_{st} = \frac{\dot{W}_{snet}}{\dot{Q}_{av}} \quad (3.29)$$

The efficiency of the combined cycle can be given by:

$$\zeta_{CC} = \zeta_{GT} + \zeta_{ST} - (\zeta_{GT}.\zeta_{ST}) \quad (3.30)$$

ISCC Efficiency:

Finally, the overall efficiency of the Integrated Solar Combined Cycle plant is:

$$\zeta_{ISCC} = \frac{\dot{W}_{snet} + \dot{W}_{gnet}}{\dot{Q}_{add} + \dot{Q}_s} \quad (3.31)$$

where $\dot{Q}_s$ is the thermal energy received from the solar field.

3.2 Design 2: ISCC with Thermal Energy Storage

In the second proposed design, the power plant consists of three main parts: the solar field, the power block and the thermal energy storage system. Figure 24 shows a schematic diagram of the integration between the conventional combined cycle, solar field and added thermal energy storage. Thermal energy storage can increase the value of the plant by allowing more thermal energy and more flexible

hour operation. The thermal energy storage system chosen is the molten salt two tank indirect storage system. The Hitec XL salt (48% $Ca(NO_3)_2$, 7% $NaNO_3$, 45% KNO_3) is the selected storage medium with an operating temperature between (120°C - 500°C). The storage capacity can be defined as the number of hours of discharge capacity. In this case, the system will operate with 7.5 full load hours of thermal energy storage. The integration of thermal energy storage is expected to decrease the plant efficiency during the time of thermal charging or discharging due to the heat transfer losses in the thermal storage system.

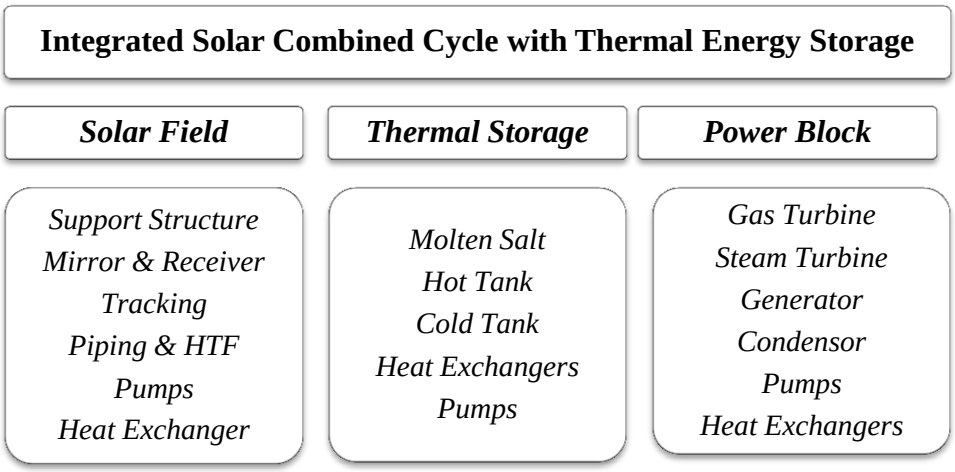

Figure 24: System components of ISCC with TES

The actual operational schemes for this system may be quite complex as the system will be charged when the thermal energy collected from the solar field exceeds the requirements of the power block. The basic operating strategy is charging the thermal energy storage system whenever the flow rate of the heat transfer fluid exceeds the design flow rate for steam generation. The surplus flow from the HTF will return to the oil-salt (shell-and-tube) heat exchanger to charge the molten salt system. The general layout of the system is illustrated in Figure 25.

The design and operating parameters for the integrated solar combined cycle with thermal energy storage is presented in Table 9.

Molten salt in the cold tank will extract heat from the HTF and then enter the hot salt tank. During operating hours, the HTF design flow rate is maintained and molten salts in the hot tank are discharged to reheat the HTF and maintain the maximum flow rate through the steam generator.

Table 9: Design and operating parameters for ISCC with TES

Parameter	***Symbol***	***Unit***	***Value***
Cold tank temperature	T_{cold}	°C	250
Hot tank temperature	T_{hot}	°C	365
Storage media density	P_{salt}	kg/m^3	1957
Storage media specific heat	Cp_{salt}	kg/kg.k	1.433
Tank height	H_{tank}	m	20
Tank diameter	D_{tank}	m	45
TES thermal capacity	$Q_{th,tank}$	MW_{th}	2205
Storage volume	V_{tank}	m^3	32923
Storage Media	-	-	Hitex XL
Storage Capacity	-	hr	7.5

The simple energy balance across the oil-salt heat exchanger can be given by

$$\dot{m}_{HTF}.C_{pHTF}.\Delta T_{HTF} = \dot{m}_{molten\ salt}.C_{pmolten\ salt}.\Delta T_{molten\ salt} \quad (3.32)$$

The required storage volume is considered to be the volume required to fill one tank of molten salt. This means when one tank is full; the other salt tank is empty. However, a minimum amount of molten salt must be maintained in each tank.

When the thermal storage system is in the *charge cycle*, a portion of the synthetic oil fluid coming from the solar collector filed is directed to the oil-salt heat exchanger. The oil inlet temperature cools down from 391°C to an outlet temperature of 293°C. The molten salt from the cold tank flows in a countercurrent arrangement through the shell and tube heat exchanger. The molten salt resides in the hot tank at a design set point temperature of 365°C while the set point temperature for the cold tank is 250°C. During the *discharge cycle*, the paths of the molten salt and oil are reversed in the heat exchanger and heat is extracted from the molten salt to oil to provide the necessary thermal energy for steam generation in the power plant.

However, there are still some concerns about the freezing possibility of the salt in the cold tank when the system is not charging for long periods. So, the use of auxiliary heaters to maintain the design point temperature for the cold tank could be used. However, Hate XL salts were proven reliable in this regard due to their low heat

capacity compared with other synthetic oils. The freezing point of the Hitec XL salt is in the range of 87°C -130°C. The performance of the system when utilizing thermal energy storage with the ISCC power plant and its impact on the levelized cost of energy is investigated by the economic and environmental analysis carried out. The operation modes of the storage system during day and night are shown in Figure 26 and 27.

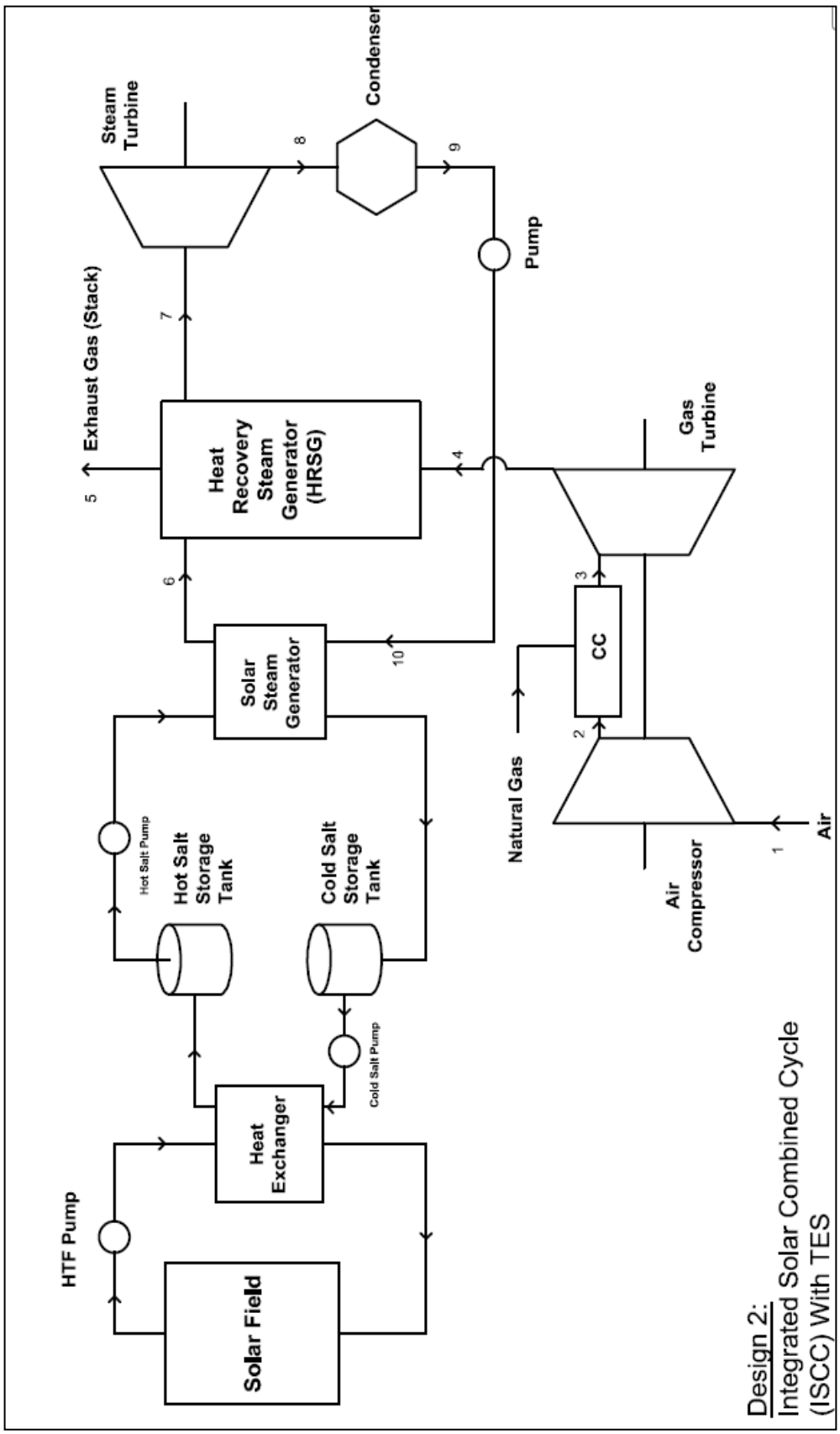

Figure 25: Schematic diagram of ISCC with TES

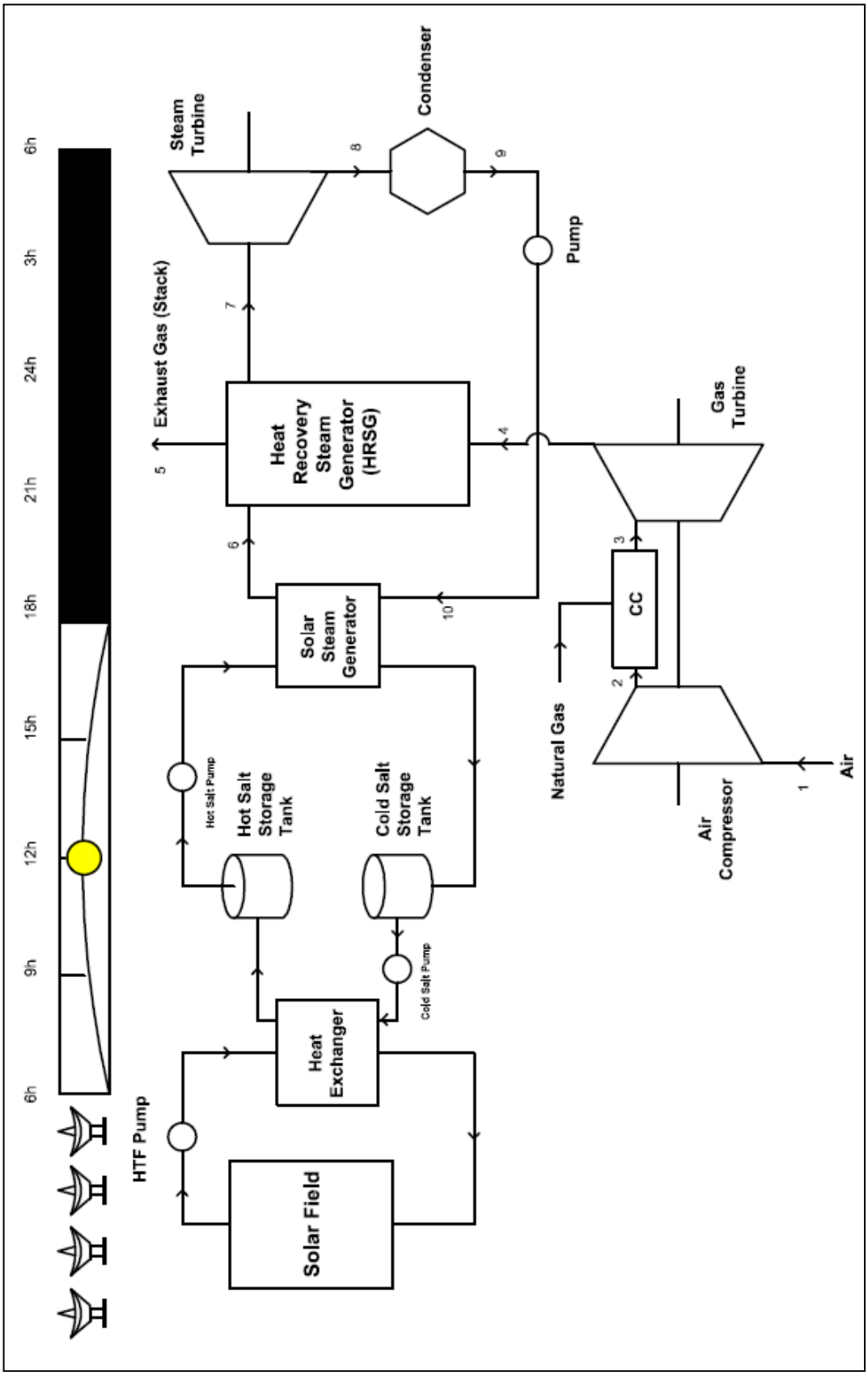

Figure 26: Thermal Energy Storage Charge Cycle (1st mode).

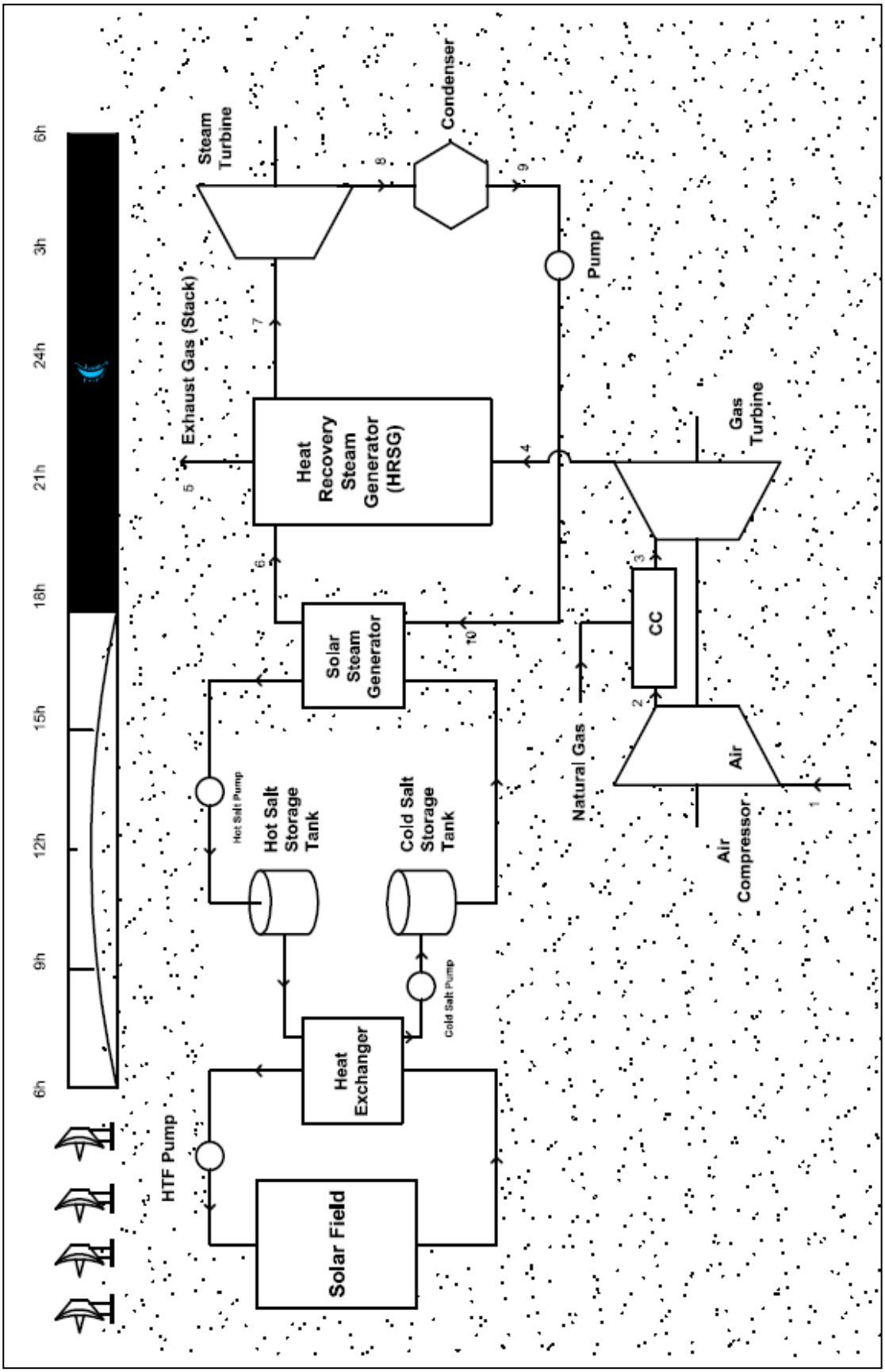

Figure 27: Thermal Energy Storage Discharge Cycle (2nd mode).

Chapter 4: System Modeling and Analysis

This chapter is divided into two sections. The first section presents a general description of the system in terms of meteorological data, solar potential, heat transfer fluid selection and the collector and receiver options for the solar field. The second section presents the thermodynamic performance model of the solar collector system based on an energy and exergy analysis. Afterwards, an economic and environmental analysis for the proposed configurations is carried out. All the analyses conducted herein are programmed using the Engineering Equations Solver (EES) and MATLAB software. The meteorological data, solar potential and collector and receiver options are discussed next.

4.1 Meteorological Data and Solar Potential

The system is located geographically at latitude 24.43°N and longitude 54.65°E and the site elevation is 27 m above sea level. Due to this geographical location, the UAE is blessed with high amounts of solar radiation with an average daily energy input of 18.48 MJ/m^2/day. The UAE is a Sun Belt country where the climate conditions and precipitation create a great potential for using solar energy for power generation.

Generally, the climate of the UAE is hot and dry. The summer months (June to September) are very hot for comfort with high midday average temperatures. Rainfall is irregular and infrequent but mainly falling in winter. Sandstorms and Gale force winds occur during summer due to the development of a low pressure area forcing the strong north-westerly winds to blow over the country. The weather data database for the UAE was downloaded from the EnergyPlus Energy Simulation Software developed by the U.S. Department of Energy - Energy Efficiency & Renewable Energy (EERE). The System Advisor Model (SAM) is used to show some of the weather data results. Figure 28 shows some weather data for Abu Dhabi.

In Figure 28, the monthly average high temperature in Abu Dhabi is shown in the upper section of the graph while the monthly low temperature values are shown in the lower section.

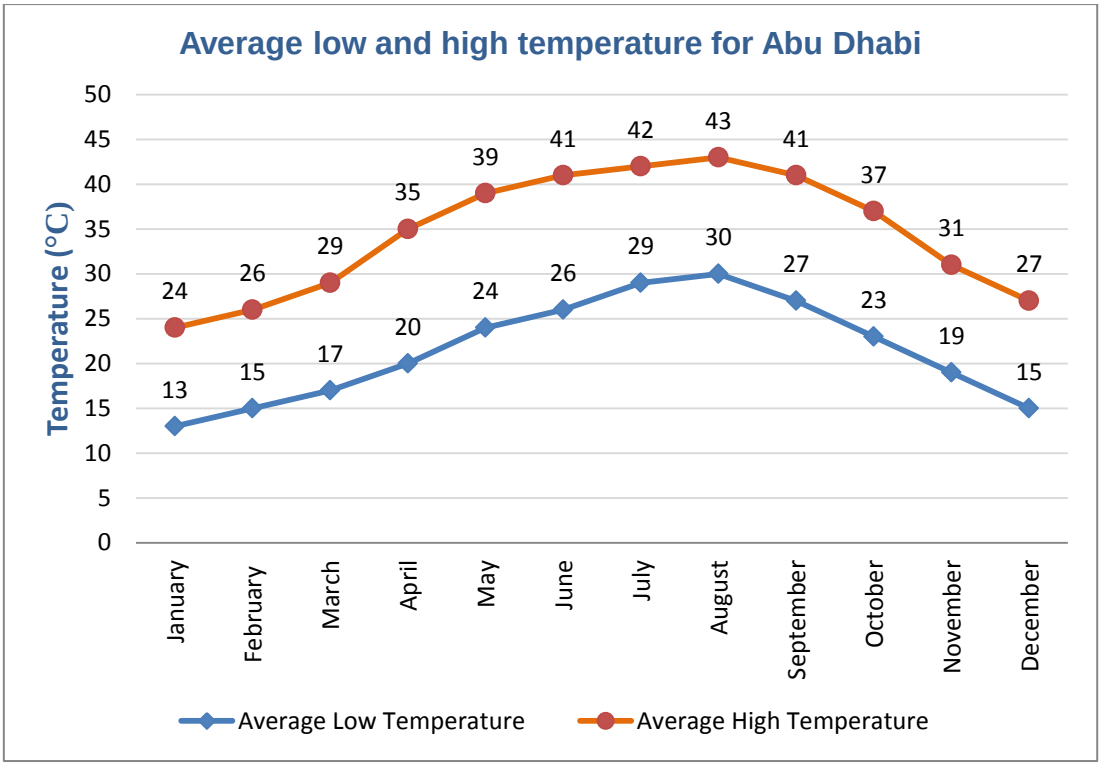

Figure 28: Monthly average low and high temperatures in Abu Dhabi

The daily low (brown) and high (blue) relative humidity during 2013 for Abu Dhabi is shown in Figure 29.

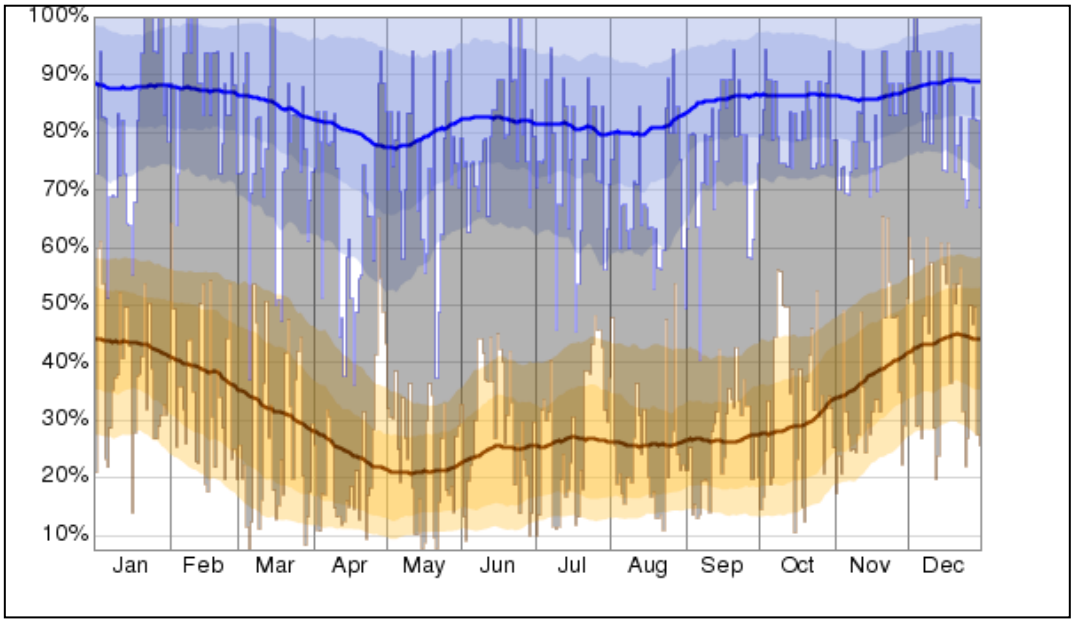

Figure 29: Monthly Wind Speed and Relative Humidity for Abu Dhabi

Observation for the last years indicated a high yearly variability in the direct normal irradiation values across the UAE. For example, the values of direct normal irradiance ranged from 1700 to 1950 kWh/m^2 in 2009. For the year 2010, the values were much higher and ranged from 1900 to 2200 kWh/m^{2}which indicates a high solar energy potential all year round.

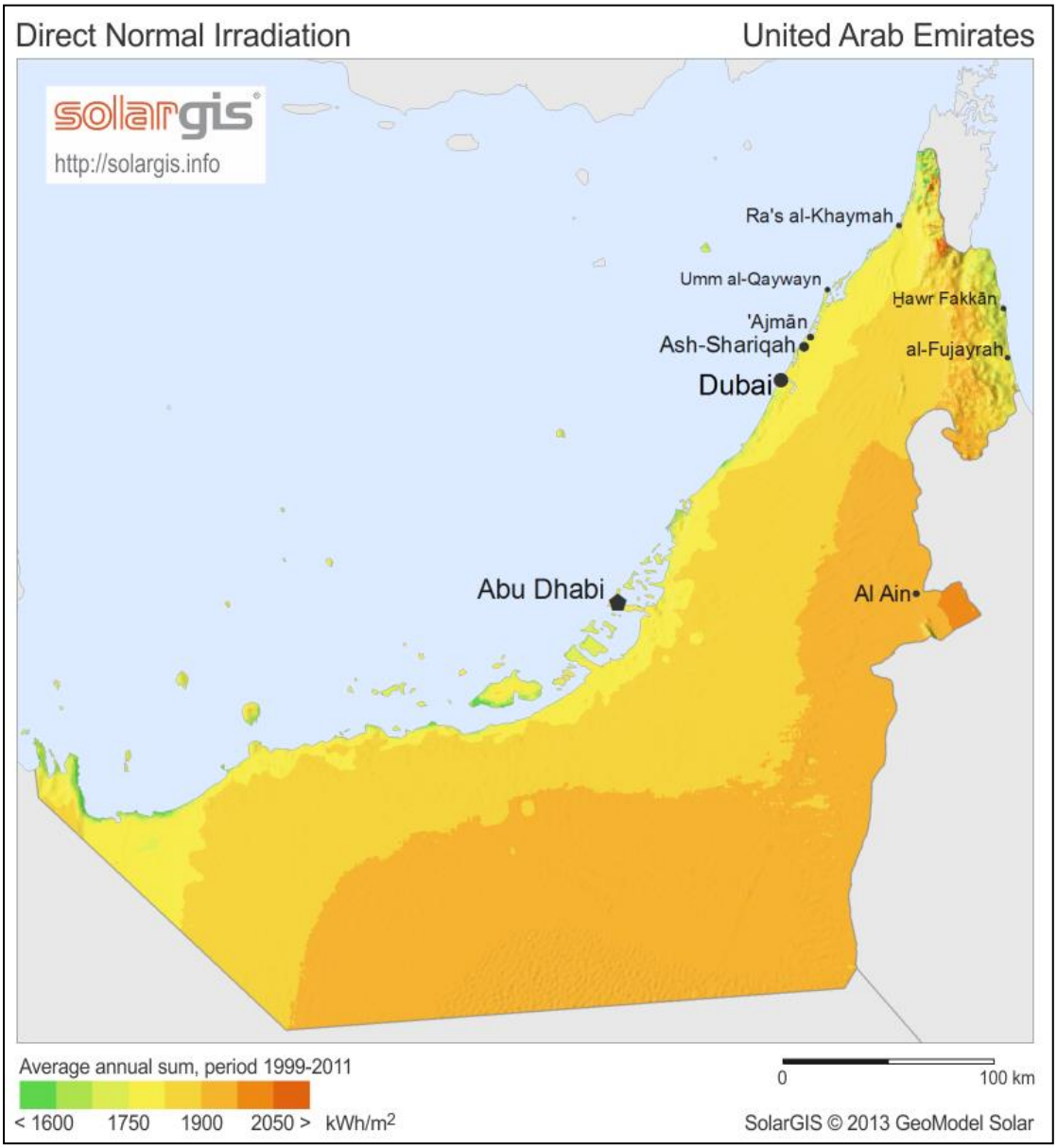

Figure 30: DNI contour plot for UAE [76]

Since the DNI values are sufficiently high, the conversion of the traditional operating gas turbine or combined cycle generating plants into an ISCC configuration should be taken into consideration by investors for future plant conversion. Figure 30

shows the direct normal irradiance map over the UAE. In Figure 31, the monthly solar beam radiation is shown while the solar global radiation is shown in Figure 32.

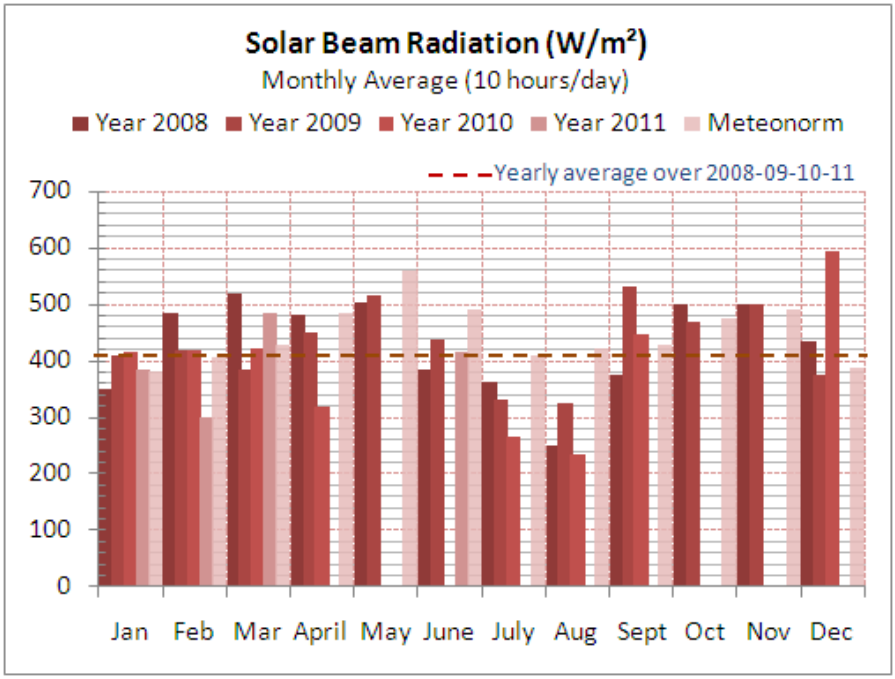

Figure 31: Monthly solar beam radiation from 2008 to 2011 (W/m^2) [77]

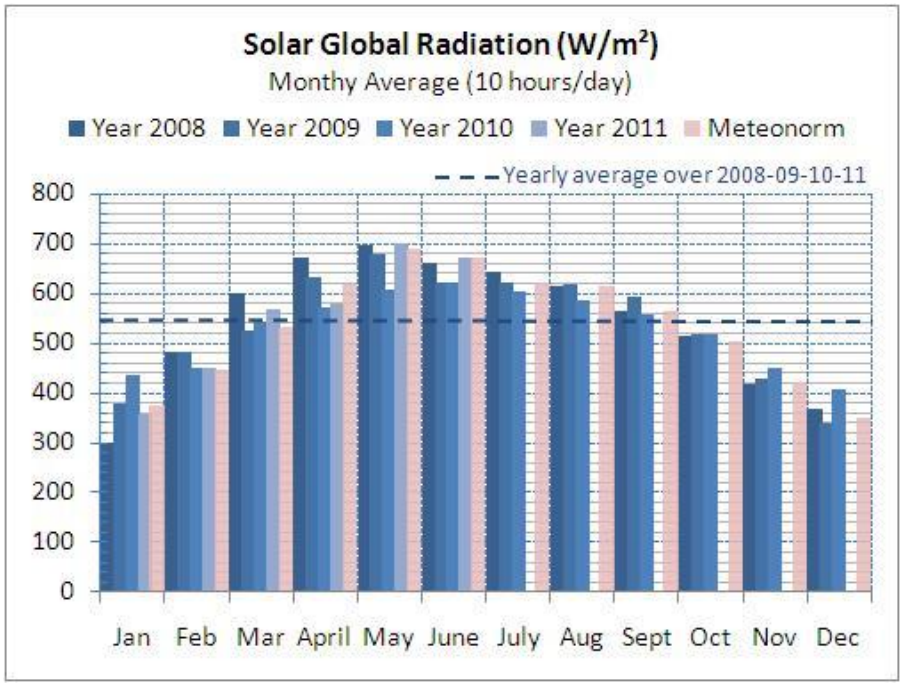

Figure 32: Monthly global horizontal radiation between 2008 to 2011 (W/m^2)[77]

The monthly profile of global horizontal irradiance (GHI) in Abu Dhabi (W/m^2) is shown in Figure 32. High values of direct normal irradiance are recorded during the summer season from May until October and are shown in Figure 33 below.

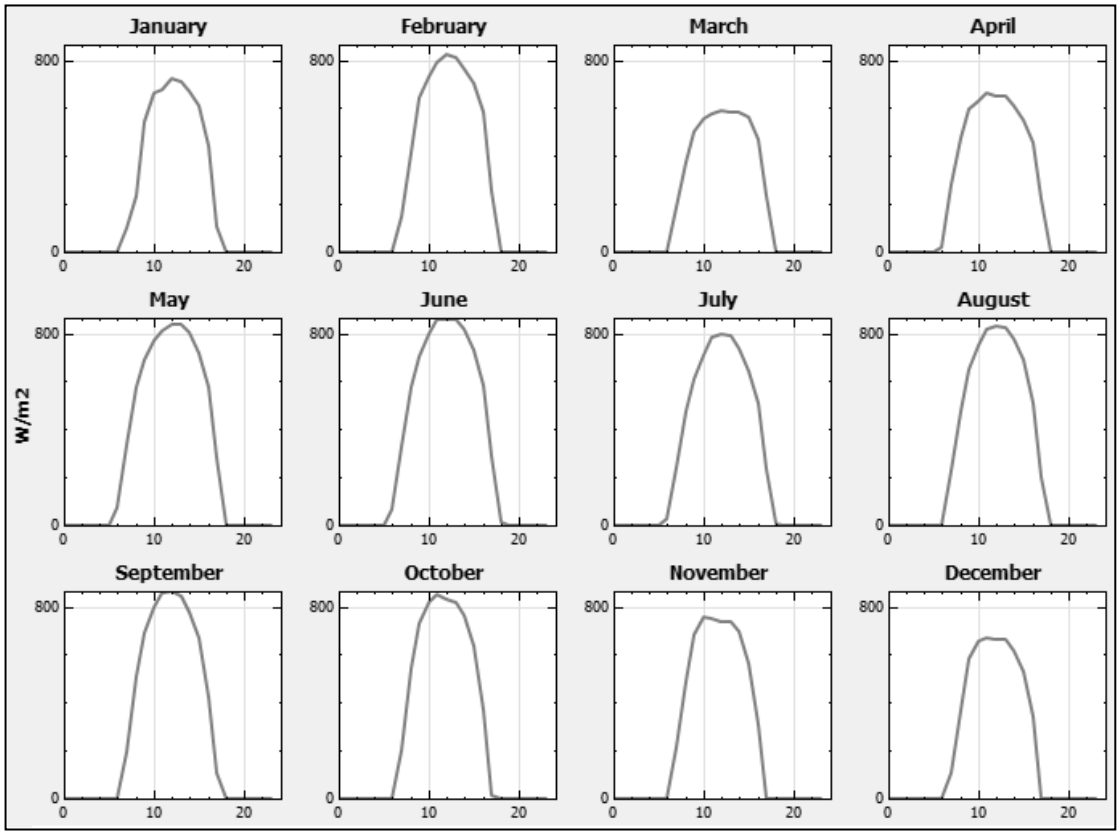

Figure 33: Monthly profile of GHI (W/m^2)

4.2 Collector and receiver options (SCA/HCE)

The solar field in a parabolic trough power plant consists of large arrays of single axis tracking solar collector assemblies (SCA). Each solar collector assembly contains multiple truss assemblies (modules) which are composed of the following:

- Concentrator Structure
- Mirrors or Reflectors
- Heat Collection Element
- Collector balance of system

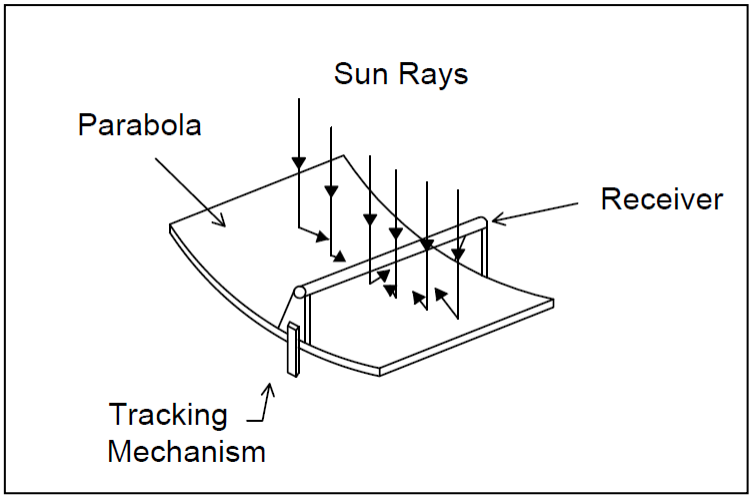

Figure 34: Solar Collector Assembly (SCA)

These are depicted in Figure 34 above.

4.2.1. Concentrator Structure. The concentrator structure is considered the skeleton of the parabolic trough collector. The objective of the concentrator structure is to support the reflective mirrors and receivers while withstanding external forces. It also allows the collector to track the sun. Some of the widely used collectors are:

- Luz system
- Eurotrough
- Solargenix

i. Luz system

Luz system collectors have been proven to be highly reliable for commercial power plant applications. There are two types of Luz system collectors used in power plants which are LS-2 and LS-3 as shown in figure 35.

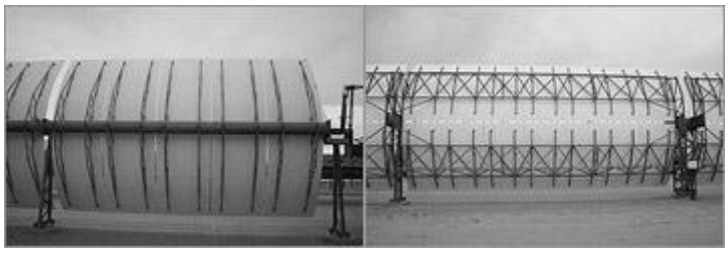

Figure 35: Back structure of LS-2 (Left) and LS-3 (Right) [78]

ii. Euro Trough Collector

The Euro Trough collector was initiated by a European consortium to develop the next generation of parabolic trough collectors building on the advantages of the LS-2 and LS-3 as shown in Figure 36. The work target was to improve the solar thermal electricity generation and develop a wide range of applications such as process heat applications and water desalination. The design task was to develop a light weight collector structure, thus being less expensive than other collector structures.

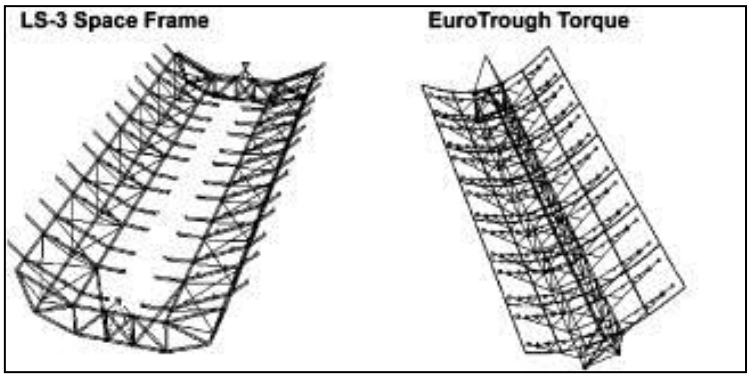

Figure 36: Different structures for LS-3 and Euro Trough Collectors [78]

iii. Solargenix Collector

The Solargenix collector – shown in Figure 37 below - was developed by the American Department of Energy and NREL. The collector is made from extruded aluminum that allows a very light design compared with other steel structures. The new collector is easy to assemble and requires no welding or specialized manufacturing.

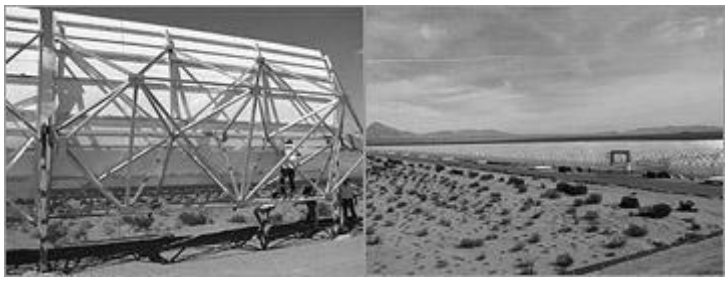

Figure 37: Solargenic SCX-1 collector (Left) and Solargenix SGX-1 (Right) [78]

The LS-3 was designed to reduce manufacturing costs in the LS-2 but the results didn't meet expectations and the design had lower than expected thermal performance. The Solargenix SGX-1 provides good performance despite having an aperture area of 470.3 m^2, approximately half the reflective aperture area of the Euro Trough ET150 collector (817.5 m^2).

Based on the above mentioned characteristics of the three parabolic trough solar collectors, the EuroTrough ET150 was selected because of its proven solar thermal performance, light weight design and high optical efficiency. Table 10 shows some parameters for the EuroTrough ET150.

Table 10: Selected Solar Collector

Parameter	***Unit***	***Value***
Configuration name	-	EuroTrough ET150
Reflective aperture area	m^2	817.5
Aperture width, total structure	m	5.75
Length of collector assembly	m	150
Number of modules per assembly	-	12
Average surface-to-focus path length	m	2.11
Piping distance between assemblies	m	1

4.2.2. Mirrors or (reflectors). The parabolic shaped glass mirrors are the most obvious feature of the solar collector. The parabola shape allows the mirrors to concentrate the solar radiation on the linear receiver. The low iron second surface tempered glass mirrors have a backside reflective silver layer and a thickness of 4 mm. The value of mirror reflectivity would be in the range between 93% and 96%. The area of each panel is approximately 2 m^2. These glass mirrors have proven to have high reliability and low annual breakage rates. However, some mirror breakage does occur and replacement of these glass mirrors has been relatively expensive. Table 10 shows suggested mirror reflectivity values for different types of glass mirrors.

4.2.3. Heat Collection Element (HCE). The linear receiver also called as the heat collection element (HCE), consists of a stainless steel metal tube and a glass envelope covering it. A special heat transfer fluid is circulated and heated through the receiver tube. The mirror reflectivity values for different glass thickness are shown in Table 11.

Table 11: Mirror reflectivity values

Glass thickness (mm)	*Iron content*	*Mirror reflectivity*
4	low	0.93 ± 0.002
1	low	0.96 ± 0.002
4	low	0.948 ± 0.003
4	Very low	0.946 ± 0.001
3	Very low	0.956 ± 0.001

Between the steel tubing and the glass envelop resides either air or a vacuum to reduce heat losses and to allow for thermal expansion at high operating temperatures. A glass-to-metal seal is crucial to achieve the necessary vacuum-tight enclosure. The metal tube is coated with a selective material that has good solar radiation absorptance and low thermal emittance. Figure 38 shows the vacuum between the glass envelop and metal tube in addition to other components of the receiver tube.

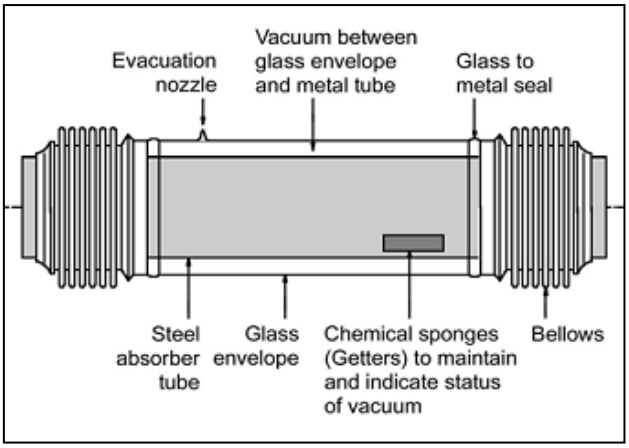

Figure 38: Structure of receiver tube [79]

The heat collection element is a primary reason the parabolic trough collector is able to acquire high efficiency with low heat losses. From the System Advisor Model library of receivers, the Schott PTR70 2008 receiver was selected due to its high reliability, lifetime and thermal performance [80]. This receiver design has the lowest heat losses of 166.25 W/m compared to other receiver tubes configurations. The detailed receiver data is presented in Table 12.

Table 12: Selected Heat Collection Element (HCE)

Parameter	***Unit***	***Value***
Configuration Name	-	Schott PTR70 2008
Absorber tube inner diameter	m	0.066
Absorber tube outer diameter	m	0.07
Glass envelope inner diameter	m	0.115
Glass envelope outer diameter	m	0.12
Absorber material type	-	304L

4.2.4. Collector balance of system. Other key components of the parabolic trough solar collector that balance the system include controls, drives, pylons and foundations. The balance system is important for rotating the collector structure and tracking the sun during the day. The local controller control monitors any alarm conditions such as low or high temperature in the receiver tube. The hydraulic drive used on the Solargenix SGX-1 collector is shown in Figure 39.

Figure 39: Hydraulic drive of SCA [78]

In this study, the configuration of the Kuraymat 150 MW integrated solar combined cycle Power Plant in Egypt can be adopted. The total area of the proposed plant is mostly occupied by the solar field. The solar field consists of 160 collectors with a collector aperture reflective area of 817.5 m^2.

The EuroTrough ET150 collector is selected as the solar collector. Each solar collector assembly consists of 12 modules with a length of 12.5 m for each module. The piping distance between assemblies is 1m and the length of the collector assembly is 150m. A detailed description of the collector and receiver system is discussed next.

4.3 Heat transfer fluid selection

The optimum selection of the heat transfer fluid (HTF) is important to improve the economic and operational characteristics of the parabolic trough collector system. For the proposed system, a HTF different from the thermal storage medium is used to circulate through the heat collection element.

Generally, the key issues that are taken into consideration when selecting the HTF include cost, availability, physical properties (freezing point, operating temperature, heat capacity) and environmental impact. The HTF type and properties are used in several solar field energy calculations such as the delivered thermal energy and heat losses. Each HTF has its own properties (mass, enthalpy, temperature and specific heat). Based on these properties, the solar field inlet temperature T_{SFin}, outlet temperature T_{SFout}, average temperature T_{SFavg} and solar field heat losses $Q_{HeatLoss}$ are computed to find the overall thermal energy delivered by the solar field Q_{SF}.

In this study, six HTF types are compared together to calculate the hourly delivered thermal energy by the solar field Q_{SF}. The minimum operating temperatures of the six HTFs are presented in Table 13.

Table 13: Minimum temperature for different HTFs

HTF Name	***Type of Fluid***	***Minimum Temperature (°C)***
Nitrate (solar salt)	Salt	260
Caloria HT 43	Hydrocarbon	-20
Therminol VP-1	Synthetic Oil	50
Hitec	Salt	142
Dowtherm Q	Synthetic Oil	-35
Dowtherm RP	Synthetic Oil	0

The performance of the six chosen heat transfer fluids is investigated using the System Advisor Model (SAM) software which uses user-input, representative default values, and approximations to predict HTF performance under the system design conditions shown in Table 14. The best suitable HTF to transfer the thermal energy received from the solar collector to the power block will be selected. The proposed location for the system is Abu Dhabi in the United Arab Emirates. This location was selected because it offers sufficient space for the plant, a high level of direct solar irradiation, and easy connection to the existing power and gas grid infrastructure. Its location also contributes to the Emirate's economic development goals by spurring economic activity in the Western Region.

Table 14: Design Parameters

Parameter	*Value*
Location Information	
Location	Abu Dhabi
Latitude	24.43°
Longitude	54.65°
Elevation	27 m
Weather Data Information	
Direct Normal	2294.9 kWh/m^2
Global Horizontal	2204.6 kWh/m^2
Dry-bulb Temp.	27.1°c
Wind Speed	3.6 m/s
Solar Field	
Aperture Area	865,352 m^2
Number of loops	230
Irradiation at design	950 W/m^2
Power Cycle	
Net Power Output	150 MW
Rated Cycle Efficiency	0.3774
Thermal Storage	
Storage Hours	7.5 hr
Storage Volume	28,815.1 m^3

4.4 Performance Model

The performance model for the components of the system is discussed next.

4.4.1 Solar Field Model. In this section, a performance model for evaluating the concentrating solar collector efficiency and the useful output of the solar field under reference conditions (ambient temperature, wind speed and global irradiance) will be introduced. The solar field efficiency and the useful heat output are the parameters that will be used to evaluate the performance. Basic concepts about solar angles used in power calculations to improve the solar collector performance are discussed followed by a thermal analysis (energy and exergy analysis) for the solar collector.

4.4.1.1 Solar Angles

Calculating the optimum solar angles is necessary to get the best out of the PTC system. However, the optimum solar angle varies through the year depending on the season and location of the system; also, a control system to track the sun movement through the day must be used. So, obtaining the optimum angle will benefit the optimum performance of the solar system. The solar angles used in the performance model to maximize the solar collector system performance are defined next.

*i. Hour angle (**ω**)*

The hour angle is the angle that the earth has rotated since solar noon as shown in Figure 40.

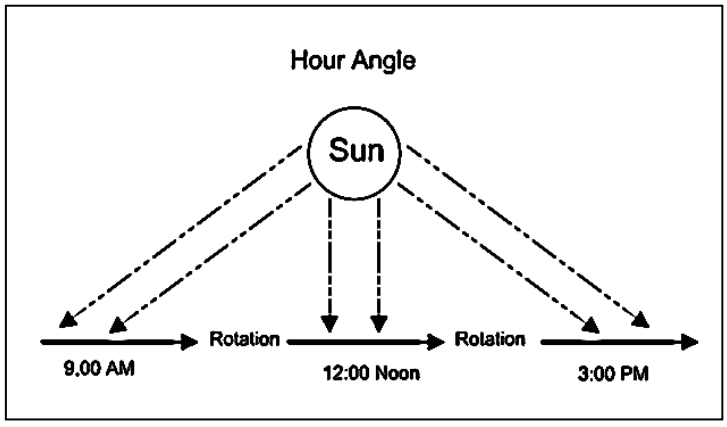

Figure 40: Hour Angle

The hour angle can be calculated by the following equation (4.1) below:

$$\omega = 15\ [\ t_s - 12] \tag{4.1}$$

where t_s is the solar time (hours), which is calculated by:

$$t_s = LCT + \left(\frac{EOT}{60}\right) - LC - DLS \tag{4.2}$$

where:

LCT Local clock time

LC Longitude correction (hours)

EOT Equation of time (minutes)

DLS Correction for daylight saving time (one hour)

The equation of time (EOT) can be given with the following approximation:

$$EOT = 0.285 \cos x - 7.416 \sin x - 3.648 \cos 2x - 9.228 \sin 2x \tag{4.3}$$

where *x* is an angle that is function of the day number N. It can be given by:

$$x = 360\ (N - 1)/365.242 \tag{4.4}$$

The longitude correction is given by:

$$LC = \frac{(Longitude\ of\ standard\ time\ zone\ meridian - Local\ longitude)}{15} \tag{4.5}$$

ii. Latitude angle (Φ)

Latitude angles are measured from the center of the earth and are used to specify the precise location on the surface of earth – see Figure 41 below.

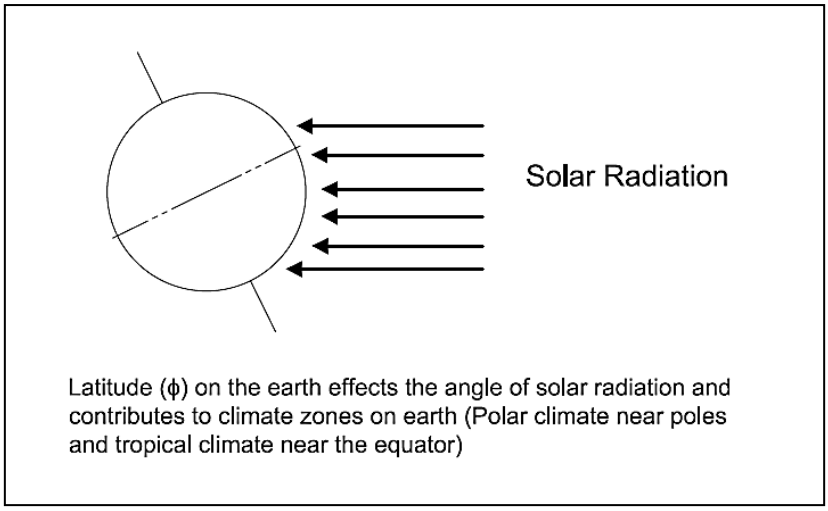

Figure 41: Latitude Angle

iii. Solar Declination angle (δ)

The solar declination angle varies throughout the year and can be defined as the angle between the earth sun line and the equatorial plane. The angle varies from 23.5° during the summer season to -23.5° during the winter season as shown in Figure 42. Stine presented an approximation equation for calculating the solar declination angle as follows:

$$\sin\delta = 0.39795 \cos\left[0.98563\,(N-173)\right] \tag{4.6}$$

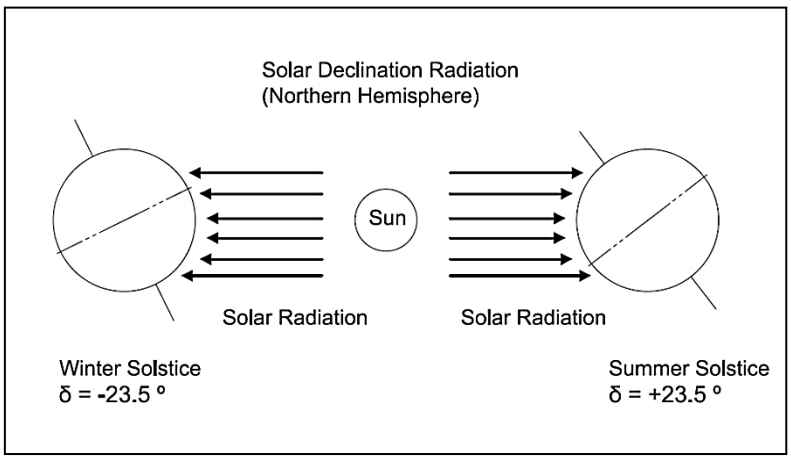

Figure 42: Solar Declination Angle

iv. Solar altitude angle (α)

The solar altitude angle is the angle between the solar rays and the horizontal plane on the surface of earth; it is given by:

$$\alpha = sin^{-1}(\sin\delta \sin\Phi + \cos\delta \cos\Phi \cos\omega) \quad (4.7)$$

v. Solar azimuth angle (β)

The solar azimuth angle is the angle between the horizontal projection of the sun rays and the due-south direction line, it is given by:

$$\beta' = cos^{-1}[\frac{(\sin\delta \cos\Phi - \cos\delta \sin\Phi \cos\omega)}{\cos\alpha}] \quad (4.8)$$

*vi. Angle of incidence (**θ**)*

The calculation of the angle of incidence θ is important for the design and performance of the solar collector system as the amount of received solar irradiance is reduced by the cosine of this angle as follows:

$$\cos\theta = \sin\alpha \cos\lambda + \cos\alpha \sin\lambda \cos(\Omega - \beta) \quad (4.9)$$

where λ is the tilt angle [81],[82] and Ω is the aperture azimuth angle. Figure 43 shows the relationship between the two solar angles. Also, an online tool to calculate the sun altitude angle, sun zenith angle, sun azimuth angle and the angle of incidence based on the previous equations can be used [83].

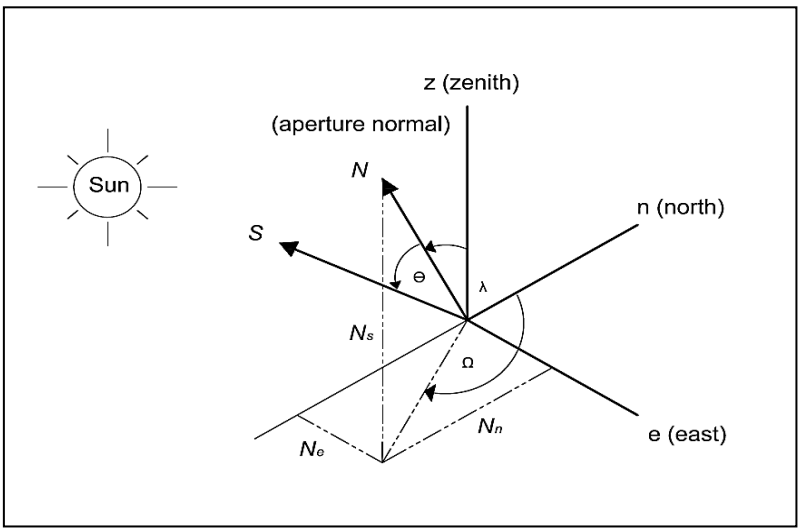

Figure 43: Tilt angle λ and aperture azimuth angle Ω

4.4.2 Energy Analysis. In general, a solar collector's overall efficiency ζ_c can be defined as the ratio between the useful output delivered by the collector $\dot{\boldsymbol{Q}}_{\boldsymbol{u}}$ (W) to the global irradiance $\boldsymbol{G}$ (W) on the collector aperture area $\boldsymbol{A_c}$ (m^2) as:

$$\zeta_C = \frac{\dot{Q}_u}{(A_c G)} \tag{4.10}$$

There are two parts of the global irradiance Gon a horizontal surface which are the diffuse irradiance G_d and the normal beam irradiance G_n

$$G = G_n \cos\theta_z + G_d \tag{4.11}$$

where:

θ_z is the solar zenith angle, which is the angle measured between the solar beam and the normal in a horizontal coordinate system.

From Equation (4.11) above we can notice that the beam Irradiance amount G_b received by the solar collector is less than the normal beam irradiance due to the cosine loss caused by the angle of incidence of the solar irradiation θ. The relationship between the beam irradiance and the normal beam irradiance can be defined as

$$G_b = G_n \cos\theta \tag{4.12}$$

In the case of concentrated solar power, the beam Irradiance is a more relevant measure of the solar resource. Therefore, the diffuse irradiance G_d under the reference conditions is neglected in this model.

So, the useful output that can be obtained by the parabolic trough solar collector can be defined as follows:

$$\dot{Q}_u = \dot{m}\bar{c}(T_o - T_i) \tag{4.13}$$

Or can be expressed as:

$$\dot{Q}_u = A_c G_b \zeta_{op}(\theta) - A_{abs} U_L (T_{abs} - T_a) \tag{4.14}$$

where:

$\dot{m}$ Mass flow rate of the heat transfer fluid (kg/s)

$\bar{c}$ Average specific heat for the heat transfer fluid (J/kg.k)

T_o Outlet temperature for the heat transfer fluid (k)

T_i Inlet temperature for the heat transfer fluid (k)

T_{abs} Absorbed surface temperature (k)

A_{abs} Surface area of the absorber (m^2)

U_L Overall heat loss coefficient ($W/m^2.k$)

$\zeta_{op}(\theta)$ Collector optical efficiency as a function of θ

Due to the difficulty of calculating the absorbed surface temperature T_{abs}, the amount of useful energy received by the collector in the above equation $\dot{Q}_u$ can be expressed as a function of the fluid inlet temperature T_i. The Hottel-Whillier equation of a concentrating solar collector is given as:

$$\dot{Q}_u = A_c F_R \left[G_b \zeta_{op}(\theta) - (A_{abs}/A_c)\, U_L\, (T_i - T_a)\right] \tag{4.15}$$

where $F_R$is the heat removal factor for the collector, defined as:

$$F_R = \frac{\dot{m} c_p A_{abs}}{A_c U_L}\left[1 - e^{-\left(\frac{A_c U_L F'}{\dot{m} c_p}\right)}\right] \tag{4.16}$$

The optical efficiency of the collector $\zeta_{op}(\theta)$ when the angle of incidence θ is normal to the aperture ($\theta = 0°$) can be given as:

$$\zeta_{op,n} = \rho_m (\tau\, \alpha_c)_e \gamma_n \tag{4.17}$$

where:

ρ_m Average specular mirror reflectance

τ The glass envelope transmittance

α_c Surface coating absorptance

$(\tau\, \alpha_c)_e$The effective product of τ and α_c

γ_n Intercept factor

However, the optical efficiency of the collector depends on the angle of incidence θ which means that any variations must be taken into account. The incident angle modifier is used to calculate the optical efficiency when there are variations in angle of incidence θ. Optical losses can occur due to mutual shading between the rows of the collector which can be accounted for by the row shading factor F_{RS}. Other

losses related to the cleanliness of the reflector will be overlooked. The optical efficiency equation can be then modified as follows:

$$\zeta_{op}(\theta) = F_{RS}\, K(\theta)\rho_m(\tau\,\alpha_c)_e\gamma_n \tag{4.18}$$

For a parabolic trough collector, Stine and Harrigan et al. [84] introduced the following model equations using the heat transfer fluid mean temperature T_m:

$$T_m = \frac{(T_o + T_i)}{2} \tag{4.19}$$

Mutual shading between the solar collectors in the solar field may occur. Therefore a heat loss as a result of mutual shading is considered in the performance model. This loss is expressed by the shading factor F_{RS}:

$$F_{RS} = \frac{(W_{e)}{}_t}{W_t} \tag{4.20}$$

where:

W_t Total aperture width of the solar field

$(W_{e)}{}_t$ Total effective width for all solar collectors

Also, due to the mirror reflection and glass envelope values various other losses could affect the performance of the collector. The incidence angle modifier can measure this effect by the following approximation:

$$K(\theta) = 1 - 5.782e^{-3}\theta + 1.485e^{-4}\theta^2 - 2.955e^{-6}\theta^3 \tag{4.21}$$

The efficiency of the parabolic trough collector is:

$$\zeta_C = \frac{\dot{Q}_u}{(A_c\, G_b)} = K(\theta)\zeta_{op,n} - \left[\frac{c_1(T_m - T_a)}{G_b}\right] - \left[\frac{c_2(T_m - T_a)^2}{G_b}\right] \tag{4.22}$$

where the values of coefficients c_1 and c_2 are found using a linear regression estimation technique.

Fischer et al. [85] discussed two alternative test methods for the collector model according to the European Standard EN 12975-2 which are the steady-state test method and the quasi-dynamic test method.

In the steady-state test, the basic equation for near normal incidence angle operation is given as:

$$\zeta_C = \frac{\dot{Q}_u}{(A_c\, G_b)} = \zeta_{op,n} - \left[\frac{c_1(T_m - T_a)}{G_b}\right] - \left[\frac{c_2(T_m - T_a)^2}{G_b}\right] \quad (4.23)$$

In the case of quasi-dynamic collector modeling the incidence angle modifier should be taken into account as well as the diffuse irradiance G_d. The specific power output is given by:

$$\frac{\dot{Q}_u}{A_c} = K(\theta)\, G_b\, \zeta_{op,n} + G_d\, \zeta_{op,d} - c_1(T_m - T_a) - c_2(T_m - T_a)^2 - c_3 \frac{dT_m}{dt} \quad (4.24)$$

Equations (4.12) and (4.13) can be simplified by the following equation [103]

$$\zeta_c = \zeta_{op,n} - U_L\, A_c \frac{T_m - T_a}{G_b A_{abs}} = \zeta_{op,n} - U_L \frac{T_m - T_a}{G_b\, CR} \quad (4.25)$$

where *CR* is the concentration ratio. ($CR = A_{abs}/A_c$).

These equations are more flexible to be used as a reference to estimate the solar field output under system reference conditions. Table 15 describes the test condition requirements and permitted deviation for the two alternative test scenarios.

Table 15: Test conditions and permitted deviation

Parameter	***Steady-state***		***Quasi-dynamic***	
	Value	***Deviation from the mean***	***Value***	***Deviation from the mean***
Global Solar Irradiance, G	> 700 W/m^2	± 50 W/m^2	300 < G < 1100 W/m^2	-
Incidence Angle, θ	< 20°	-	-	-
Diffuse Fraction, G_d/G	< 30%	-	-	-
Surrounding air temperature, T_a	-	± 1 k	-	-
Surrounding air speed, u	3 m/s ± 1 m/s	-	-	-
Collector inlet temperature, T_i	-	± 0.1 k	-	± 1 k

The following general assumptions are made to simplify the performance model:

a) Clear sky conditions are considered for this model. Therefore, the diffuse irradiance G_d will be neglected.

b) Due to the variation of wind speed values u, heat loss may occur in the model and a new term $c_4\,(T_m - T_a)$ will be added to the performance model equations.

c) Piping heat loss will be introduced to the performance model equation by the term $\dot{Q}_P$

d) In order to apply the performance model equations on the parabolic trough system, the collector aperture area A_c is used in the efficiency equation.

The reference conditions for each month in Abu Dhabi during 2012 in Table 16 were obtained from SoDa Service – Knowledge in solar radiation [76] and the National Center of Meteorology & Seismology [86] and were used as input values for the concentrated solar collector in this study.

Table 16: Reference conditions for Abu Dhabi

Month	***Average Wind Speed, u (m/s)***	***Ambient Temperature, T_a (°C)***	***Global Irradiance, G (W/m^2)***	
			Average	***Maximum***
January	3.7	19.8	140	404
February	4.0	21.1	182	469
March	3.9	23.7	204	584
April	3.8	27.5	246	635
May	3.5	31.3	282	695
June	3.7	33.3	290	693
July	3.7	34.6	274	655
August	3.6	35.5	266	631
September	3.4	33.5	246	586
October	3.3	30.8	218	525
November	3.5	26.9	176	446
December	3.6	22.2	146	392

The piping heat loss $\dot{Q}_P$ of the heat transfer fluid is given as:

$$\dot{Q}_P = U_L A_O (T_m - T_a) \tag{4.26}$$

where A_O is the outer surface area of the insulated pipe and is given by:

$$A_O = \pi D_3 L \tag{4.27}$$

The overall heat transfer coefficient U_L($W/m^2.k$) for the insulated pipe is calculated by:

$$U_L = \frac{1}{\frac{D_3}{D_1 h_m} + \frac{\ln(\frac{D_2}{D_1})D_3}{2k_p} + \frac{\ln(\frac{D_3}{D_2})D_3}{2k_f} + \frac{1}{h_a}} \tag{4.28}$$

where:

h_m Heat transfer coefficient inside the pipe (W/m^2.k)

h_a Heat transfer coefficient on the insulated pipe surface (W/m^2.k)

k_p Thermal conductivity of the pipe (W/m.k)

k_f Thermal conductivity of insulation (W/m.k)

D_1 Inside pipe diameter (m)

D_2 Outside pipe diameter (m)

D_3 Insulated pipe outside diameter (m)

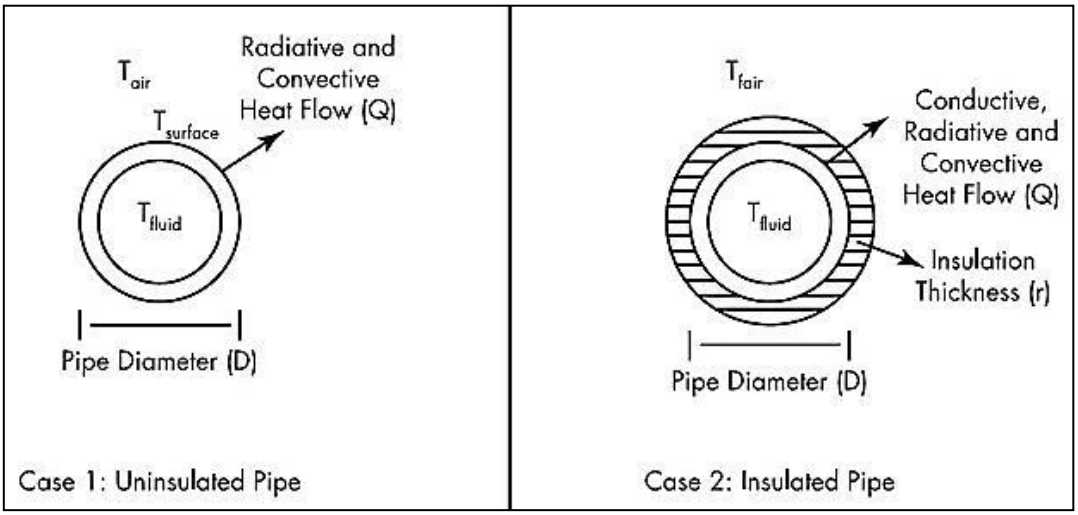

Figure 44: Piping heat loss

The heat transfer coefficient inside the pipe h_m can be obtained from the following set of equations:

$$h_m = \frac{k_{HTF}\, N_u}{D_1} \tag{4.29}$$

$$N_u = \frac{\frac{f}{8}(Re - 1000)\, Pr}{1 + 12.7\left(\frac{f}{8}\right)^{0.5}(Pr^{0.67} - 1)} \tag{4.30}$$

$$Re = \frac{\rho_{HTF}\, V\, D_1}{\mu_{HTF}} \tag{4.31}$$

$$f = (0.79 \ln Re - 1.64)^{-2} \tag{4.32}$$

$$P_r = \frac{\mu_{HTF}\, c_{pHTF}}{k_{HTF}} \tag{4.33}$$

where:

k_{HTF}	The mal conductivity of the heat transfer fluid (W/m.k)
N_u	Nusselt Number
f	Moody friction factor
Re	Reynlods Number
Pr	Prandtl Number
ρ_{HTF}	Density of heat transfer fluid (kg/m^3)
μ_{HTF}	Dynamic viscosity of heat transfer fluid (N.s/m^2)
c_{pHTF}	Specific heat of heat transfer fluid (J/kg.k)

Similarly, the heat transfer coefficient h_a is calculated by

$$h_a = \frac{k_a\, N_u}{D_3} \tag{4.34}$$

$$P_r = \frac{\mu_a\, c_{pa}}{k_a} \tag{4.35}$$

$$G_r = \frac{D_3^3\, \rho_a^2\, \Delta T\, b}{\mu_a^2} \tag{4.36}$$

$$N_u = [0.6 + \frac{0.387\, Ra^{\frac{1}{6}}}{[1 + \left(\frac{0.599}{Pr}\right)^{\frac{9}{16}}]^{\frac{8}{27}}}]^2 \tag{4.37}$$

where:

k_a	Thermal conductivity of the heat transfer fluid (W/m.k)
c_{pa}	Specific heat of air (J/kg.k)
μ_a	Dynamic viscosity of air (N.s/m^2)
b	Expansion coefficient for air (1/k)
G_r	Grashof Number
Ra	Rayleigh Number

Therefore, the final set of equations of the parabolic trough performance model can be summarized below:

$$T_m = \frac{(T_o + T_i)}{2} \tag{4.38}$$

$$\dot{Q}_{SF} = \dot{m}\, \bar{c}\, (T_o - T_i) \tag{4.39}$$

$$\dot{Q}_{SF} = A_a \Big[K(\theta) F_{RS}\, G_b\, \zeta_{op,n} - c_1(T_m - T_a) - c_2(T_m - T_a)^2 - c_3 \frac{dT_m}{dt} - c_4 u\, (T_m - T_a)\Big] - \dot{Q}_P \tag{4.40}$$

$$\zeta_{SF} = \frac{\dot{Q_{SF}}}{(A_a G_b)} = \left[K(\theta) F_{RS}\, \zeta_{op,n} - \frac{c_1(T_m - T_a)}{G_b} - \frac{c_2(T_m - T_a)^2}{G_b} - \frac{c_3 \frac{dT_m}{dt}}{G_b} - \frac{c_4 u\, (T_m - T_a)}{G_b}\right] - \frac{\dot{Q}_P}{A_a G_b} \tag{4.41}$$

where:

ζ_{SF} Efficiency of the solar field

$\dot{Q}_{SF}$ Solar field useful output (W)

A_a Solar field total aperture area (m^2)

c_1 Heat loss coefficient at $(T_m - T_a) = 0$ ($W/m^2.k$)

c_2 Temperature dependence of the heat losses ($W/m^2.k^2$)

c_3 Effective thermal capacitance ($J/m^2.k$)

c_4 Wind speed dependence of heat loss ($J/m^3.k$)

4.4.3 Exergy Analysis. Using exergy analysis in evaluating the thermodynamic performance of the system is a good tool for optimizing the design of power production cycles and to reduce exergy losses for the system. Exergy can be defined as the maximum theoretical useful work received from energy in a system. Exergy cannot be stored in a single process but may be destroyed due to irreversibility. This can be achieved by decreasing exergy destruction or by maximizing exergetic efficiency.

The exergy balance for the solar collector is given by:

$$\sum \dot{E}_{in} - \sum \dot{E}_{out} - \sum \dot{E}_{loss} - \sum \dot{E}_{change} - \sum \dot{E}_{des} = 0 \tag{4.42}$$

In parabolic trough collectors, exergy can be exchanged either by the fluid flow or by heat transfer through the absorbed solar radiation. Therefore, the inlet exergy rate is expressed by:

$$\dot{E}_{in,f} = \dot{m} c_p \left(T_{in} - T_a - T_a ln \frac{T_{in}}{T_a} \right) + \frac{\dot{m}\, \Delta P}{\rho} \tag{4.43}$$

where:

T_{in} Inlet fluid temperature (k)

T_a Ambient air temperature (k)

ΔP Pressure difference between the fluid and ambient temperature

In order to find the exact exergy solar radiation for the parabolic solar collector, the Petela's approach is used next. The approach considers the formula:

$$\dot{E}_{in,r} = G_b A_c \, \zeta_P \tag{4.44}$$

where ζ_P is the Petela's efficiency which can be obtained from the relation:

$$\zeta_P = 1 - \frac{4T_a}{3T_s} + \frac{1}{3}\left(\frac{T_a}{T_s}\right)^4 \tag{4.45}$$

where T_s is the black body temperature of the sun ($T_s \approx 6000\ k$).

The outlet exergy rate includes only the exergy exchanged through the fluid flow which is given by:

$$\dot{E}_{f,out} = \dot{m}c_p(T_{out} - T_a - T_a ln\frac{T_{out}}{T_a}) + \frac{\dot{m}\,\Delta P}{\rho} \tag{4.46}$$

The total gain exergy which is the difference between the inlet and outlet exergies of the flow fluid through the receiver is given by:

$$\sum \dot{E}_{gain} = \sum \dot{E}_{out,f} - \sum \dot{E}_{in,f} \tag{4.47}$$

Finally, the exergy efficiency is:

$$\zeta_E = \frac{\dot{E}_{gain}}{\dot{E}_{in,r}} = 1 - \frac{\left(\sum \dot{E}_{loss} - \sum \dot{E}_{change} - \sum \dot{E}_{des}\right)}{\dot{E}_{in,r}} \tag{4.48}$$

For each component of the combined cycle power plant, the exergy balance can be obtained by:

$$\dot{E}x_Q + \sum \dot{m}_i ex_i = \sum \dot{m}_e ex_e + \dot{E}x_W + \dot{E}x_D \tag{4.49}$$

where $\dot{E}x_D$ the exergy destruction rate and *ex* is the total specific exergy. Here:

$$\dot{E}x_Q = \left(1 - \frac{T_0}{T_i}\right)\dot{Q}_i \tag{4.50}$$

$$\dot{E}x_W = \dot{w} \tag{4.51}$$

The physical exergy is obtained from:

$$ex_{ph} = (h - h_0) - T_0(s - s_0) \tag{4.52}$$

The chemical exergy is given by:

$$ex_{mix}^{ch} = \left[\sum_{i=1}^{n} X_i ex^{ch_i} + RT_0 \sum_{i=1}^{n} X_i lnX_i\right] \tag{4.53}$$

The total specific exergy is:

$$\dot{e}x = \dot{e}x_{ph} + \dot{e}x_{ch} \tag{4.54}$$

4.4.4 Thermo-Economic Analysis. Thermo-economic analysis deals with investigation of the exergy and economics of a system to minimize the cost of exergy. The governing equation for the thermodynamic model is given by:

$$\sum_{e}^{N}\left(c_e\dot{E}_e\right)_k + c_{w,k}\dot{W}_k = c_{q,k}\dot{E}_{q,k} + \sum_{i}^{N}\left(c_i\dot{E}_i\right)_k + \dot{Z}_k \tag{4.55}$$

In this equation, the sum cost rates in exergies of output flows denoted by the k^{th} component are equal to total cost rates of exergies in input flows plus the cost rate of the capital investment and operating and maintenance (O&M) expenses $\dot{Z}_k$. This exergetic balance may be written also as:

$$\sum_{e}\dot{C}_{e,k} + \dot{C}_{w,k} = \dot{C}_{q,k} + \sum_{i}\dot{C}_{i,k} + \dot{Z}_k \tag{4.56}$$

$$\dot{Z}_k = \frac{f\, I_k\, \varphi}{H} \tag{4.56}$$

where:

$\dot{C}$ Cost rate, \$ h^{-1}

c Cost per exergy unit, \$ kWh^{-1}

$\dot{E}$ Exergy rate, MW

f Annuity factor.

I_k Investment cost, \$

φ Maintenance factor

H Operation period, h

Each exergy flow is represented with a thermodynamic value where the cost of the exergy flows is related to the exergy transfer rate. This concept is known as exergy costing where *I* denotes input flows while *e* denotes output flows. Also, *w* denotes work and *q* heat transfer. The economic model for the integrated solar combined cycle power plant used to calculate exergy was obtained from Bejan et. al. [86]. The model is represented by the following cost balance set of equations.

a. Air Compressor

$$I_{AC} = \left(\frac{c_{11}\dot{m}_{air}}{c_{12} - \zeta_{AC}}\right)\left(\frac{P_e}{P_i}\right) ln\left(\frac{P_e}{P_i}\right) \quad (4.57)$$

$$c_{11} = 75\ \$\ kg^{-1}s\ , \qquad c_{12} = 0.9$$

b. Combustion Chamber

$$I_{CC} = c_{21}.\dot{m}_{air}.\left(1 + exp(c_{22}T_e + c_{23})\right).\frac{1}{0.995 - \frac{P_e}{P_i}} \quad (4.58)$$

$$c_{21} = 84.64\ \$\ kg^{-1}s\ , \qquad c_{22} = 0.018\ K^{-1}\ , \qquad c_{23} = 26.4$$

c. Gas Turbine

$$I_{GT} = \left(\frac{c_{31}\dot{m}_g}{c_{32} - \zeta_{GT}}\right) ln\left(\frac{P_i}{P_e}\right)\left(1 + exp(c_{33}T_i - c_{34})\right) \quad (4.59)$$

$$c_{31} = 1536\ \$\ kg^{-1}s\ , \qquad c_{22} = 0.92\ , \qquad c_{23} = 0.036\ K^{-1}\ , \qquad c_{34} = 54.4$$

d. Heat Recovery Steam Generator (HRSG)

$$I_{HRSG} = c_{41}\left(\frac{\dot{m}h_s}{log(T_i - T_e)}\right)^{0.8} + c_{42}\dot{m}_s + c_{43}\dot{m}_g \quad (4.60)$$

$$c_{41} = 4745\ \$\ (kW^{-1}K)^{0.8}\ , \qquad c_{42} = 0.11820\ \$\ kg^{-1}s$$

$$c_{43} = 658\$\ kg^{-1}s$$

e. Condenser

$$I_{COND} = c_5\dot{m}_s, \quad c_5 = 1773\$\ kg^{-1}s \quad (4.61)$$

f. Steam Turbine

$$\mathrm{I_{ST}} = \mathrm{c_6}\dot{\mathrm{W}}_{\mathrm{ST}}^{0.71}\ , \quad c_6 = 6000\$(kW^{0.7})^{-1} \quad (4.62)$$

g. Pump

$$\mathrm{I_P} = \mathrm{c_7}\dot{\mathrm{W}}_{\mathrm{P}}^{0.71}\ , \quad c_7 = 3450\$(kW^{0.7})^{-1} \quad (4.63)$$

$$f = \left[\frac{q^{(k+cp)} - 1}{(q-1)q^{(k+cp)}} - \frac{q^{cp} - 1}{(q-1)q^{cp}}\right]^{-1} \tag{4.64}$$

$$q = \left(1 + \frac{in}{100}\right)\left(1 + \frac{ri}{100}\right) \tag{4.65}$$

where*k* is the system economic life (years) while *cp* is the construction period (years). The interest rate is denoted by *in* and the rate of inflation is *ri.*

The following system of equations is developed for each component of the ISCC system including the cost of each stream. The schematic diagram for the system is shown in Figure 45.

a. Air Compressor

$$\dot{C}_2 = \dot{C}_1 + \dot{C}_{27} + \dot{Z}_{AC} \tag{4.66}$$

b. Combustion Chamber

$$\dot{C}_3 = \dot{C}_2 + \dot{C}_{23} + \dot{Z}_{CC} \tag{4.67}$$

c. Gas Turbine

$$\dot{C}_4 + \dot{C}_{28} = \dot{C}_3 + \dot{Z} \tag{4.68}$$

d. HRSG super heater

$$\dot{C}_{15} + \dot{C}_5 = \dot{C}_4 + \dot{C}_{14} + \dot{Z}_{SH} \tag{4.69}$$

e. HRSG evaporator

$$\dot{C}_{13} + \dot{C}_6 = \dot{C}_5 + \dot{C}_{12} + \dot{Z}_{EVA} \tag{4.70}$$

f. HRSG economizer

$$\dot{C}_{11} + \dot{C}_7 = \dot{C}_6 + \dot{C}_{10} + \dot{Z}_{ECO} \tag{4.71}$$

g. Steam Turbine

$$\dot{C}_8 + \dot{C}_{29} = \dot{C}_{15} + \dot{Z}_{ST} \tag{4.72}$$

h. Condenser

$$\dot{C}_9 + \dot{C}_{22} = \dot{C}_8 + \dot{C}_{21} + \dot{Z}_{COND} \quad (4.73)$$

i. Condensate Extraction pump

$$\dot{C}_{10} = \dot{C}_9 + \dot{C}_{26} + \dot{Z}_{CEP} \quad (4.74)$$

j. Solar Steam Generator (SSG)

$$\dot{C}_{17} + \dot{C}_{18} = \dot{C}_{16} + \dot{C}_{20} + \dot{Z}_{SSG} \quad (4.75)$$

k. HTF pump

$$\dot{C}_{19} = \dot{C}_{18} + \dot{C}_{25} + \dot{Z}_{HTF} \quad (4.76)$$

l. Solar Collector

$$\dot{C}_{20} = \dot{C}_{19} + \dot{C}_{24} + \dot{Z}_{COLL} \quad (4.77)$$

m. Separation point

$$\dot{C}_{12} + \dot{C}_{16} = \dot{C}_{11} \quad (4.78)$$

n. Mixing Point

$$\dot{C}_{14} = \dot{C}_{13} + \dot{C}_{17} \quad (4.79)$$

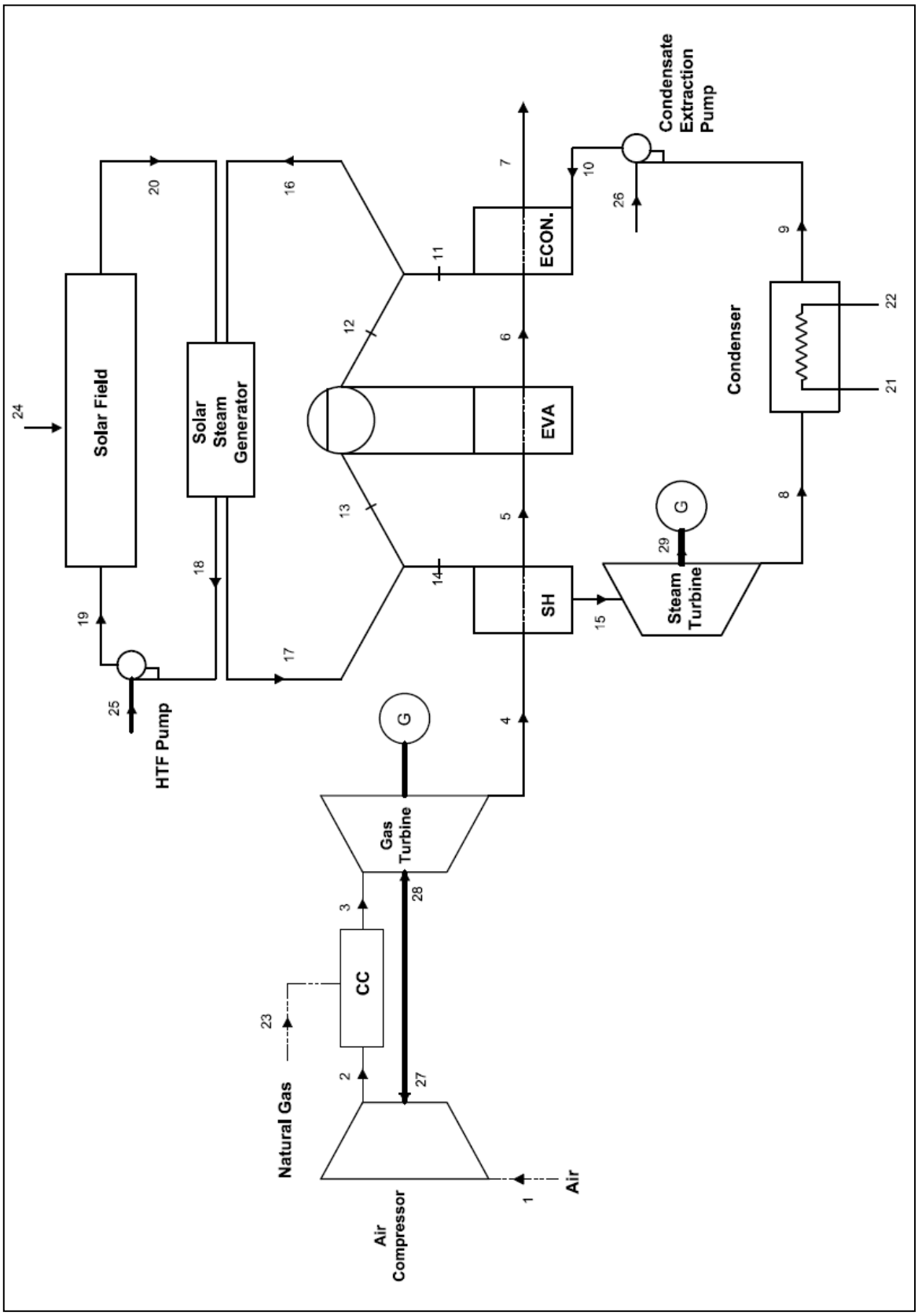

Figure 45: Schematic diagram of the ISCC

4.4.5 Economic and Environmental Analysis. An economic analysis has been carried out for the two proposed power plants. The levelized cost of energy (LCOE) and the amount of avoided CO_2 emissions per year are the selected factors to indicate the economic effectiveness of the proposed designs. The assessment for the different configurations will help the investor determine the best suitable economic choice that is worthy of the investment. However, the lower LCOE does not necessarily indicate a higher efficiency of the power plant. The analysis is carried out using the I.P.P algorithm (Independent Power Producer technology selection algorithm) proposed by Poullikkas [59]. The algorithm takes into account many parameters such as the plant capacity, efficiency; capital cost, fuel cost, operation and maintenance cost (O&M) and fuel type. The next part will describe the method of calculating the LCOE. In Table 17, the economic assumptions for calculating the LCOE for the proposed design are presented.

Table 17: Economic parameters for the system

Parameter	***Symbol***	***Unit***	***Value***
Combined Cycle			
System economic life	n	Year	25
Plant Capacity	E_{CC}	MW	120
Specific capital cost	Ccj	$/kWh	500-1500
Fixed O&M cost	O_{MFj}	$/kWh	2.5
Variable O&M cost	O_{MVj}	$/kWh	1.5
Integrated Solar Combined Cycle (ISCC)			
Plant Capacity	E_{ISCC}	MW	150
Specific capital cost	Ccj	$/kWh	5000-12000
Fixed O&M cost	O_{MFj}	$/kWh	5.5
Variable O&M cost	O_{MVj}	$/kWh	3
Discount rate	i	%	6
Loan interest	m	%	4
Annual Inflation	r	%	2
Fuel net calorific value	CV	GJ/t	50
Fuel Carbon content	FCC	%	76.24

The following set of equations is used to find the value of the Levelized Cost of Energy:

The Annual Energy Production *Pj* given by:

$$P_j = 8760\ xP_c xLF \tag{4.80}$$

The Annual Capital Expenditure (*Ccj*):

$$C_{cj} = qx(1+m)^j x(1+r)^{j-1} xEx\ 1000\ xC_{sc} \tag{4.81}$$

The Fuel Cost (*Cfj*) is calculated by:

$$C_{fj} = 3{,}153{,}6000\ x\left(\frac{F_j xP_C xLF}{\zeta xCV}\right) \tag{4.82}$$

The Fixed O&M cost (*Comf*):

$$C_{OMf} = 12\ x\ OM_F\ x\ P_c\ x\ (1+r)^{j-1}\ x\ 1000 \tag{4.83}$$

The Variable O&M cost (*Comf*) is calculated by:

$$C_{OMv} = 8760\ x\ (1+r)^{j-1}\ x\ P_c\ x\ LF\ x\ OM_v \tag{4.84}$$

The Annual CO_2 Cost can be found from the following equation:

$$Annual\ CO_2\ Cost = CO_2\ Generated\ per\ year\ x\ Cost\ per\ ton \tag{4.85}$$

where:

Amount of CO2 Generated per year

$$= CO_2\ Environmental\ Indicator\ x\ P_j \tag{4.86}$$

The CO2 Environmental Indicator

$$= \frac{440}{12\ x\ Fuel\ Consumption\ Indicator\ x\ Fuel\ Carbon\ Content\ x\ X_0} \tag{4.87}$$

$$Fuel\ Consumption\ Indicator = \frac{3600}{\zeta\ x\ CV\ x\ 1000} \tag{4.88}$$

The total expenses of the power plant is:

$$Expenses = Fuel\ Cost + Fixed\ O\&M\ Cost + Variable\ O\&M\ Cost + CO_2\ Cost \tag{4.89}$$

Finally, by substitution of all the values in equation (4.90), the Levalized Cost of Energy is given by:

$$LCOE = \frac{\frac{\left(\begin{matrix}Annual\ Capital\ Expenditure+\\ Fuel\ Cost+Fixed\ OM+Variable\ OM+\\ CO_2\ Cost\end{matrix}\right)}{(1+i)^j}}{\frac{Annual\ Energy\ Production}{(1+i)^j}} \tag{4.90}$$

Chapter 5: Results and Discussion

In this study, the objective was to perform a technical, economic and environmental analysis for investigating the performance of various power generation technologies. First, a comparative analysis for six different HTFs was performed using the system advisor model (SAM) software to determine the best suitable HTF to be used in the parabolic trough collector. Afterwards, a thermodynamic analysis for the parabolic trough collector based on energy and exergy analysis was carried out. The effect of integrating solar energy to the combined cycle power plant was investigated and a comparison was made between a gas turbine, combined cycle and the integrated solar combined cycle is done. Also, an economic and environmental analysis was performed using the I.P.P algorithm to calculate the levelized cost of electricity, generated CO_2 emissions and fuel savings for the proposed configurations. Finally, a parametric analysis is carried out by varying the capital cost for the two designs to help identify the most cost effective option to be implemented in the UAE.

5.1 Heat Transfer Fluid Selection

The performance of the system was investigated for different types of heat transfer fluids. The chosen HTFs in this study were Nitrate Solar Salt, Caloria HT 43, Therminol VP-1, Hitec, Dowtherm Q and Dowtherm RP. Some properties of these HTFs including mass, enthalpy, temperature and specific heat are discussed in the appendix. The annual output data for the six HTFs is obtained using the system advisor model (SAM).

The main indicators used in this study to select the optimum HTF were:

- Net Electric Output (kWh)
- Annual Energy (kWh)
- LCOE (c/kWh)
- Thermal Energy absorbed by the HTF (kWh)

The comparative analysis for the different HTFs was carried out and the final results are presented in Table 18.

Table 18: Comparison between different HTFs, annual output data

HTF Name	*Net Electric Output (MWh) annual*	*Annual Energy to grid (MWh)*	*LCOE Real (cents/kWh)*	*HTF System (cents/kWhreal)*	*Thermal Energy From Solar Field (MWh) annual*
Nitrat Solar Salt	324,813.00	311,821.00	8.01	0.63	1,009,920.00
Caloria HT 43	363,631.00	349,086.00	7.18	0.57	1,098,110.00
Therminol VP-1	363,193.00	348,666.00	7.19	0.57	1,097,240.00
Hitec	342,612.00	328,907.00	7.61	0.60	1,027,300.00
Dowtherm Q	364,415.00	349,838.00	7.16	0.56	1,097,620.00
Dowtherm RP	364,520.00	349,939.00	7.16	0.56	1,096,940.00

The output data obtained from the simulation software is presented graphically from Figure 46 to Figure 50 below to simplify the comparison between the six HTFs according to the main indicators mentioned earlier. The results will be discussed afterwards to determine the HTF with the best operational and economical characteristics.

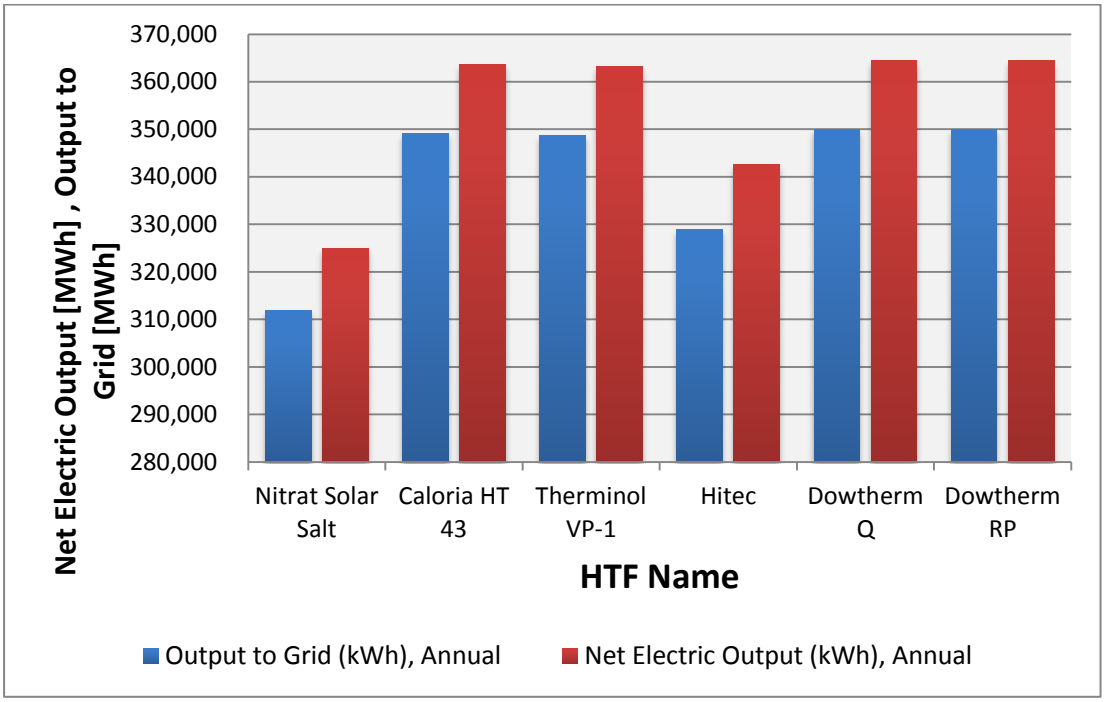

Figure 46: Annual Energy & Net Electricity for different HTFs

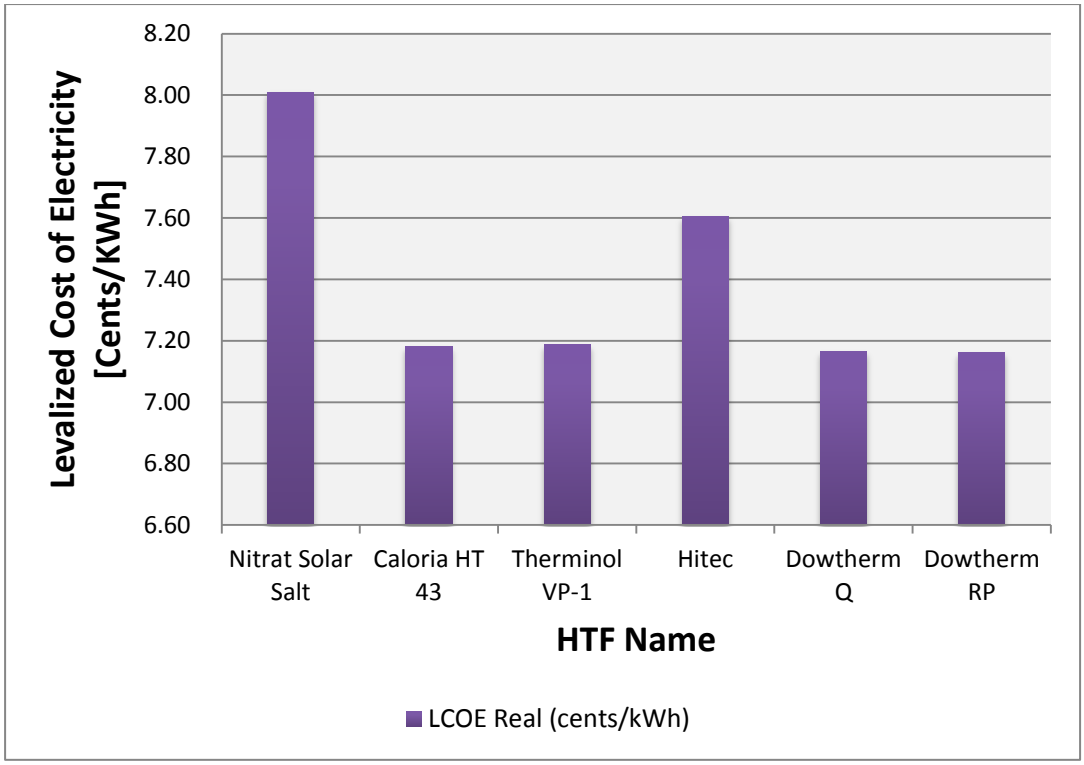

Figure 47: Levelized Cost of Electricity using different HTFs

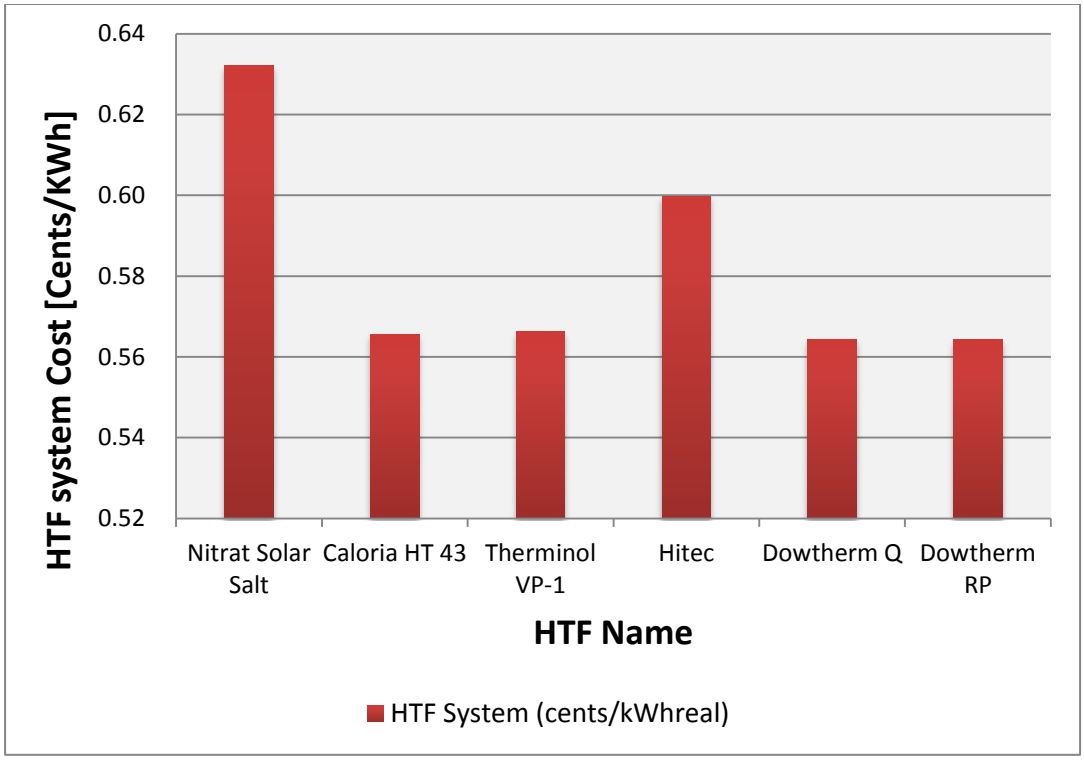

Figure 48: HTF System (Cents/kWh.real)

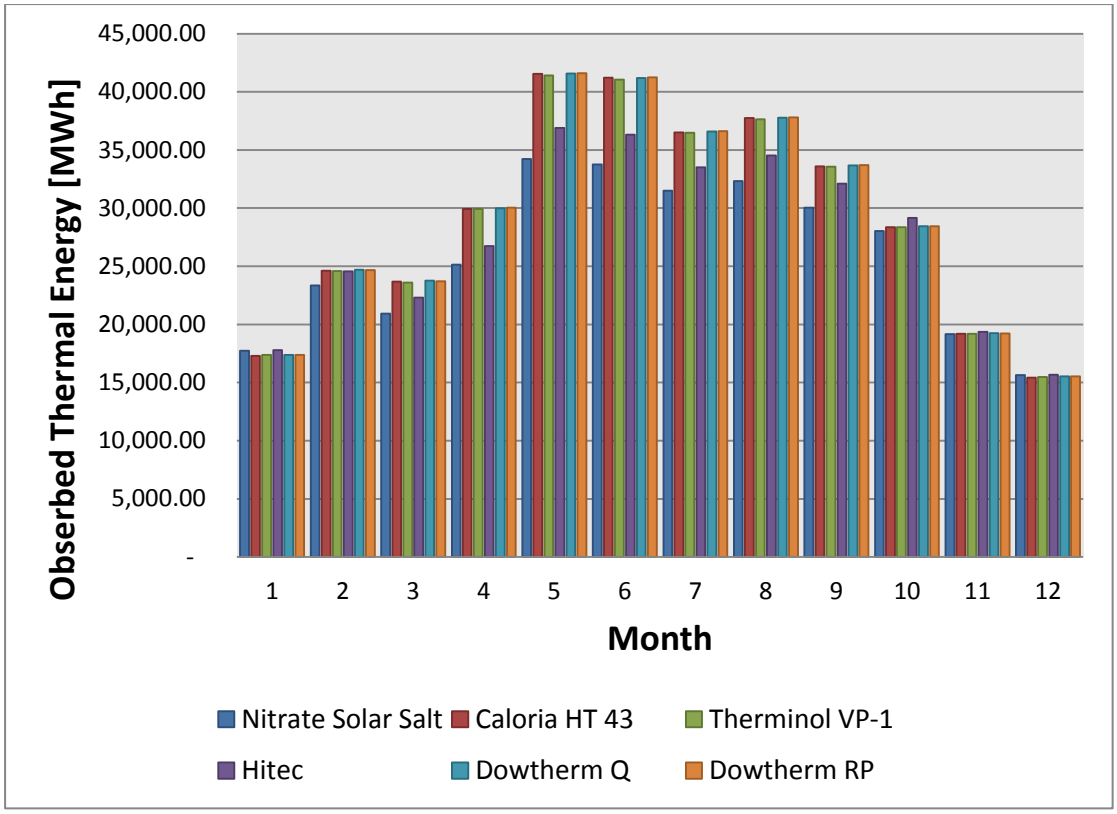

Figure 49: Monthly Thermal Energy absorbed by different HTFs (kWh)

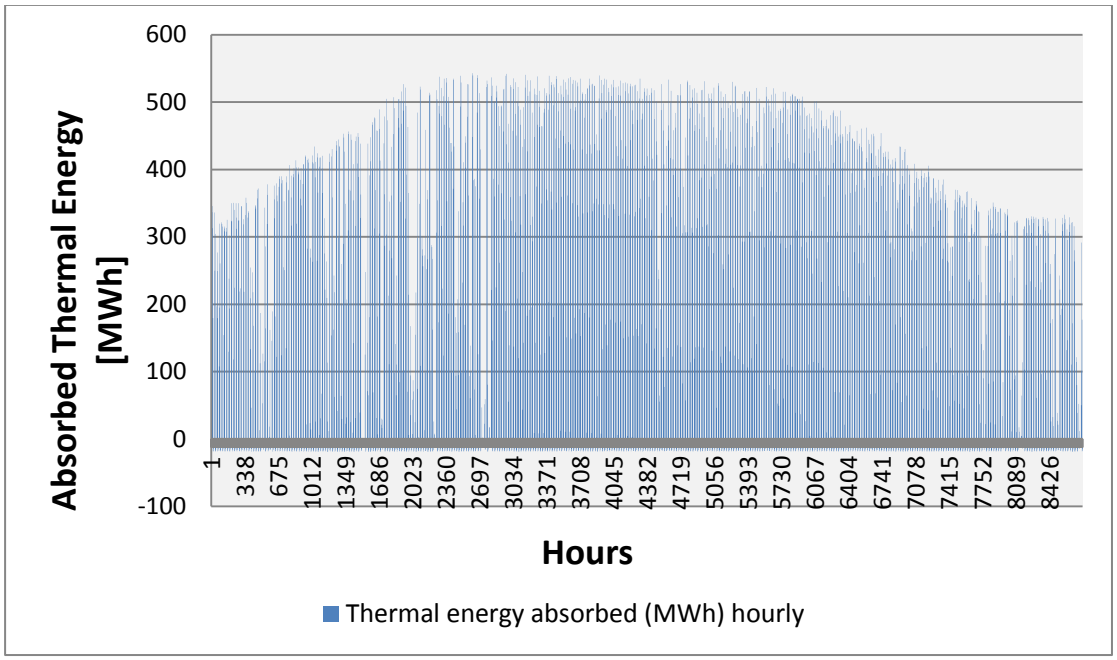

Figure 50: Hourly absorbed thermal energy throughtout the year (MWh)

Figure 50 shows the net electric output and the annual energy (kWh) for the six HTFs. The Caloria HT 43, Therminol VP-1, Dowtherm Q and Dowtherm RP are the

HTFs with highest values of annual energy produced to the grid. In Table18, the same four HTFs have the lowest cost of energy (c/kWh) values which are 7.18, 7.19, 7.16 and 7.16 respectively. The cost of each HTF per kWh is shown in Figure 46 where the Nitrate and Hitec salt values are 0.63 and 0.6 c/kWh more than the other four HTFs. The last indicator for evaluating the HTFs performance is the amount of thermal energy absorbed by the HTF. The monthly data for the delivered thermal energy was obtained and compared for all HTFs. It can be seen from Figure 47 that the amount of thermal energy delivered is increasing during the summer season between May and September. This is due to the increased solar radiation potential during these months. The amount of thermal energy absorbed by the Dowtherm Q and Dowtherm RP HTFs was slightly higher than that absorbed by the Caloria HT 43 and Therminol VP-1. However, the required outlet temperatures of the Caloria HT 43, Dowtherm Q and Dowtherm RP were outside of the fluid's operating temperature range during the simulation. The required outlet fluid temperature of 390.5°c is outside the Caloria HT 43'soperating range of -12°c - 315°c. This temperature also lies outside the Dowtherm Q operating range of -35°c - 330°c and the Dowtherm RP operating range of 0°c - 350°c. Based on the previous comparison, the Therminol VP-1 which is a synthetic heat transfer fluid designed to meet the demanding requirements of vapor and liquid phase systems is selected as the suitable HTF for the parabolic trough system and Hitec Solar Salt is selected as the storage media. Some characteristics of the selected HTF are mentioned in Table 19.

Table 19: Therminol VP-1 characteristics

Parameter	***Unit***	***Value***
Appearance	-	Clear, water white liquid
Composition	-	Biphenyl/diphenyl oxide (DPO) eutectic mixture
Density at 25°c	kg/m^3	1060
Field HTF min operating temp.	°C	12
Field HTF max operating temp.	°C	400
Min field flow velocity	m/s	0.356106
Max field flow velocity	m/s	4.9655

Therminol VP-1 has low viscosity and excellent heat transfer properties as it has the highest thermal stability among all other organic heat transfer fluids. The

thermal energy received by the solar collectors system is transferred to the power block through the heat transfer fluid. The heat transfer fluid passes through the receiver tube with material type 304L with internal surface roughness of 4.5e-005 m. The loss diagram for the system is shown in Figure 51. The operating losses percentage of the energy to the power block is 1.20 % reducing the amount of solar field energy from 1,097,244 MWht to 1,084,085 MWht. The energy from the power block is then decreased by an operating loss of 63.97 % due to the thermal-to-electric conversion. Also, a loss of 7.01 % accrued as a result of conversion from the gross to net electricity output. Finally, the system output to the grid calculated as 348,666 MWth is shown in the loss diagram using a performance adjustment of 4 %.

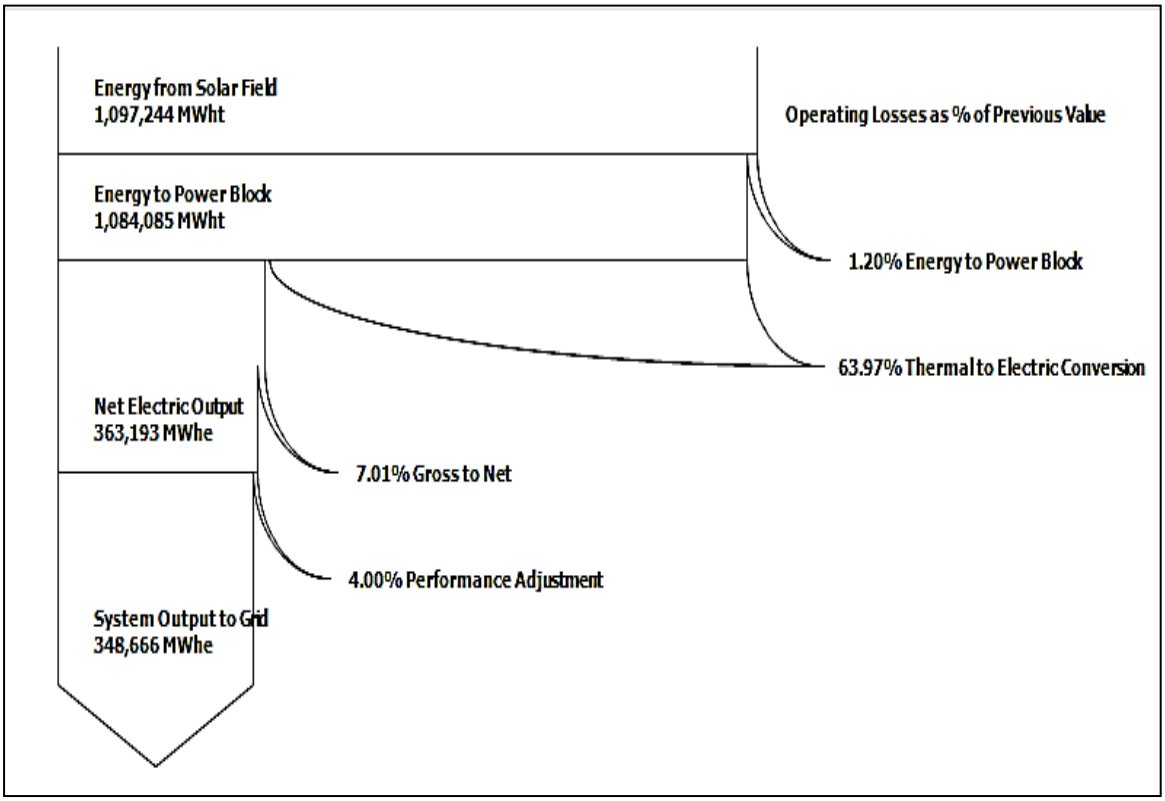

Figure 51: Loss Diagram

In the next section, the results of the thermodynamic analyses are shown and used for the performance evaluation of the presented candidate technologies to determine the most suitable option for the UAE.

5.2 Thermodynamic Analysis

The evaluation of the performance of the parabolic trough collector is based on the energy and exergy equations presented earlier in the performance model for the solar field. The energy and exergy efficiency values were found depending on certain parameters such as the global irradiance, inlet HTF temperature, outlet HTF temperature and the ambient temperature. The average and maximum monthly values for global irradiance in Abu Dhabi are shown in Table 20. This input data was used to calculate the energetic and exergetic efficiency for the solar collector. The solar data values were obtained from the National Center of Meteorology & Seismology.

Table 20: Average and Maximum Global Radiation

Month	***Average Irradiation (W/m^2)***	***Maximum Irradiation (W/m^2)***
Jan	144	404
Feb	182	496
March	204	584
April	246	635
May	282	696
June	290	692
July	274	655
Aug	266	631
Sep	246	586
Oct	218	525
Nov	176	446
Dec	146	392

The energy and exergy analysis was conducted on the solar collector to obtain the efficiency values based on the average and maximum solar radiation values. The average and maximum energy and exergy efficiency monthly variations throughout the year were then plotted on the following graphs. Figure 52 shows the bar chart of the average and maximum global irradiance values in Abu Dhabi. The highest values were recorded in May and June with average and maximum global irradiance values of 290 W/m^2 and 696 W/m^2 respectively.

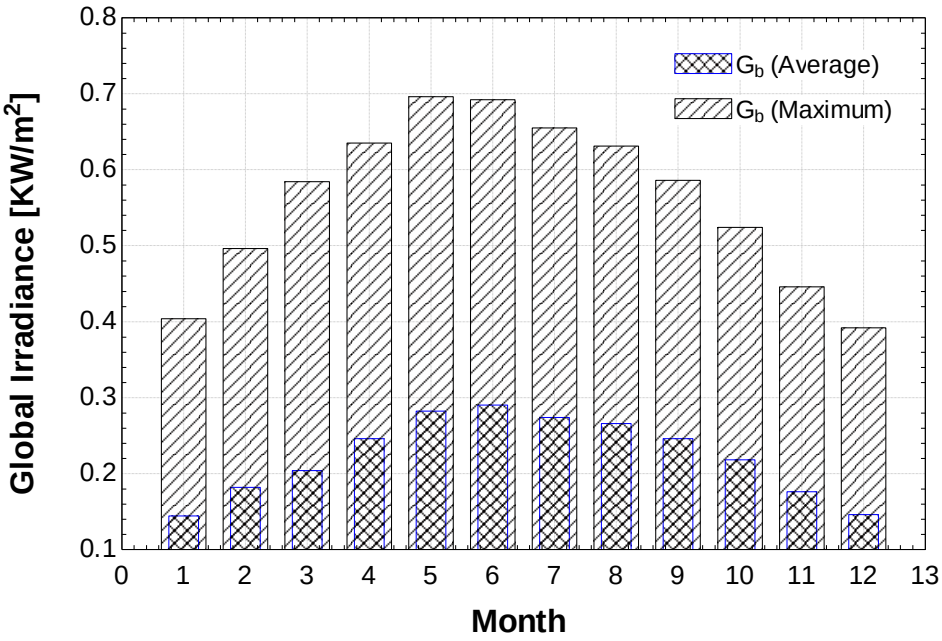

Figure 52: Average and maximum solar radiation for Abu Dhabi

In Figure 53, the energy and exergy efficiency values were found based on the average global irradiance ranging between 144 W/m^2 and 290 W/m^2. The results show a decrease in the energetic and exergetic efficiencies from January until June as a result of the increasing global irradiance and ambient temperature. The highest values for energy and exergy efficiency were 68.64% and 64.93% respectively. The average energy efficiency for the solar collector ranged between 34.08% and 68.64% while the average exergy efficiency ranged between 32.24% and 64.93% in the same period.

Figure 54 shows the drop in the energy and exergy efficiency values. The efficiency values were found based on the maximum global solar irradiance values ranging between 404 W/m^2 and 696 W/m^2. The highest values for energy and exergy efficiency were calculated as 24.46% and 23.14% respectively. The maximum energy efficiency values varied between 14.2% and 24.46% while the maximum exergy efficiency values were in the range between 13.43% and 23.14%. The monthly average and maximum energy and exergy efficiencies for the whole year from January to December were compared together and are shown in Figures 54 and 55. It is expected for the exergy efficiencies to be lower for the energy efficiencies due to the irreversibilities in the process that destroy some of the input exergy.

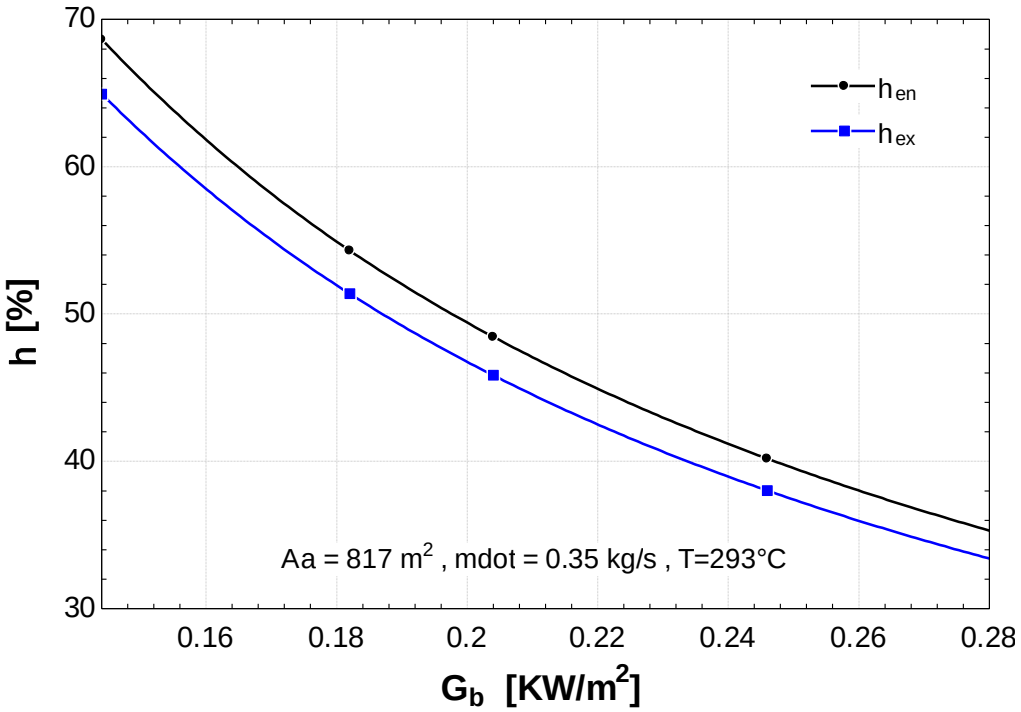

Figure 53: Energy and Exergy Efficiency based on average global radiation

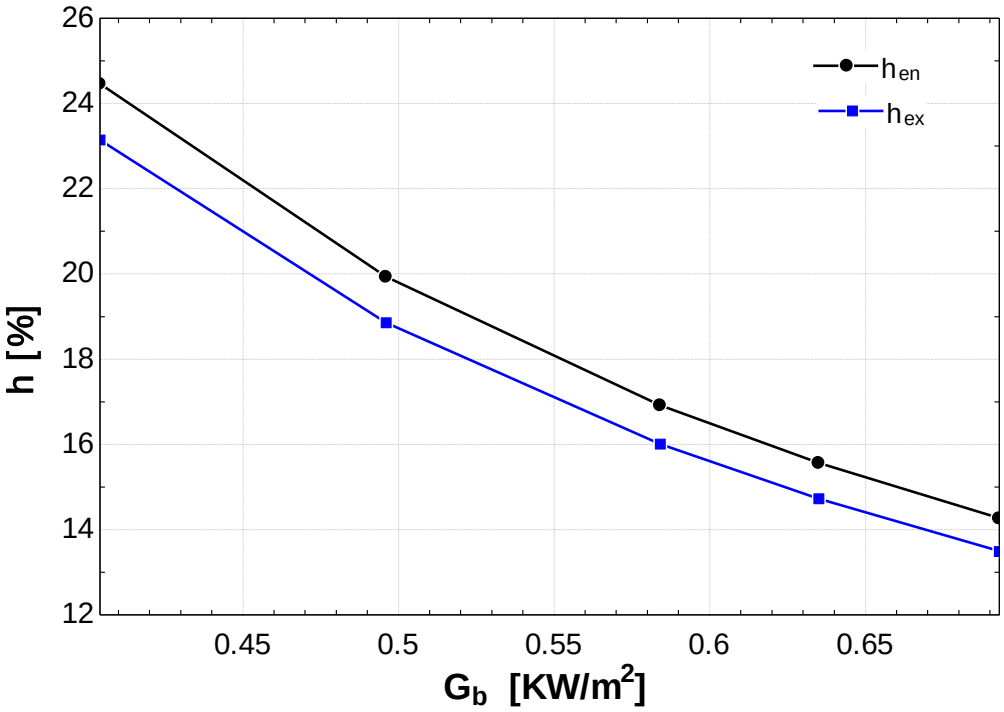

Figure 54: Energy and Exergy Efficiency based on maximum global radiation

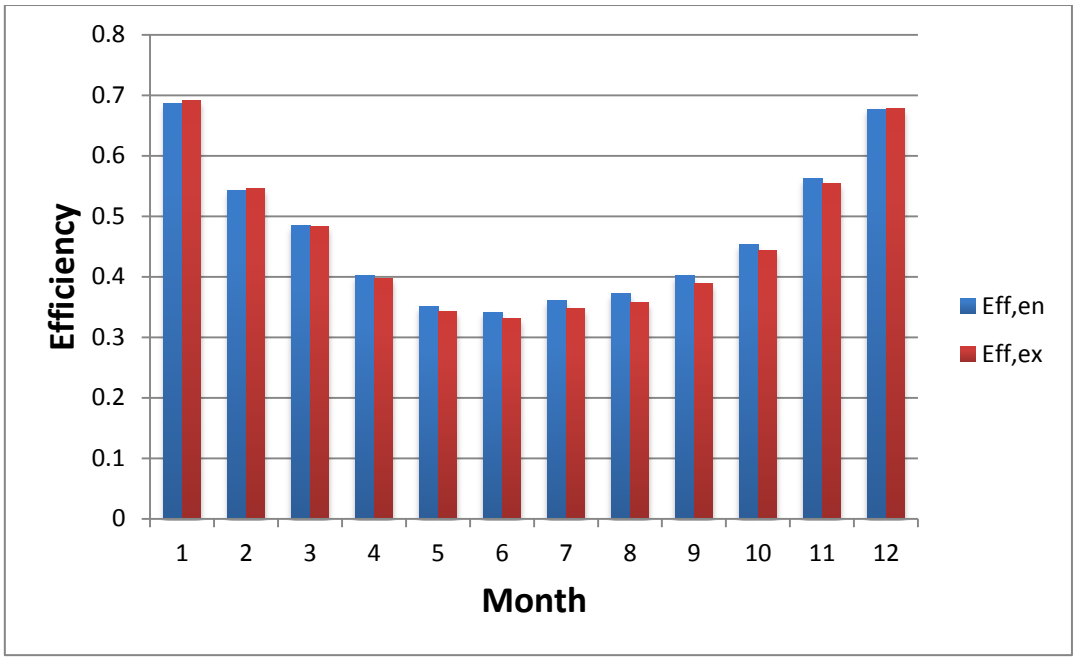

Figure 55: Energy and Exergy Efficiencies for average global radiation

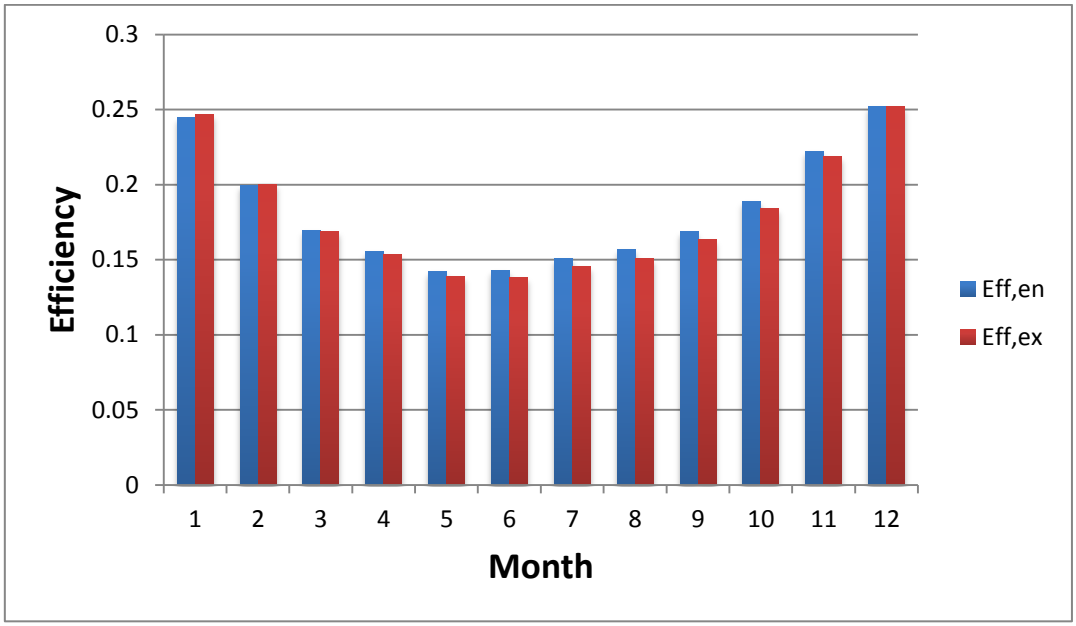

Figure 56: Energy and Exergy Efficiencies for maximum global radiation

Petela's Efficiency

In order to evaluate the performance of the solar energy system based on exergy analysis, the calculation of exergy radiation is necessary. Various approaches were suggested to calculate the exergy to energy ratio of radiation. Among these, is

the approach developed by Petela [87]. The Petela's efficiency was presented earlier in equation 4.45 as:

$$\zeta_P = 1 - \frac{4T_a}{3T_s} + \frac{1}{3}\left(\frac{T_a}{T_s}\right)^4$$

Where T_s is the solar radiation temperature

Figure 57 shows the slight decrease in the Petela's efficiency value with varying ambient temperatures. The efficiency values are then used to calculate the exact exergy solar radiation for the parabolic trough collector.

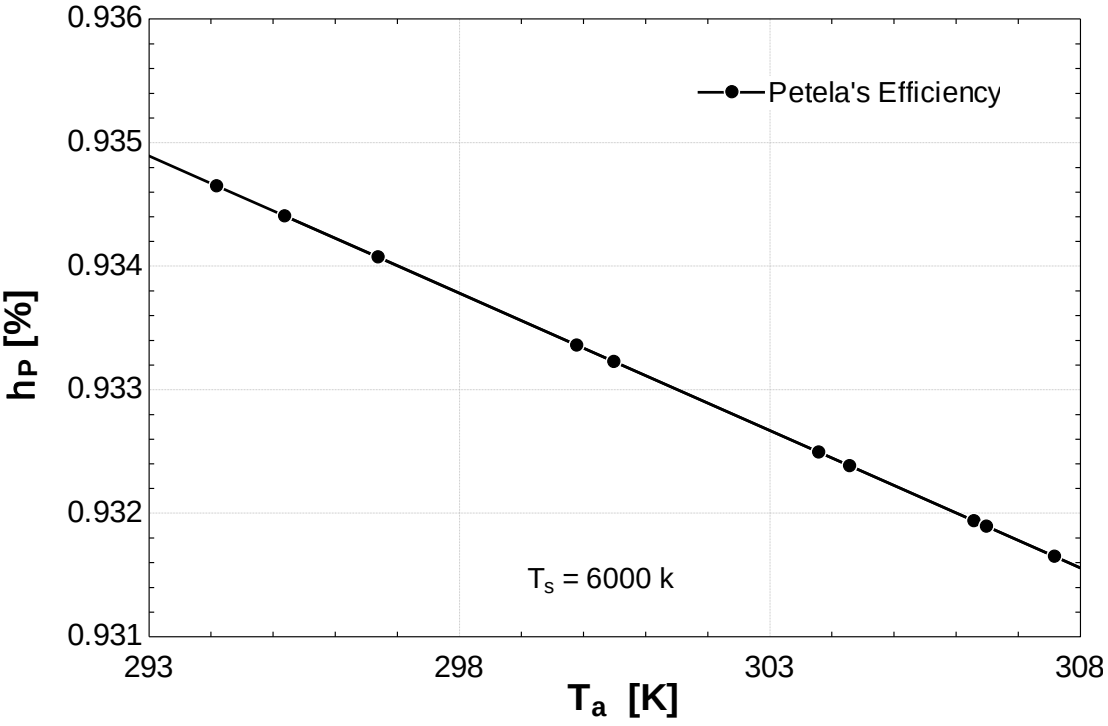

Figure 57: Petela's Efficiency variation with ambient temperature

The effect of varying the heat transfer fluid flow rate value is shown in the figures that follow. The energy and exergy efficiencies are based on the average global beam radiation value of 144 W/m^2 and collector aperture reflective area of 817.5 m^2.

Figure 58 shows the rise of both the energy and exergy efficiency values when increasing the flow rate value from 0.2 kg/s to 0.4 kg/s. The energy efficiency increased from 39.22% to 68.64% at a flow rate value of 0.35 kg/s.

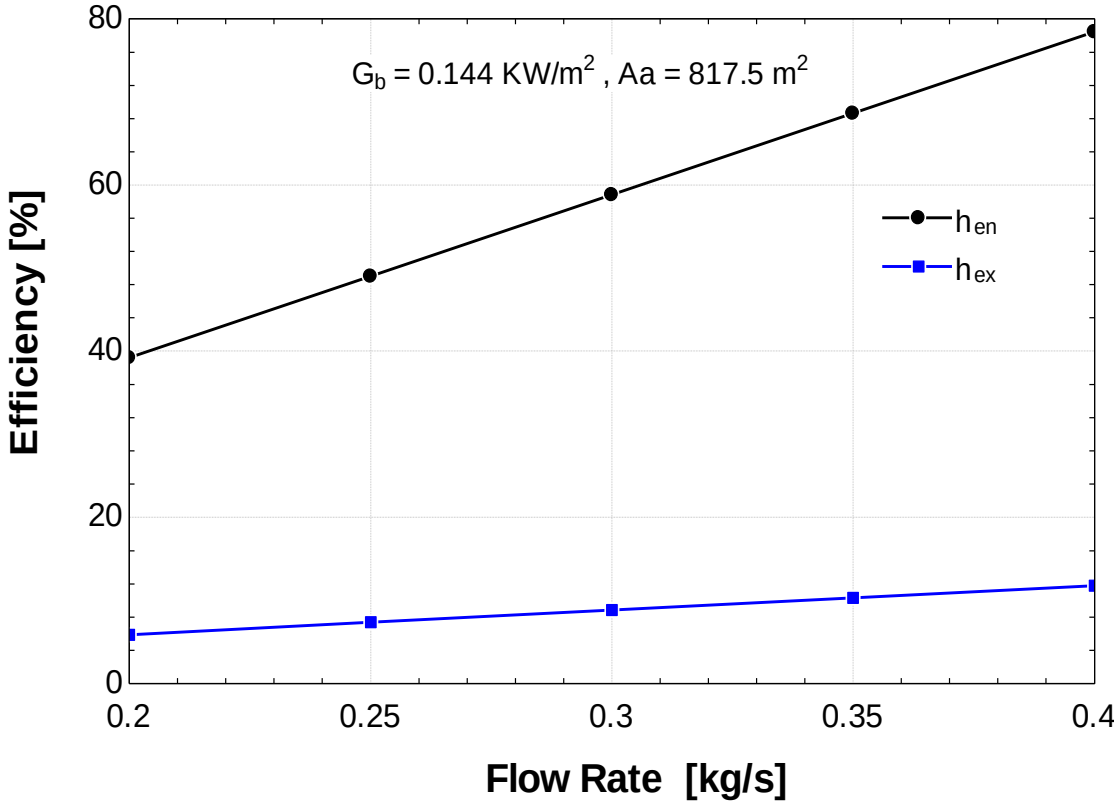

Figure 58: Effect of varying flow rate on average energy and exergy efficiency

In Figure 58, the energy and exergy efficiencies are found based on the maximum global radiation value of 404 W/m^2 occurring in the month of January. The maximum energy efficiency for the parabolic trough collector is calculated as 27.96% at the heat transfer fluid rate of 0.4 kg/s while the highest exergetic efficiency recorded was 4.2%. The inlet temperature for the heat transfer fluid is 293°C while the outlet heat transfer fluid temperature was 393°C. The amount of useful heat generated will increase with the rise of the flow rate value leading to raise the energy and exergy efficiency values.

Figure 59 shows arise in the efficiency of the integrated solar combined cycle when increasing the gas flow rate. The efficiency increased from 49.03% at a flow rate of 120 kg/s for the heat transfer fluid to around 65% at the flow rate of 160 kg/s. The design input value for the gas turbine inlet temperature (TIT) was 1100°C. These results were obtained at an ambient temperature of 35°C and a compression ratio of 6:1 for the compressor. The effect of varying the gas turbine inlet temperature with the compression ratio on the efficiency of the gas turbine, combined cycle and integrated solar combined cycle is investigated in the following figures.

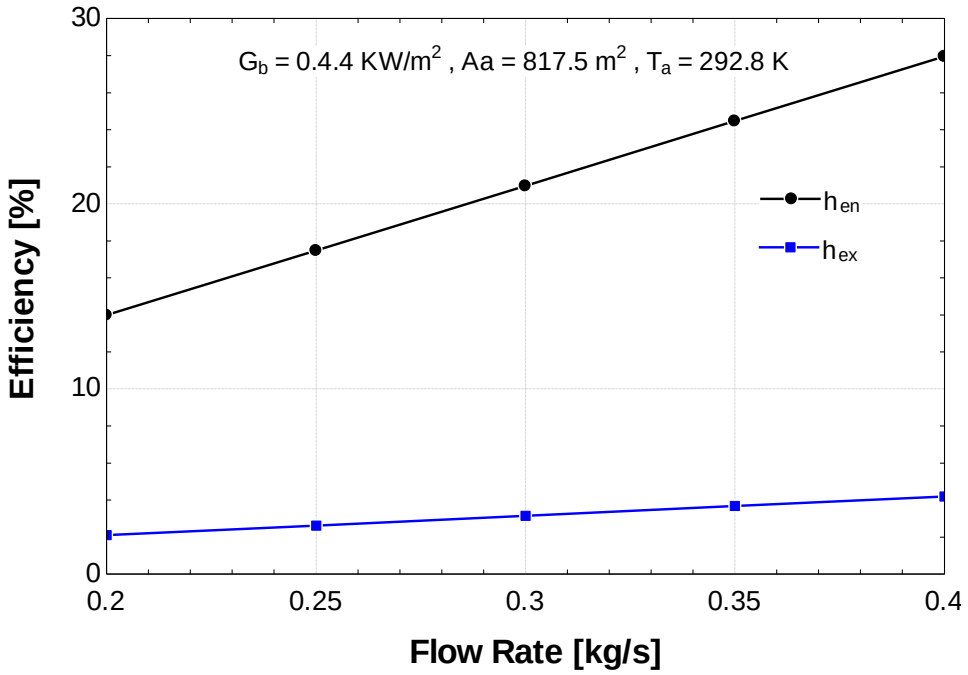

Figure 59: Effect of varying flow rate on average energy and exergy efficiency

In Figure 59, the efficiency values for both the gas turbine and the combined cycle are increasing with the rise of the compression ratio value from 4:1 to 10:1 while the integrated solar combined cycle efficiency value is decreasing in the same range for the turbine inlet temperature of 1100°C.

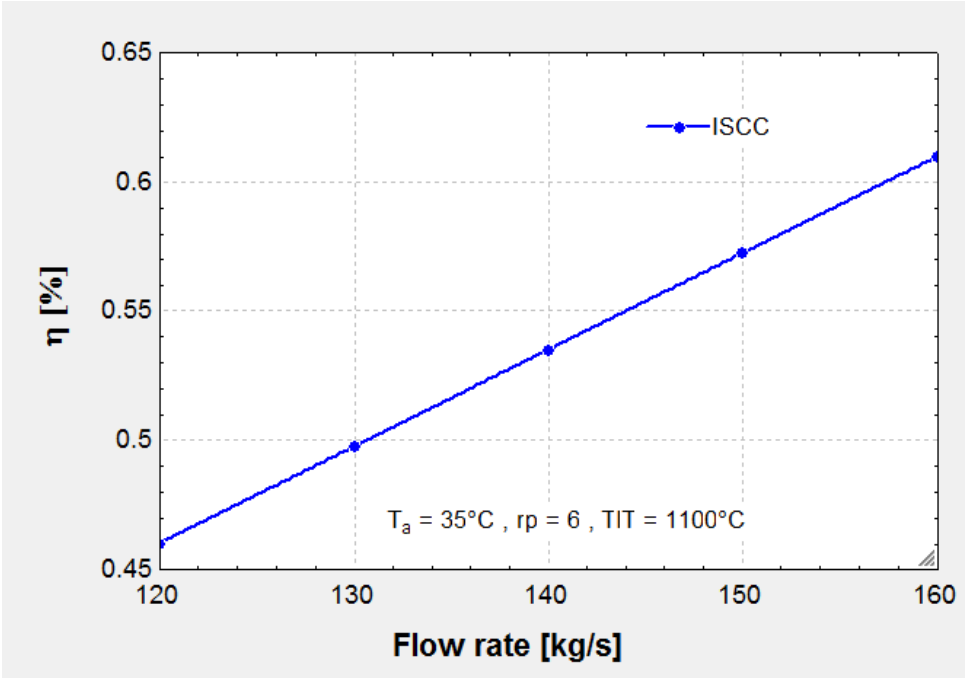

Figure 60: Effect of varying flow rate value on the ISCC efficiency

The highest values recorded for the gas turbine, combined cycle and ISCC efficiencies were 39.16%, 53.21% and 51.11% respectively. In Figure 62, the efficiencies of the three energy systems are shown with a gas turbine inlet temperature of 1200°C. The effect of increasing the turbine inlet temperature can be clearly shown on the ISCC efficiency curve. The efficiency values for the ISCC system were decreasing from about 57.53% to 44.39% while the efficiency for the gas turbine and combined cycle efficiency varied slightly. Figure 63 shows the variation of the efficiency values for the gas turbine unit from 26.25% to 38.95%. The efficiency of the combined cycle increased from 43.29 % to 53.05 % while the highest recorded efficiency for the ISCC system was 70.19% at compression ratio 4:1 and a gas turbine inlet temperature of 1400°C. For a turbine inlet temperature of 1400°C in Figure 64, a drop in efficiency values for the ISCC system continued while the efficiency values increased for the gas turbine and combined cycle system. The energy efficiency values varied between 26.15% and 38.83% for the gas turbine. In the case of the combined cycle, the efficiency increased from 43.21% to about 52.96%. Finally, the energy efficiency for the ISCC system decreased to 55.02% at the compression ratio of 10:1 and a gas turbine inlet temperature of 1400°C.

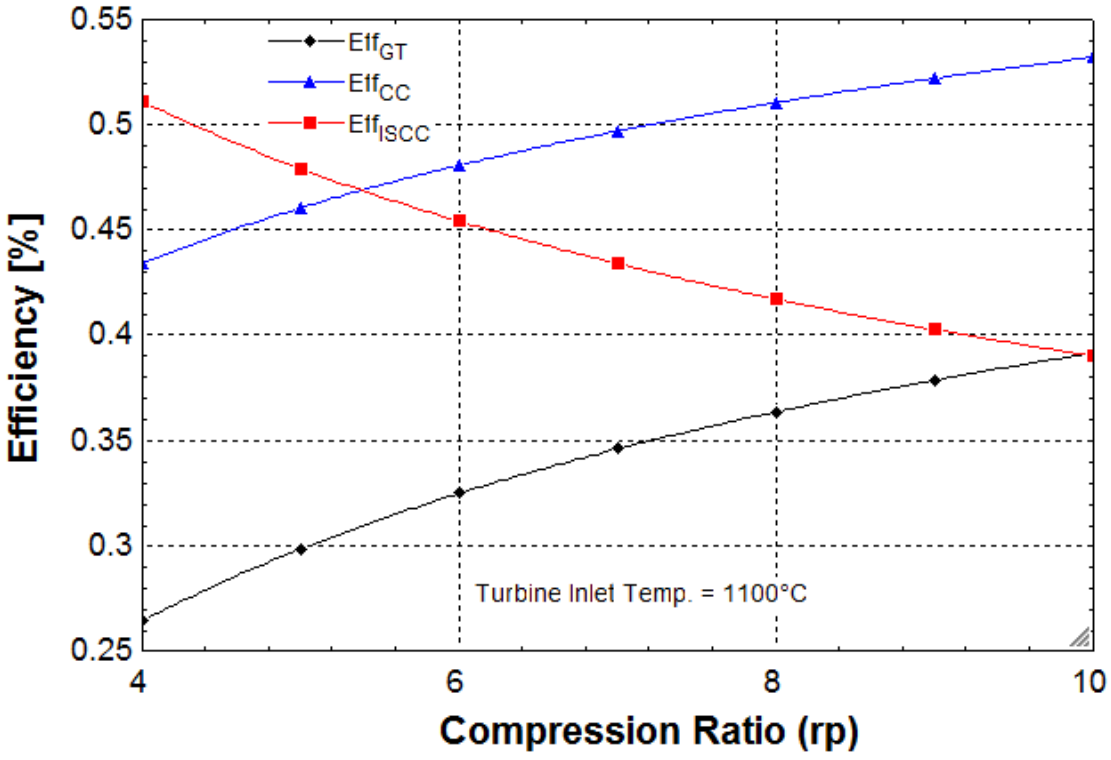

Figure 61: Effect of varying compression ratio on efficiency [TIT=1100°C]

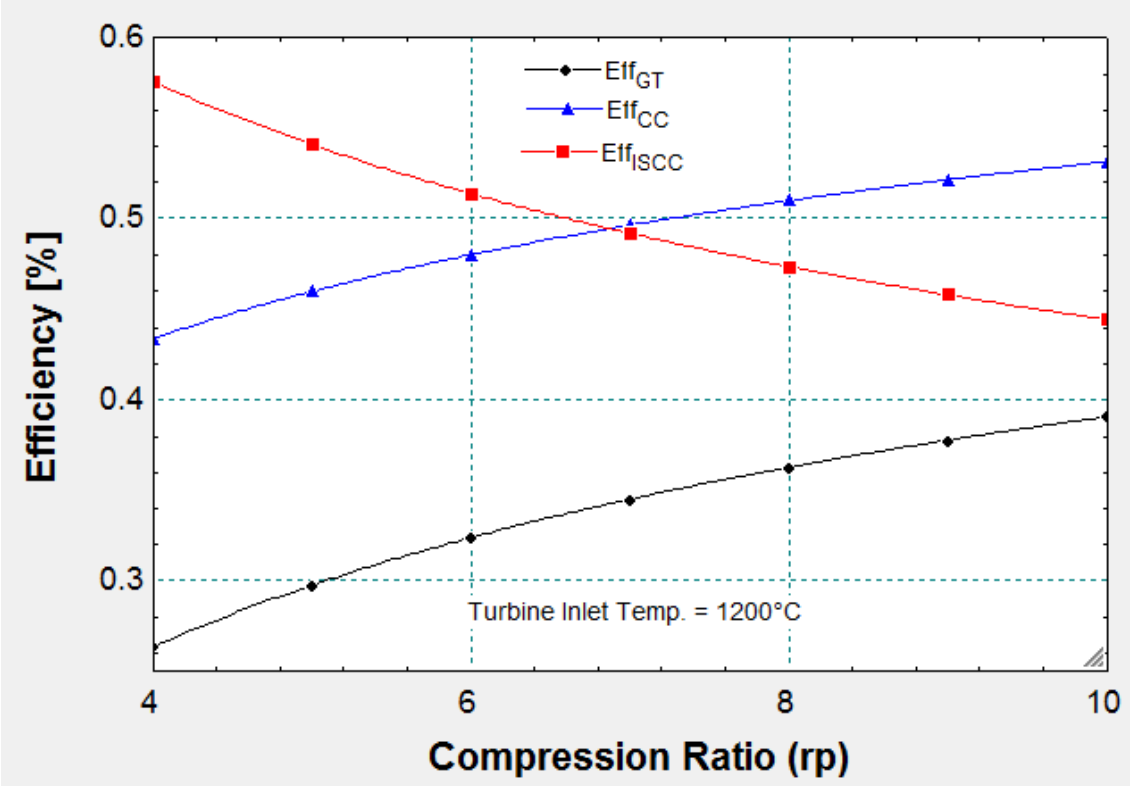

Figure 62: Effect of varying compression ratio on efficiency [TIT=1200°C]

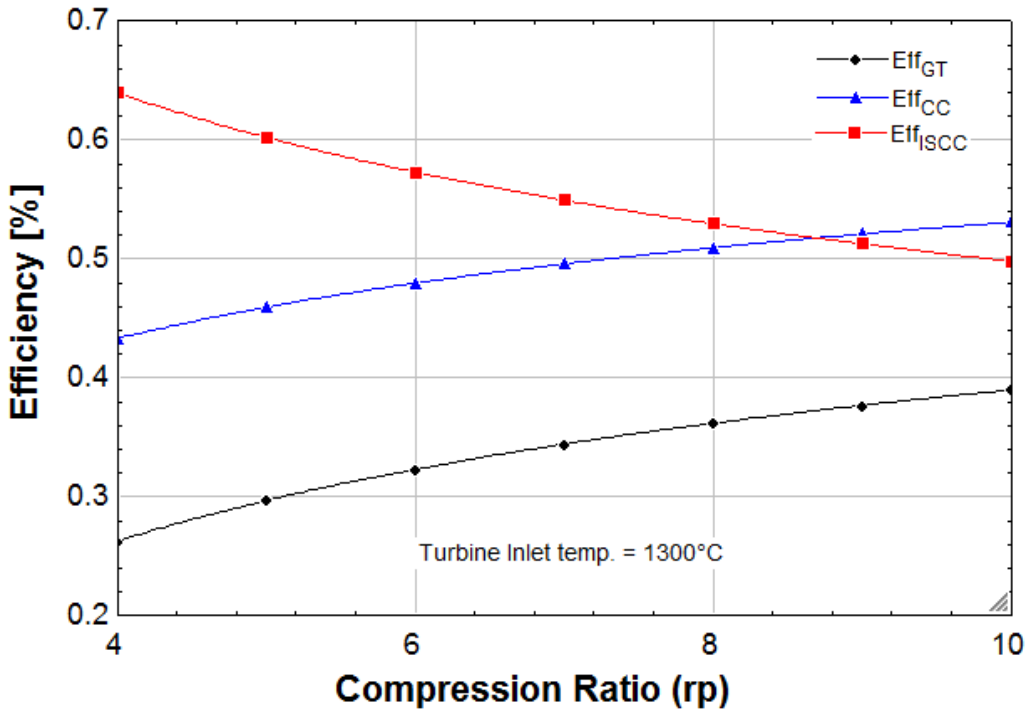

Figure 63: Effect of varying compression ratio on efficiency [TIT=1300°C]

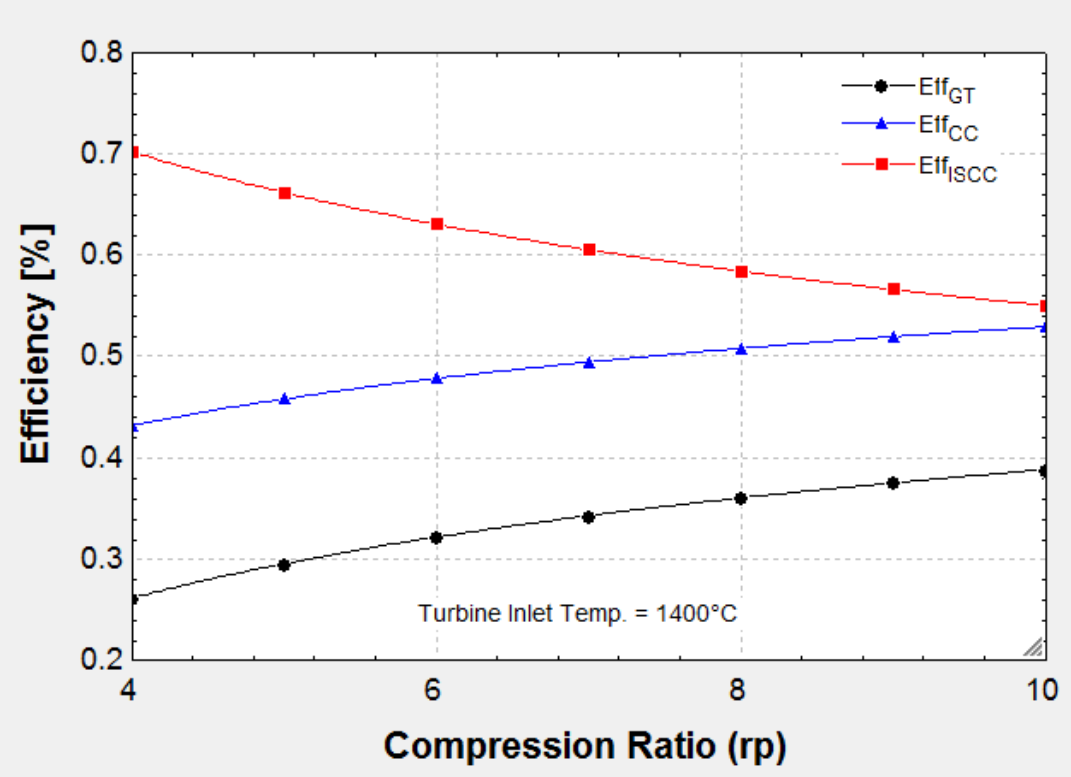

Figure 64: Effect of varying compression ratio on efficiency [TIT=1400°C]

5.3 Thermo economic analysis

An exergy and economic analysis for the proposed system is performed to estimate the exergy cost for all the flows in the system. The solving equations based on mass and energy conservation were discussed back in Chapter 4. The parameters used for determination of the properties for all the defined streams in the system are shown in Table 21. In Table 22, the exergy rate for all the streams in the system is presented. The costs of the intermediate flows in the system are shown in Table 23. The equations used to find the exergy destruction and the exergetic efficiency for the components of the power plant is shown in Table 24. Finally, the results obtained from the exergy destruction and exergetic efficiency equations are shown in Table 25.

Table 21: Parameters of the ISCC system

Parameter	***Symbol***	***Unit***	***Value***
Economic Life of System	*k*	Years	25
Interest Rate	*in*	%	6
Rate of Inflation	*ri*	%	2
Construction Period	*CP*	Years	3
Low heating Value	*LHV*	kJ kg^{-1}	50,000
Maintenance Factor	φ	-	1.06
Operation Period	*H*	Hours	7500
Compression Ratio	*rp*	-	7
Isentropic efficiency of compressor	ζ_{ac}	%	85
Isentropic efficiency of turbine	ζ_T	%	90
Mechanical efficiency for compressor	ζ_m	%	95
Gas Turbine inlet temperature	*TIT*	K	1473.15

Table 22: State properties of the ISCC system

State	*Phase*	T_i *(K)*	P_i *(bar)*	*h (kJ/kg)*	*s (kJ/kg.K)*	$\dot{E}$*(MW)*
0	Air	300.15	1.013	300.613	6.871	
0'	Water	300.15	1.013	79.82	0.281	
0"	Oil	300.15	1.013	12	0.283	
1	Air	300.15	1.01	300.61	6.87	0.00
2	Air	562.74	11.14	639.60	6.94	64.8
3	Gas	1404.80	10.58	1523.00	7.86	420.1
4	Gas	821.50	1.05	846.20	7.90	250.1
5	Gas	729.70	1.07	745.80	7.77	220.8
6	Gas	536.90	1.04	541.60	7.45	172.0
7	Gas	479.70	1.04	482.60	7.34	145.3
8	Water	321.19	0.11	2293.40	7.19	1.6
9	Water	321.19	0.11	201.15	0.67	0.2
10	Water	391.71	119.00	506.00	1.50	2.2
11	Water	488.15	118.00	923.80	2.45	15.0
12	Water	488.15	118.00	923.80	2.45	6.2
13	Saturated Steam	578.66	92.77	2738.00	5.66	38.9
14	Saturated Steam	578.66	92.77	2738.00	5.66	32.5
15	Superheated Steam	779.15	84.80	3408.60	6.71	47.1
16	Water	488.15	118.00	923.80	2.45	1.4
17	Water	578.66	92.77	2738.20	5.66	7.3
18	Oil	571.15	11.00	550.34	1.55	13.0
19	Oil	573.82	16.00	552.63	1.55	13.2
20	Oil	666.50	26.00	790.00	1.93	25.1
21	Water	292.15	1.01	79.82	0.28	0.00
22	Water	320.35	1.01	197.71	0.67	5.23
23	Fuel	292.15	20.00	292.43	4.78	401.89

Table 23: Cost of the intermediate streams of the systems

State Points	***c*** ***($ kWh^{-1})***	$\dot{C}$ ***($ h^{-1})***
1	0	0.0
2	0.24	15.6
3	0.21	88.2
4	0.21	52.5
5	0.21	46.4
6	0.21	36.1
7	0.21	30.5
8	0.26	0.4
9	0.26	0.0
10	0.36	0.8
11	0.30	4.5
12	0.30	1.9
13	0.25	9.7
14	0.27	8.8
15	0.26	12.2
16	0.30	0.4
17	0.33	2.4
18	0.23	3.0
19	0.23	3.0
20	0.23	5.8
21	0.00	0.0
22	0.52	0.5
23	0.12	46.8

Table 24: Exergy destruction rate and exergy efficiency equation for plant components

Component	***Exergy Destruction***	***Exergy Efficiency***
Air Compressor	$\dot{E}_1 - \dot{E}_2 - \dot{W}_{27}$	$\frac{\dot{E}_2 - \dot{E}_1}{\dot{W}_{27}}$
Combustion Chamber	$\dot{E}_2 + \dot{E}_{23} - \dot{E}_3$	$\frac{\dot{E}_3}{\dot{E}_2 + \dot{E}_{23}}$
Gas Turbine	$\dot{E}_3 - \dot{W}_{28} - \dot{E}_4$	$\frac{\dot{W}_{28}}{\dot{E}_3 - \dot{E}_4}$
HRSG – Super Heater	$(\dot{E}_4 + \dot{E}_{14}) - (\dot{E}_5 + \dot{E}_{15})$	$\frac{(\dot{E}_5 + \dot{E}_{15})}{(\dot{E}_4 + \dot{E}_{14})}$
HRSH - Evaporator	$(\dot{E}_5 + \dot{E}_{12}) - (\dot{E}_6 + \dot{E}_{13})$	$\frac{(\dot{E}_6 + \dot{E}_{13})}{(\dot{E}_5 + \dot{E}_{12})}$
HRSG - Economizer	$(\dot{E}_6 + \dot{E}_{10}) - (\dot{E}_7 + \dot{E}_{11})$	$\frac{(\dot{E}_7 + \dot{E}_{11})}{(\dot{E}_6 + \dot{E}_{10})}$
Steam Turbine	$\dot{E}_{15} - \dot{E}_8 - \dot{W}_{29}$	$\frac{\dot{W}_{29}}{\dot{E}_{15} - \dot{E}_8}$
Condenser	$(\dot{E}_8 + \dot{E}_{21}) - (\dot{E}_{22} + \dot{E}_9)$	$\frac{(\dot{E}_{22} + \dot{E}_9)}{(\dot{E}_8 + \dot{E}_{21})}$
Condensate Extraction Pump	$\dot{E}_9 - \dot{W}_{26} - \dot{E}_{10}$	$\frac{\dot{E}_9 - \dot{E}_{10}}{\dot{W}_{26}}$
Solar Steam Generator	$(\dot{E}_{16} + \dot{E}_{20}) - (\dot{E}_{18} + \dot{E}_{17})$	$\frac{(\dot{E}_{18} + \dot{E}_{17})}{(\dot{E}_{16} + \dot{E}_{20})}$
HTF Pump	$\dot{E}_{18} - \dot{W}_{25} - \dot{E}_{19}$	$\frac{\dot{E}_{18} - \dot{E}_{19}}{\dot{W}_{25}}$

Table 25: Exergy destruction and exergetic efficiency results

Component	***Exergy Destruction (MW)***	***Exergy Efficiency (%)***
Air Compressor	6.76	0.91
Combustion Chamber	34.82	0.92
Gas Turbine	14.94	0.91
HRSG – Super Heater	14.68	0.95
HRSH - Evaporator	16.19	0.93
HRSG - Economizer	13.78	0.92
Steam Turbine	6.77	0.99
Condenser	0.42	0.74
Condensate Extraction Pump	4.52	0.81
Solar Steam Generator	6.11	0.77
HTF Pump	0.45	0.80

5.4 Economic and Environmental Analysis

An economic and environmental analysis of the proposed power plants has also been carried out. The levelized cost of electricity (LCOE), annual CO_2 avoided emissions and fuel savings are calculated for the combined cycle, ISCC and the ISCC with thermal energy storage. All the parameters associated with the economic and environmental analysis are listed before. The economic life for the proposed designs is 25 years. First, the effect of integrating the combined cycle power plant with a capacity of 120 MW with the solar energy source is investigated. Afterwards, the addition of a thermal energy storage system with a storage capacity of 7.5 hours is evaluated. The annual electricity generation for the combined cycle and integrated solar combined cycle power plants is shown in Figure 65. The power plants are assumed to start operation and electricity generation after two years of experimental runs. The amount of electricity generated can be shown to increase gradually as the loading factor value increases over time. The annual electricity generated for the ISCC plant is higher than that of the combined cycle power plant and the electricity generation reaches between 1000 GWh and 1200 GWh.

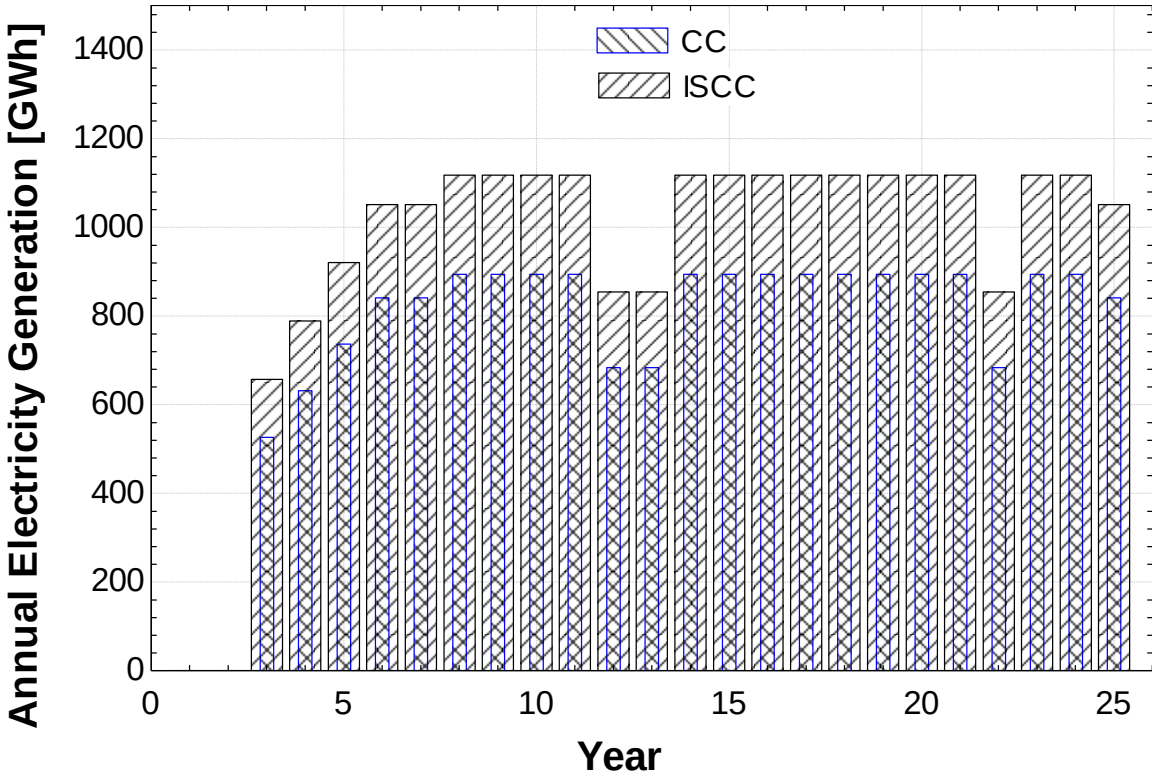

Figure65: Annual electricity generation (GWh)

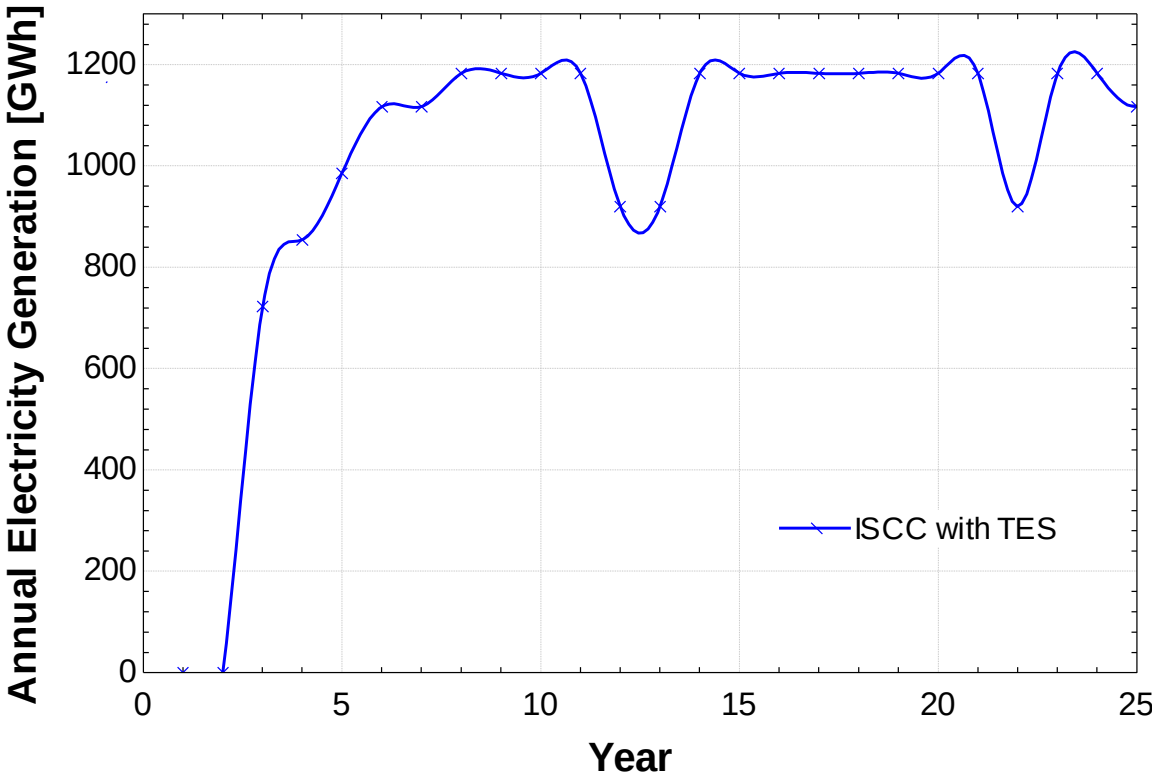

Figure 66: Annual electricity generation for ISCC with TES

Similarly, Figure 66 shows the annual electricity generated by the ISCC and with 7.5 hours of thermal storage. One of the main parameters that have a direct impact on the LCOE value is the fuel cost. The fuel used in the proposed system is natural gas with a lower heating value of 50 GJ/T. The fuel price projection for the proposed power plans during the period of 25 years is assumed according to forecasts taking into account the variation in the fuel price. In Figure 67, the fuel cost along the period of the power plant's operating life is shown for the six candidate configurations. It is expected for the fuel cost for the combined cycle power plant to be higher than the other technology options. This is due to the continuous consumption of fuel during the 24 hour operation of the CC power plant. The fuel cost is shown to reach around 35 million US$ for the CC pant in Figure 67. Integrating solar energy to the conventional CC power plant will improve the economics of the plant as part of the thermal energy delivered from the solar field which will assist in the steam production to generate electricity and increase the amount of fuel saved. Adding thermal energy storage to the ISCC power plant will add many advantages as the number of hours for the power block operating on fossil fuels will decrease. It can be seen from the graph that the fuel cost curve throughout the economic life for the

system is decreasing. The option of integrating the ISCC power plant with 4.5, 7.5, 10.5 and 12.5 hours of storage is investigated. The results show that adding a thermal energy storage system with a storage capacity of 12.5 hours is the least cost feasible option in terms of fuel costs for the proposed power plants.

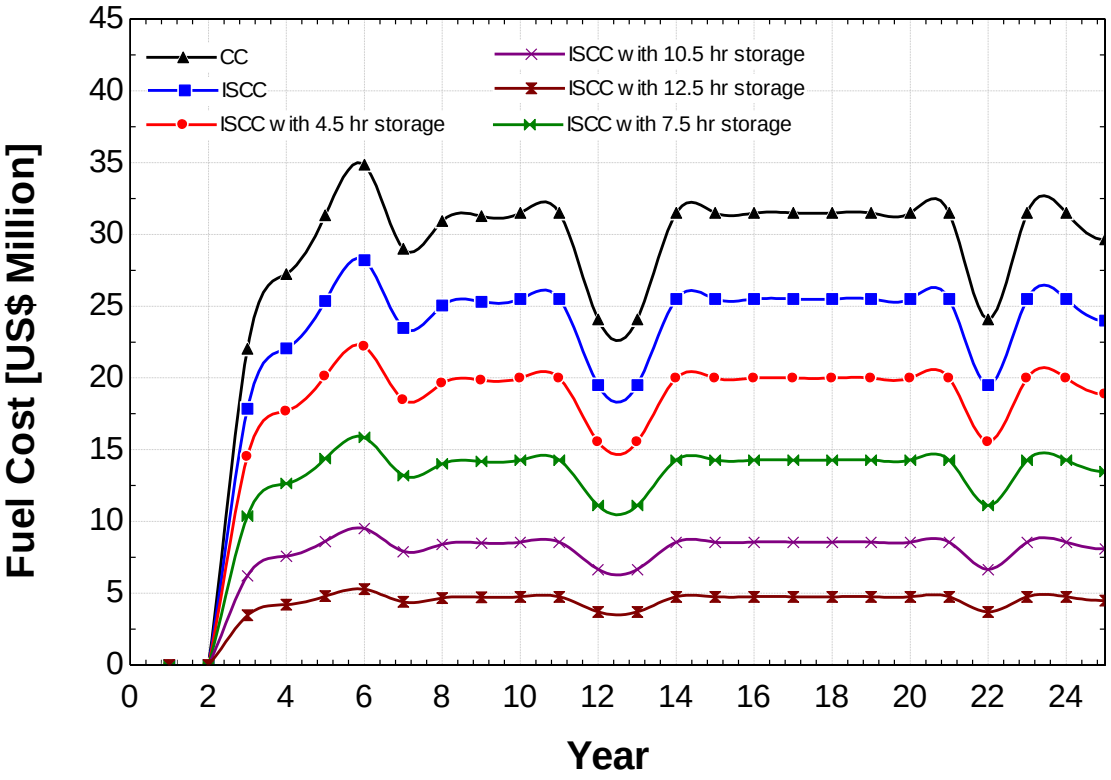

Figure 67: Fuel Cost (Million USD)

Figure 68 shows the total production costs for the six configuration options. The total production cost for the power plant includes the annual values for capital cost, operation and maintenance costs (O&M) and the fuel cost. A parametric analysis was conducted to evaluate the most suitable option in technical, economic and environmental terms. For the combined cycle power plant of capacity 120 MW, the specific capital cost ranged from 500 US$/KW to 1500 US$/KW. In the case of the ISCC and the ISCC with thermal storage, the capital cost value was varied between 5000 US$/KW to 12,000 US$/KW.

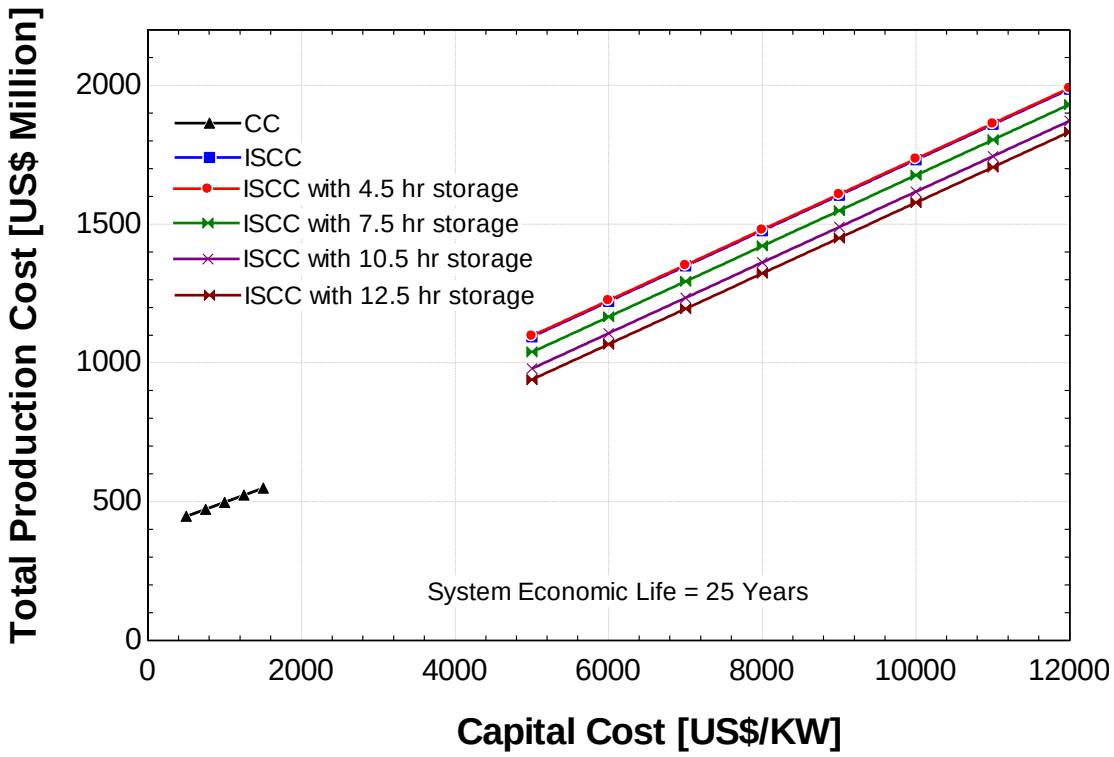

Figure 68: Total electricity production cost (Million USD)

The total production cost for the six mentioned power plants over the period of 25 years is shown in Figure 68. The least production cost option is the combined cycle power plant with a total production cost of around 549.1 million US$ at a specific capital cost of 1500 US$/KW. The ISCC without thermal storage and the ISCC with 4.5 hours of storage had the highest total production costs of 1986 million US$ and 1990 million US$ respectively due to the additional cost of the solar field and high fuel cost. Increasing the storage capacity for the system will reduce the total production cost as a result of the decrease of fuel consumed in the power plant. It is evident that the ISCC with 12.5 hours of storage followed by the ISCC with 10.5 hours storage are both cost-effective options to be utilized. The total production cost for the ISCC with 12.5 hours storage varied between 940 million US$ to 1832 million US$. Figure 69 illustrates a comparison between the two proposed designs in terms of the LCOE value. The ISCC design with 7.5 hours of storage capacity had a calculated electricity cost of 8.86 Cents/KWh at a specific capital cost of 5000 US$/KW. This cost increases to 16.47 Cents/KWh at specific capital cost of 12,000 US$/KW. The ISCC design without thermal storage had a lower LCOE value in the same range of the capital cost increasing from 9.94 Cents/KWh to 18.05 Cents/KWh. The LCOE for

the combined cycle power plant ranged from 5.08 Cents/KWh to 6.24 Cents/KWh at a specific capital cost of 1500 US$ per KW.

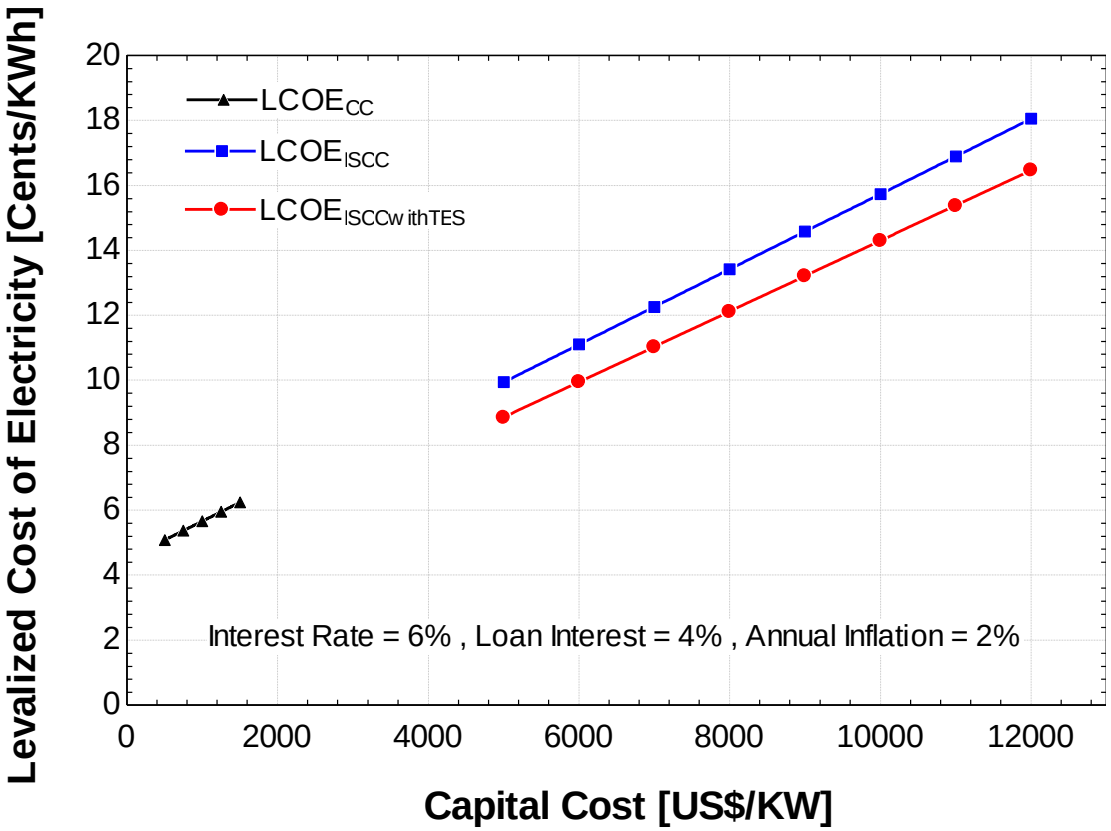

Figure 69: LCOE for the two proposed designs

Adding thermal energy storage with different capacities to the ISCC will reduce the LCOE value as discussed earlier. It is shown that the ISCC design without thermal storage had the highest LCOE value of 17.85 Cents/KWh at the specific capital cost of 5000 US$/KW and increasing to reach 25.5 Cents/KWh at capital cost of 12,000 US$/KW. As the number of storage hours increase for the system, the cost of electricity drops gradually. For the ISCC design with 7.5 hours of storage, the LCOE value increased from 10.38 Cents/KWh to 14.28 Cents/KWh at a specific capital cost of 12,000 US$/KW. The ISCC with 12.5 hours storage capacity had the lowest LCOE after the combined cycle with an LCOE value ranging from 3.46 Cents/KWh to 4.76 Cents/KWh which makes it the least cost feasible choice among the proposed integration options.

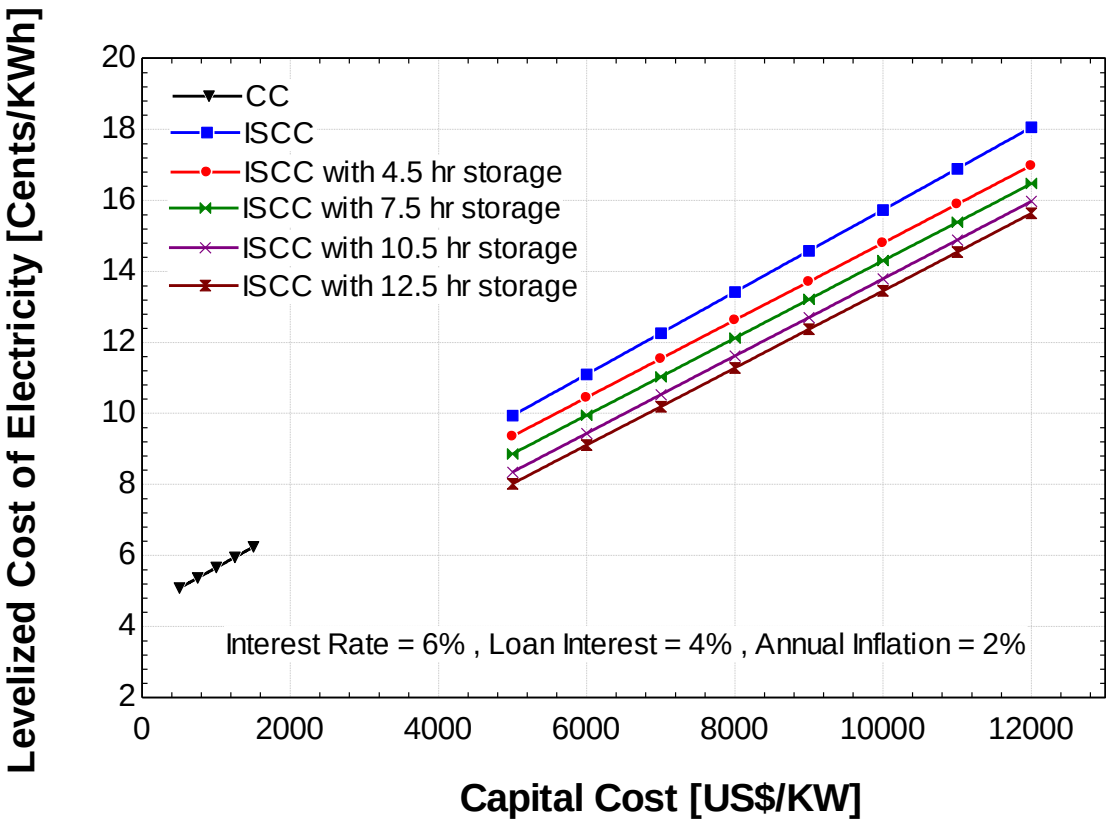

Figure 70: LCOE for the ISCC with different storage capacities

Figure 70 shows a comparison between the conventional combined cycle with the ISCC and the ISCC with thermal storage (7.5 hours) in terms of the total electricity generated during the operating life of the system (25 years). It is shown in the bar chart that the ISCC with TES had the highest value for electricity generation of 25,228.80 GWh. The total electricity generation for the ISCC design was calculated as 23,717.70 GWh while the combined cycle power plant had an amount of only 18,974.16 GWh of generated electricity in the same period. Figure 71 shows the amount of annual avoided CO_2 emissions for the ISCC and ISCC with thermal storage systems. In the case of the ISCC design, the annual CO_2 emissions were recorded as 380,842 tons compared with 427,989 tons of CO_2 avoided emission for the ISCC design with 7.5 hours of thermal storage. The integration of thermal storage has proven to make the renewable energy source (solar) more viable while also adding environmental benefits and its serving as a back-up source of power. Thermal energy storage allows for storage for surplus thermal energy at times of low demand and in order to provide power at peak demand periods. The option of utilizing thermal energy storage with a maximum storage capacity of 12.5 hours leads to more

greenhouse gas reduction potential and a reduction in the amount of fossil fuels consumed in the power plant.

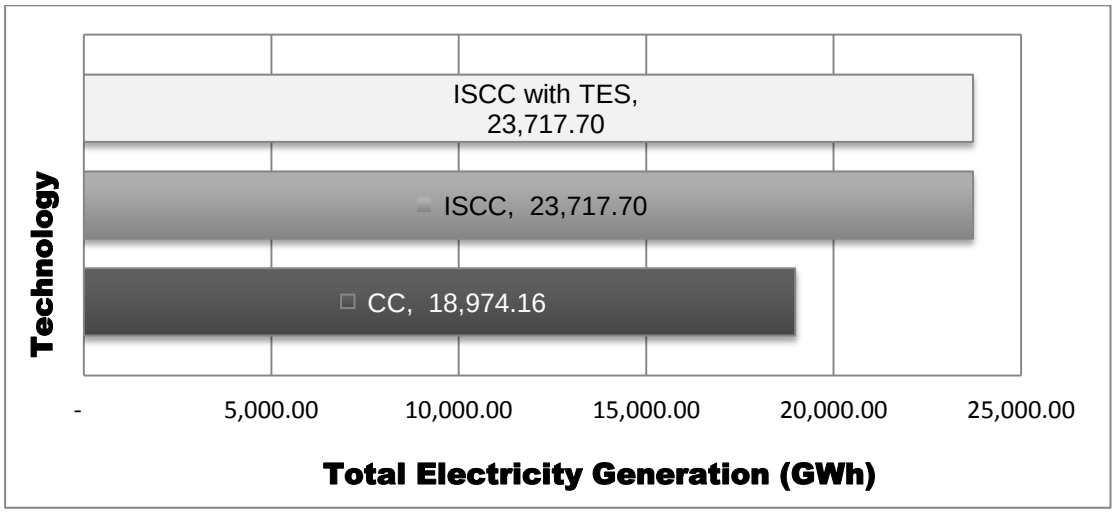

Figure 71: Total electricity generation for CC, ISCCM ISCC with TES

As discussed in the above section, the addition of a thermal energy storage system to the power plant can improve the economics of the power plant as the fuel cost will decrease and the amount of fuel savings will increase. Figure 72 shows that amount of fuel savings are calculated as 382,657 barrels for the case of the ISCC with 7.5 hours storage capacity compared with only 133,757 barrels of crude oil not consumed by the ISCC power plant.

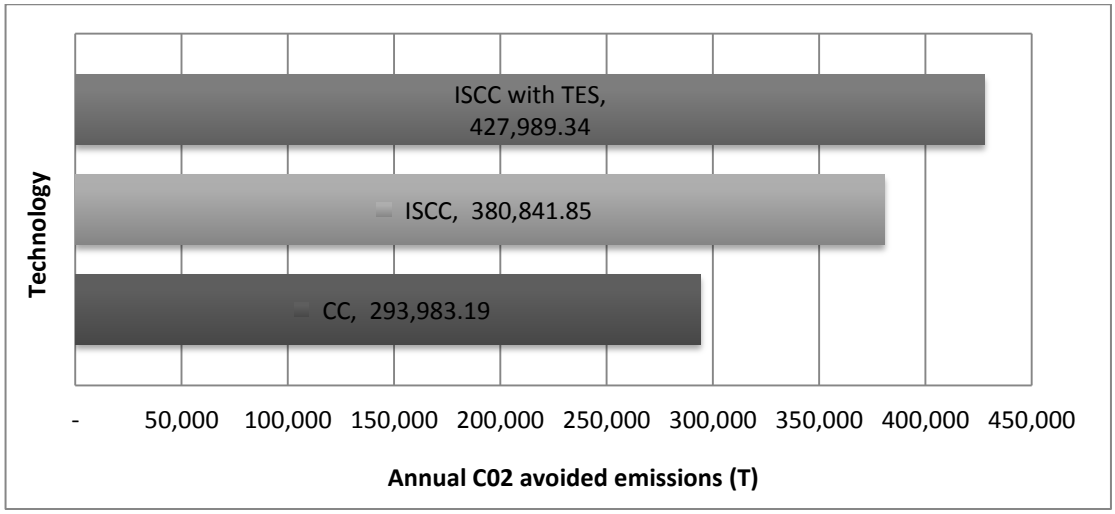

Figure 72: Annual CO_2 avoided emissions

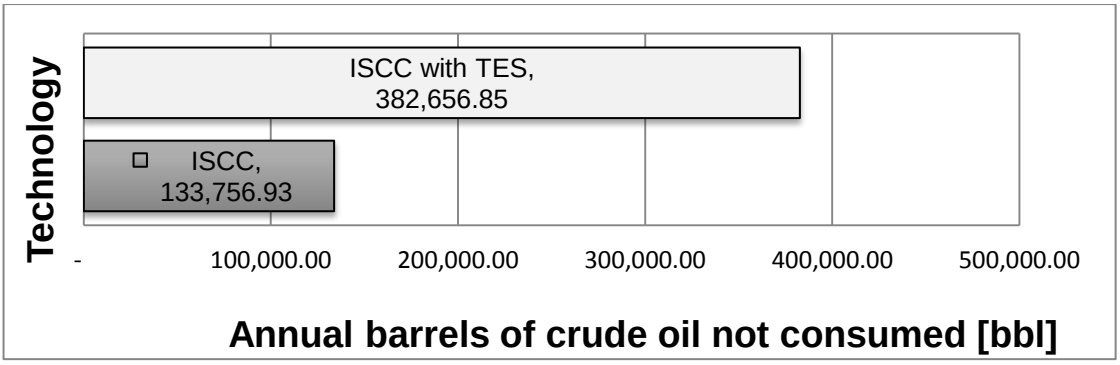

Figure 73: Fuel saving for ISCC and ISCC with TES

In Figure 74, the cost breakdown for the conventional combined cycle power plant is shown. The cost breakdown which is the total production cost consists of three main parameters: annual capital expenditure, fuel cost and O&M cost, respectively. For the combined cycle case, fuel cost formed the highest cost element of the power plant because the power plant was fully dependent on fossil fuels for power generation.

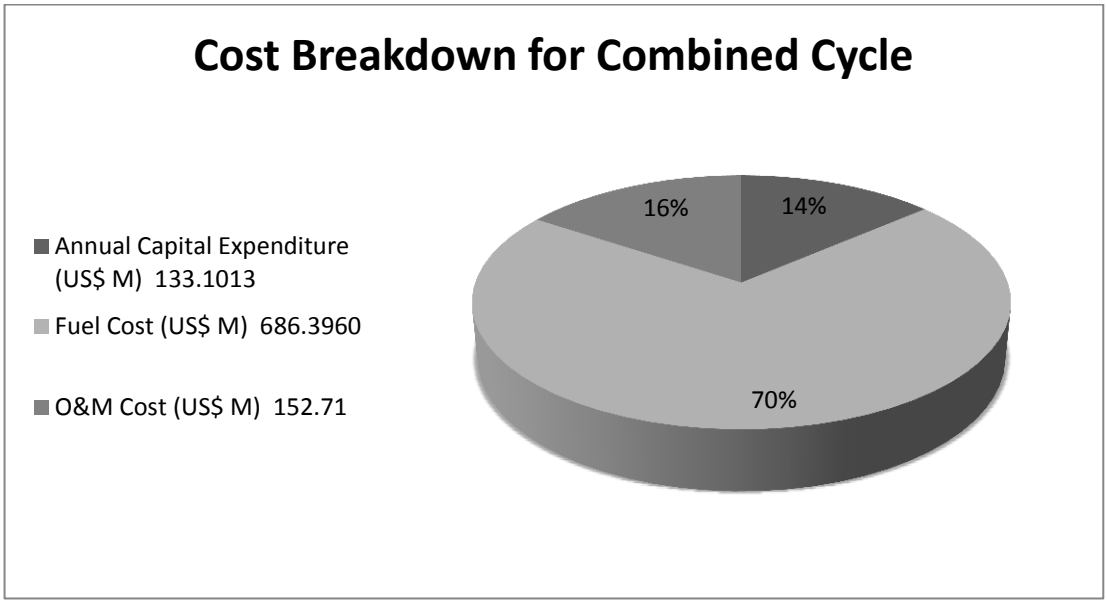

Figure 74: Cost breakdown for Combined Cycle

Figure 75 shows the cost breakdown for the ISCC design with around 66% annual capital expenditure estimated at 1,091 million US$ followed by the fuel cost and then the O&M cost. In Figure 76, the fuel cost percentage decreased from 20% to 11% as a result of integrating thermal energy storage with the ISCC design.

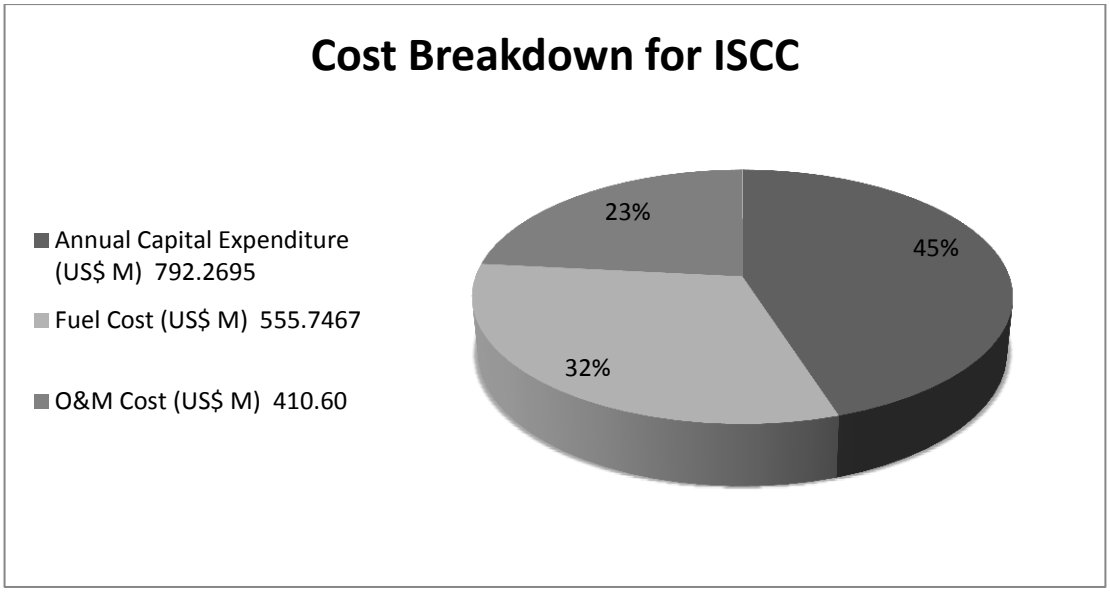

Figure 75: Cost breakdown for ISCC

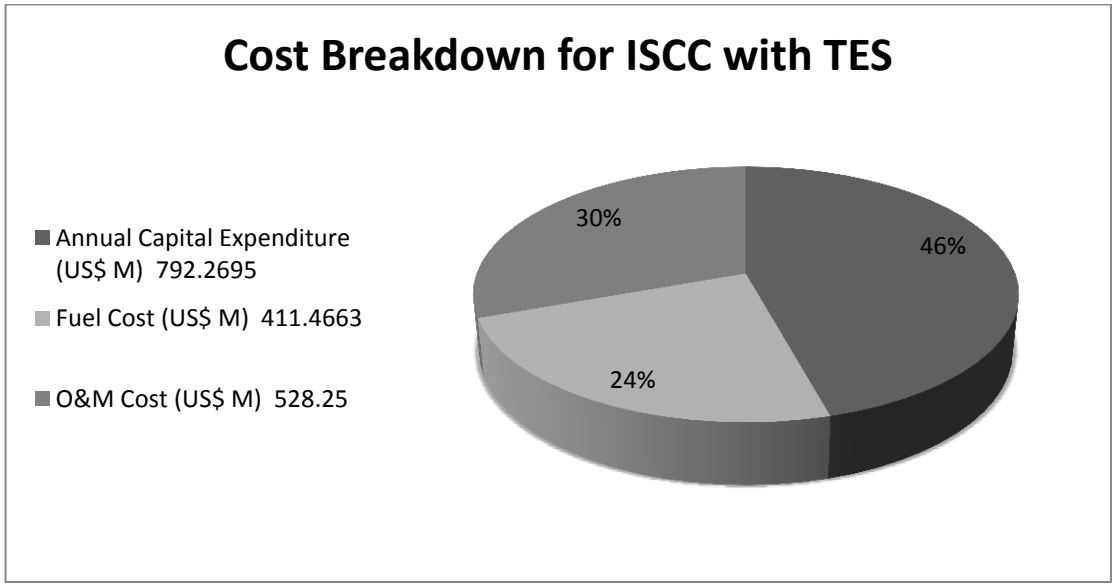

Figure 76: Cost breakdown for ISCC with TES

Chapter 6: Conclusion and Recommendations

In this thesis, the integration of solar energy technology with the conventional combined cycle and addition of thermal energy storage to the power plant were investigated. Energy, exergy and thermo economic analyses were performed to evaluate the performance of the system. Also, an economic and environmental analysis for the two proposed designs was conducted. The results of these analyses are given here.

6.1 Conclusions

1) Two different configurations of the combined cycle system are proposed. The first configuration is an integrated solar combined cycle (ISCC) power plant. In the second configuration, adding thermal energy storage with different storage capacity hours is proposed to find the most suitable option to be implemented in the UAE.
2) The meteorological data and solar potential for Abu Dhabi is discussed in Chapter 4. A detailed description of the collector and receiver options is also presented.
3) A preliminary comparative analysis for six different HTFs is performed to determine the most suitable HTF to be used in the parabolic trough collector. The main indicators used were the net electric output (kWh), annual energy (kWh), LCOE (c/kWh) and the thermal energy absorbed by the HTF (kWh). Based on this comparative analysis, the Therminol VP-1 which is a synthetic heat transfer fluid was selected as the suitable HTF for the parabolic trough system and Hitec Solar Salt was selected as the storage medium.
4) The evaluation of the performance of the parabolic trough collector is based on the energy and exergy equations presented earlier in the performance model for the solar field. The results obtained shows a decrease in the energetic and exergetic efficiencies from January until June as a result of the increasing global irradiance and ambient temperature. The highest values for energy and exergy efficiency were 68.64% and 64.93% respectively. The average energy efficiency for the solar collector ranged between 34.08% and 68.64% while the average exergy efficiency ranged between 32.24% and 64.93% in the same period. The energy and exergy efficiencies were based on the average global beam radiation

value of 144 W/m2 and collector aperture reflective area of 817.5 m2.The highest values recorded for the gas turbine, combined cycle and ISCC efficiencies were 39.16%, 53.21% and 70.18% respectively.

5) Based on the thermo economic analysis, it was found that the highest exergy destruction value was recorded in the combustion chamber with 34.82 MW.

6) The least production cost option is the combined cycle power plant with a total production cost of around 549.1 million US$ at a specific capital cost of 1500 US$/KW. The ISCC without thermal storage and the ISCC with 4.5 hours of storage had the highest total production costs with 1986 million US$ and 1990 million US$ respectively due to the additional cost of the solar field and high fuel cost. Increasing the storage capacity for the system will lead to a reduction in the total production cost as a result of the decrease of fuel consumed in the power plant. It is evident that the ISCC with 12.5 hours of storage followed by the ISCC with 10.5 hours storage are both viable cost-effective options to be utilized. The total production cost for the ISCC with 12.5 hours storage varied between 940 million US $ to 1832 million US$. The ISCC design with 7.5 hours storage capacity had a calculated electricity cost of 8.86 Cents/KWh at a specific capital cost of 5000 US$/KW. This cost increases to 16.47 Cents/KWh at a capital cost of 12,000 US$/KW. The ISCC design without thermal storage had a lower LCOE value in the same range of the capital cost increasing from 9.94 Cents/KWh to 18.05 Cents/KWh. The LCOE for the combined cycle power plant ranged from 5.08 Cents/KWh to 6.24 Cents/KWh at a specific capital cost of 1500 US$ per KW. Adding thermal energy storage with different capacities to the ISCC will reduce the LCOE value as discussed earlier. It is shown that the ISCC design without thermal storage had the highest LCOE value of 17.85 Cents/KWh at the specific capital cost of 5000 US$/KW, increasing to reach 25.5 Cents/KWh at a capital cost of 12,000 US$/KW. As the number of storage hours increases for the system, the cost of electricity drops gradually. The LCOE value increases with the variation of the capital cost value from 5000 US$/KW to 12,000 US$/KW. For the ISCC design with 7.5 hours of storage, the LCOE value increased from 10.38 Cents/KWh to 14.28 Cents/KWh at 12,000 US$/KW, specific capital cost. The ISCC with 12.5 hours storage capacity had the lowest LCOE after the combined cycle with an LCOE value ranging from 3.46 Cents/KWh to 4.76 Cents/KWh

which makes it the least cost feasible choice among the proposed integration options.

7) It is shown above that the ISCC with TES had the highest value for electricity generation with 25,228.80 GWh. The total electricity generation for the ISCC design was calculated as 23,717.70 GWh while the combined cycle power plant had an amount of only 18,974.16 GWh of generated electricity in the same period.
8) The integration of thermal storage has proven to make the renewable energy source (solar) more viable in addition to the environmental benefits and its deployment as a back-up source of energy.

6.2 Recommendations for future work

In this thesis, advanced thermodynamic and economic techniques were used to analyze the proposed systems. An Energy, exergy and thermo economic analyses were deployed. Based on this, a basis for optimization of this work is ready. Also, there is more work to be improved upon regarding exergy and its links to the economy and environment. Also, the high temperatures required for producing energy requires the suitable selection of heat transfer fluids. So, it is recommended to conduct comprehensive research on methods to help narrow the fluids down to the best choice for the required application. Furthermore, this could lead to achievement of the same desired performance with a highly cost-effective HTF. Other Concentrated Solar Power methods such as the Linear Fresnel and the Parabolic Dish reflectors are promising technologies for electricity generation, although more research and development for them is needed to prove viable commercially. It would also be useful to investigate other thermal energy storage options that can convert sunlight into electric power when needed. Finally, the work presented in this thesis can contribute to the research towards the fulfillment of the UAE's goal towards sustainability and diversifying the energy mix.

References

[1] J. Adeoye, Y. Amha, V. Poghosyan, K. Torchyan and H. Arafat, "Comparative LCA of Two Thermal Energy Storage Systems for Shams1 Concentrated Solar Power Plant: Molten Salt vs. Concrete," *Journal of Clean Energy Technologies*, pp. 274-281, 2014.

[2] A. Al-Sabounchi, E. Al-Hammadi, S. Yalyali and H. Al-Thani, "Photovoltaic-grid connection in the UAE: Technical perspective," *Renewable Energy*, vol. 49, pp. 39-43, 2013.

[3] T. Mezher, G. Dawelbait and Z. Abbas, "Renewable energy policy options for Abu Dhabi: Drivers and barriers," *Energy Policy*, vol. 42, pp. 315-328, 2012.

[4] G. Vidican, L. McElvaney, D. Samulewicz and Y. Al-Saleh, "An empirical examination of the development of a solar innovation system in the United Arab Emirates," *Energy for Sustainable Development*, vol. 16, no. 2, pp. 179-188, 2012.

[5] H. Radhi, "On the Effect of Global Warming and the UAE Built Environment," *Global Warming*, Stuart Arthur Harris (Ed.), ISBN: 978-953-307-149-7, InTech Open Access Publisher, 2010.

[6] W. Alnaser and N. Alnaser, "The status of renewable energy in the GCC countries," *Renewable and Sustainable Energy Reviews*, vol. 15, no. 6, pp. 3074-3098, 2011.

[7] H. Hejase and A. Assi, "Global and Diffuse Solar Radiation in the United Arab Emirates," *International Journal of Environmental Science and Development*, pp. 470-474, 2013.

[8] D. Reiche, "Renewable Energy Policies in the Gulf countries: A case study of the carbon-neutral 'Masdar City' in Abu Dhabi," *Energy Policy*, vol. 38, no. 1, pp. 378-382, 2010.

[9] Enipedia.tudelft.nl, "United Arab Emirates/Powerplants - Enipedia," 2015. [Online]. Available: http://enipedia.tudelft.nl/wiki/United_Arab_Emirates/Powerplants. [Accessed: 16- May- 2015].

[10] A. Khalil and A. Alnajjar, "Experimental and theoretical investigation of global

and diffuse solar radiation in the United Arab Emirates, "*Renewable Energy*, vol. 6, no. 5-6, pp. 537-543, 1995.

[11] K. Gairaa and S. Benkaciali, "Analysis of solar radiation measurements at Ghardaia area, south Algeria," *Energy Procedia*, vol. 6, pp. 122-129, 2011.

[12] L. El Chaar and L. Lamont, "Global solar radiation: Multiple on-site assessments in Abu Dhabi, UAE," *Renewable Energy*, vol. 35, no. 7, pp. 1596-1601, 2010.

[13] E. Harder and J. Gibson, 'The costs and benefits of large-scale solar photovoltaic power production in Abu Dhabi, United Arab Emirates," *Renewable Energy*, vol. 36, no. 2, pp. 789-796, 2011.

[14] Eia.gov, "United Arab Emirates - U.S. Energy Information Administration (EIA)," 2015. [Online]. Available: http://www.eia.gov/countries/country-data.cfm?fips=TC. [Accessed: 16- May- 2015].

[15] Appbook.org, "Energy Policy in the Gulf Arab States: Shortage and Reform in the World's Storehouse of Energy," 2015. [Online]. Available: http://www.appbook.org/read-files/energy-policy-in-the-gulf-arab-states-shortage-and-reform. [Accessed: 16- May- 2015].

[16] J. Sathaye, "Renewable Energy in the Context of Sustainable Development," *Renewable Energy Sources and Climate Change Mitigation*, pp. 707-790, 2009.

[17] M. Qader, "Electricity Consumption and GHG Emissions in GCC Countries," *Energies*, vol. 2, no. 4, pp. 1201-1213, 2009.

[18] F. Carl Knopf, "Modeling, Analysis and Optimization of Process and Energy Systems - Knopf - Wiley Online Library," 2015. [Online]. Available: http://onlinelibrary.wiley.com/book/10.1002/9781118121160. [Accessed: 16- May- 2015].

[19] A. Helal and S. Al-Malek, "Design of a solar-assisted mechanical vapor compression (MVC) desalination unit for remote areas in the UAE," *Desalination*, vol. 197, no. 1-3, pp. 273-300, 2006.

[20] N. Raj, S. Iniyan and R. Goic, "A review of renewable energy based cogeneration technologies," *Renewable and Sustainable Energy Reviews*, vol. 15, no. 8, pp. 3640-3648, 2011.

[21] M. Elhaj, M. Mahgub and K. Matrawy, "Thermal Analysis of Combined Cycle Power Plant with Desalination Unit," *AMR*, vol. 658, pp. 430-436, 2013.

[22] C. Christou, I. Hadjipaschalis and A. Poullikkas, "Assessment of integrated gasification combined cycle technology competitiveness," *Renewable and Sustainable Energy Reviews*, vol. 12, no. 9, pp. 2459-2471, 2008.

[23] A. Poullikkas and A. Kellas, "The use of sustainable combined cycle technologies in Cyprus: a case study for the use of LOTHECO cycle," *Renewable and Sustainable Energy Reviews*, vol. 8, no. 6, pp. 521-544, 2004.

[24] I. Kessides, "The future of the nuclear industry reconsidered: Risks, uncertainties, and continued promise," *Energy Policy*, vol. 48, pp. 185-208, 2012.

[25] H. AlFarra and B. Abu-Hijleh, "The potential role of nuclear energy in mitigating CO2 emissions in the United Arab Emirates," *Energy Policy*, vol. 42, pp. 272-285, 2012.

[26] O. Torres, "Life cycle assessment of a pumped storage power plant," M.S. thesis, Dept. of Energy and Process Eng., Norwegian University of Science and Technology, Trondheim, 2011.

[27] Cleanenergysolutions.org, "Clean Energy Solutions Center | Large Scale Offshore Wind Power in the United States: Assessment of Opportunities and Barriers," 2015. [Online]. Available: https://cleanenergysolutions.org/resources/large-scale-offshore-wind-power-united-states-assessment-opportunities-and-barriers. [Accessed: 16- May- 2015].

[28] K. Li, H. Bian, C. Liu, D. Zhang and Y. Yang, "Comparison of geothermal with solar and wind power generation systems," *Renewable and Sustainable Energy Reviews*, vol. 42, pp. 1464-1474, 2015.

[29] R. Saidur, G. BoroumandJazi, S. Mekhlif and M. Jameel, "Exergy analysis of solar energy applications," *Renewable and Sustainable Energy Reviews*, vol. 16, no. 1, pp. 350-356, 2012.

[30] S. Kalogirou, "Seawater desalination using renewable energy sources," *Progress in Energy and Combustion Science*, vol. 31, no. 3, pp. 242-281, 2005.

[31] A. Kazim, "Strategy for a sustainable development in the UAE through

hydrogen energy," *Renewable Energy*, vol. 35, no. 10, pp. 2257-2269, 2010.

[32] M. Ball and M. Wietschel, "The future of hydrogen - opportunities and challenges," *International Journal of Hydrogen Energy*, vol. 34, no. 2, pp. 615-627, 2009.

[33] S. Therien, "Distributed Generation: Issues Concerning a Changing Power Grid Paradigm," *Research Gate*, 2015. [Online]. Available: http://www.researchgate.net/publication/44165402_Distributed_Generation_Issues_Concerning_a_Changing_Power_Grid_Paradigm. [Accessed: 16- May- 2015].

[34] M. Islam, A. Alili, I. Kubo and M. Ohadi, "Measurement of solar-energy (direct beam radiation) in Abu Dhabi, UAE," *Renewable Energy*, vol. 35, no. 2, pp. 515-519, 2010.

[35] M. Islam, I. Kubo, M. Ohadi and A. Alili, "Measurement of solar energy radiation in Abu Dhabi, UAE," *Applied Energy*, vol. 86, no. 4, pp. 511-515, 2009.

[36] G. Elsaket, "Simulating the Integrated Solar Combined Cycle for Power Plants Application in Libya," M.S. thesis, School of Engineering, Cranfield University, Cranfield, 2015. [Online]. Available: http://www.abstract.xlibx.com/a-economy/111671-1-gamal-elsaket-simulating-the-integrated-solar-combined-cycle-f.php. [Accessed: 16- May- 2015].

[37] R. Pitz-Paal, J. Dersch, B. Milow, A. Ferriere, U. Langnickel, A. Steinfeld, J. Karni, E. Zarza and O. Popel, "Development Steps for Parabolic Trough Solar Power Technologies With Maximum Impact on Cost Reduction," *Journal of Solar Energy Engineering*, vol. 129, no. 4, p. 371, 2007.

[38] G. Augsburger and D. Favrat, "Thermo-economic optimisation of large solar tower power plants," Ph.D dissertation, Swiss Federal Institute of Technology Lausanne: EPFL, 2013.

[39] A. Cabane Fernandez, "Economic Study of Solar Thermal Plant based on Gas Turbines," M.S. thesis, LTH School of Engineering, Lund University, Lund, 2013. [Online]. Available: https://lup.lub.lu.se/student-papers/search/publication/3634057. [Accessed: 16- May- 2015].

[40] X. Py, Y. Azoumah and R. Olives, "Concentrated solar power: Current technologies, major innovative issues and applicability to West African countries," *Renewable and Sustainable Energy Reviews*, vol. 18, pp. 306-315, 2013.

[41] A. Fernandez-Garcia, E. Zarza, L. Valenzuela and M. Perez, "Parabolic-trough solar collectors and their applications," *Renewable and Sustainable Energy Reviews*, vol. 14, no. 7, pp. 1695-1721, 2010.

[42] A. Rovira, M. Montes, F. Varela and M. Gil, "Comparison of Heat Transfer Fluid and Direct Steam Generation technologies for Integrated Solar Combined Cycles," *Applied Thermal Engineering*, vol. 52, no. 2, pp. 264-274, 2013.

[43] S. Kaushik, V. Reddy and S. Tyagi, "Energy and exergy analyses of thermal power plants: A review," *Renewable and Sustainable Energy Reviews*, vol. 15, no. 4, pp. 1857-1872, 2011.

[44] O. Behar, A. Khellaf and K. Mohammedi, "A review of studies on central receiver solar thermal power plants," *Renewable and Sustainable Energy Reviews*, vol. 23, pp. 12-39, 2013.

[45] E. Pihl, D. Kushnir, B. Sanden and F. Johnsson, "Material constraints for concentrating solar thermal power," *Energy*, vol. 44, no. 1, pp. 944-954, 2012.

[46] E. Kane, D. Favrat, K. Ziegler and Y. Allani, "Thermoeconomic Analysis of Advanced Solar-Fossil Combined Power Plants," *International Journal of Applied Thermodynamics*, vol. 3, no. 4, pp. 191-198, 2000.

[47] H. Derbal-Mokrane, S. Bouaichaoui, N. Gharbi, M. Belhamel and A. Benzaoui, "Modeling and numerical simulation of an Integrated Solar Combined Cycle System in Algeria," *Procedia Engineering*, vol. 33, pp. 199-208, 2012.

[48] H. Nezammahalleh, F. Farhadi and M. Tanhaemami, "Conceptual design and techno-economic assessment of integrated solar combined cycle system with DSG technology," *Solar Energy*, vol. 84, no. 9, pp. 1696-1705, 2010.

[49] A. Baghernejad and M. Yaghoubi, "Exergy analysis of an integrated solar combined cycle system," *Renewable Energy*, vol. 35, no. 10, pp. 2157-2164, 2010.

[50] G. Ordorica-Garcia, A. Delgado and A. Garcia, "Novel integration options of

concentrating solar thermal technology with fossil-fuelled and CO2 capture processes," *Energy Procedia*, vol. 4, pp. 809-816, 2011.

[51] Z. Yang and S. Garimella, "Thermal analysis of solar thermal energy storage in a molten-salt thermocline," *Solar Energy*, vol. 84, no. 6, pp. 974-985, 2010.

[52] S. Odeyale, A. Oguntola and E. Odeyale, "Evaluation and selection of an effective green supply chain management strategy: A case study," *International Journal of Research Studies in Management*, vol. 3, no. 1, 2014.

[53] T. Boukelia and M. Mecibah, "Parabolic trough solar thermal power plant: Potential, and projects development in Algeria," *Renewable and Sustainable Energy Reviews*, vol. 21, pp. 288-297, 2013.

[54] M. Montes, A. Rovira, M. Munoz and J. Martinez-Val, "Performance analysis of an Integrated Solar Combined Cycle using Direct Steam Generation in parabolic trough collectors," *Applied Energy*, vol. 88, no. 9, pp. 3228-3238, 2011.

[55] G. Cau, D. Cocco and V. Tola, "Performance and cost assessment of Integrated Solar Combined Cycle Systems (ISCCSs) using CO2 as heat transfer fluid," *Solar Energy*, vol. 86, no. 10, pp. 2975-2985, 2012.

[56] R. Hosseini, M. Soltani and G. Valizadeh, "Technical and economic assessment of the integrated solar combined cycle power plants in Iran," *Renewable Energy*, vol. 30, no. 10, pp. 1541-1555, 2005.

[57] G. Barigozzi, G. Bonetti, G. Franchini, A. Perdichizzi and S. Ravelli, "Thermal performance prediction of a solar hybrid gas turbine," *Solar Energy*, vol. 86, no. 7, pp. 2116-2127, 2012.

[58] J. Dersch, M. Geyer, U. Herrmann, S. Jones, B. Kelly, R. Kistner, W. Ortmanns, R. Pitz-Paal and H. Price, "Trough integration into power plants - a study on the performance and economy of integrated solar combined cycle systems," *Energy*, vol. 29, no. 5-6, pp. 947-959, 2004.

[59] A. Poullikkas, "A Technology Selection Algorithm for Independent Power Producers," *The Electricity Journal*, vol. 14, no. 6, pp. 80-84, 2001.

[60] G. Li, "Review of Thermal Energy Storage Technologies and Experimental Investigation of Adsorption Thermal Energy Storage for Residential

Application," *Drum.lib.umd.edu*, 2013. [Online]. Available: http://drum.lib.umd.edu/handle/1903/14698. [Accessed: 16- May- 2015].

[61] Arrow.dit.ie, "A Life Cycle Cost Analysis of Large-scale Thermal Energy Storage Techn" by Kenneth Gaine and Aidan Duffy," 2015. [Online]. Available: http://arrow.dit.ie/dubencon2/8/. [Accessed: 16- May- 2015].

[62] Y. Zhang and A. Faghri, "Analysis of thermal energy storage system with conjugate turbulence forced convection," *Journal of Thermophysics and Heat Transfer*, vol. 9, no. 4, pp. 722-726, 1995.

[63] L. Moens and D. Blake, "Advanced Heat Transfer and Thermal Storage Fluids," presented at the DOE Solar Energy Technologies Program Review Meeting, Denver, Colorado, NREL/CP-510-37083, 2005.

[64] H. Fath, "Technical assessment of solar thermal energy storage technologies," *Renewable Energy*, vol. 14, no. 1-4, pp. 35-40, 1998.

[65] S. Kuravi, J. Trahan, D. Goswami, M. Rahman and E. Stefanakos, "Thermal energy storage technologies and systems for concentrating solar power plants," *Progress in Energy and Combustion Science*, vol. 39, no. 4, pp. 285-319, 2013.

[66] Y. Tian and C. Zhao, "A review of solar collectors and thermal energy storage in solar thermal applications," *Applied Energy*, vol. 104, pp. 538-553, 2013.

[67] Y. Jian, F. Bai, Q. Falcoz, C. Xu, Y. Wang and Z. Wang, "Thermal analysis and design of solid energy storage systems using a modified lumped capacitance method," *Applied Thermal Engineering*, vol. 75, pp. 213-223, 2015.

[68] G. Kolb, "Economic evaluation of solar-only and hybrid power towers using molten-salt technology," *Solar Energy*, vol. 62, no. 1, pp. 51-61, 1998.

[69] J. Birnbaum, M. Eck, M. Fichtner, T. Hirsch, D. Lehmann and G. Zimmermann, "A Direct Steam Generation Solar Power Plant With Integrated Thermal Storage," *Journal of Solar Energy Engineering*, vol. 132, no. 3, p. 031014, 2010.

[70] S. Sharma, H. Kitano and K. Sagara, "Phase Change Materials for Low Temperature Solar Thermal Applications," *Research Gate*, 2015. [Online]. Available: http://www.researchgate.net/publication/241091651_Phase_Change_Materials_f

or_Low_Temperature_Solar_Thermal_Applications. [Accessed: 16- May- 2015].

[71] B. Zalba, J. Marin, L. Cabeza and H. Mehling, "Review on thermal energy storage with phase change: materials, heat transfer analysis and applications," *Applied Thermal Engineering*, vol. 23, no. 3, pp. 251-283, 2003.

[72] X. Wei, Q. Peng, J. Ding, X. Yang, J. Yang and B. Long, "Theoretical study on thermal stability of molten salt for solar thermal power," *Applied Thermal Engineering*, vol. 54, no. 1, pp. 140-144, 2013.

[73] C. Turchi and G. Heath, "Molten salt power tower cost model for the System Advisor Model (SAM)," Tech. Rep. NREL/TP-5500-57625, National Renewable Energy Laboratory, Contract No. DE-AC36-08GO28308, 2013.

[74] D. Max Lieblich, "Electricity generation using molten salt technology," School of Chem. Eng., Univ. of Manchester, 2015. [Online]. Available: http://marxiv-org.lieblich.us/?query=id%3A1312.2258&page=0&type=search. [Accessed: 16- May- 2015].

[75] H. Auer, "Global Warming Blog by Henry Auer: The Sun Shines at Night: Solar Thermal Power with Storage," *Warmgloblog.blogspot.ae*, 2013. [Online]. Available: http://warmgloblog.blogspot.ae/2013/10/the-sun-shines-at-night-solar-thermal.html. [Accessed: 16- May- 2015].

[76] Soda-is.com, "SoDa Service - Knowledge in Solar Radiation," 2015. [Online]. Available: http://www.soda-is.com/eng/index.html. [Accessed: 16- May- 2015].

[77] Csem-uae.com, "CSEM-uae - Swiss Center for Electronics and Microtechnology United Arab Emirates," 2015. [Online]. Available: http://www.csem-uae.com/busiandserv25.php. [Accessed: 16- May- 2015].

[78] Nrel.gov, "NREL: TroughNet - Parabolic Trough Solar Field Technology," 2010. [Online]. Available: http://www.nrel.gov/csp/troughnet/solar_field.html. [Accessed: 16- May- 2015].

[79] Mtholyoke.edu, "Concentrated Solar Power:Parabolic Trough Power Plant," 2015. [Online]. Available: http://www.mtholyoke.edu/~wang30y/csp/PTPP.html. [Accessed: 16- May- 2015].

[80] F. Burkholder and C. Kutscher, "Heat loss testing of Schott's 2008 PTR70 parabolic trough receiver," Tech, Rep. NREL/TP-550-45633, National Renewable Energy Laboratory, Contract No. DE-AC36-08-GO28308, 2009.

[81] O. Idowu, O. Olarenwaju and O. Ifedayo, "Determination of optimum tilt angles for solar collectors in low-latitude tropical region," *International Journal of Energy Environment Eng*ineering, vol. 4, no. 1, p. 29, 2013.

[82] G. Tiwari and M. Ahmad, "Optimization of Tilt Angle for Solar Collector to Receive Maximum Radiation," *The Open Renewable Energy J*ournal, vol. 2, no. 1, pp. 19-24, 2009.

[83] Powerfromthesun.net, "Solar Angle Calculations," 2015. [Online]. Available: http://www.powerfromthesun.net/calculators/AngleCalc.html. [Accessed: 16- May- 2015].

[84] W. Stine and R. Harrigan, *Solar Energy Fundamentals and design*, 536 pp. New York: John Wiley & Sons, 1985.

[85] S. Fischer, W. Heidemann, H. Muller-Steinhagen, B. Perers, P. Bergquist and B. Hellstrom, "Collector test method under quasi-dynamic conditions according to the European Standard EN 12975-2," *Solar Energy*, vol. 76, no. 1-3, pp. 117-123, 2004.

[86] Ncms.ae, "Ministry of Presidential Affairs - National Center of Meteorology & Seismology - Index," 2015. [Online]. Available: http://www.ncms.ae/en. [Accessed: 16- May- 2015].

[87] A. Bejan, G. Tsatsaronis and M. Moran, *Thermal design and optimization*. 542 pp. New York: John Wiley & Sons, 1996.

[88] A. Hepbasli, "A key review on exergetic analysis and assessment of renewable energy resources for a sustainable future," *Renewable and Sustainable Energy Reviews*, vol. 12, no. 3, pp. 593-661, 2008.

[89] R. Sioshansi and P. Denholm, "The Value of Concentrating Solar Power and Thermal Energy Storage," *IEEE Transactions on Sustainable Energy*, vol. 1, no. 3, pp. 173-183, 2010.

[90] A. Baghernejad and M. Yaghoubi, "Exergoeconomic analysis and optimization of an Integrated Solar Combined Cycle System (ISCCS) using genetic

algorithm," *Energy Conversion and Management*, vol. 52, no. 5, pp. 2193-2203, 2011.

[91] P. Harper, "TRNSYS Modelling Of A 100 MWe Hybrid Combined Cycle Concentrating Solar Power Plant," *Academia.edu*, 2015. [Online]. Available: http://www.academia.edu/11372229/TRNSYS_Modelling_Of_A_100_MWe_Hybrid_Combined_Cycle_Concentrating_Solar_Power_Plant. [Accessed: 16- May- 2015].

[92] M. Elhaj, K. Matrawy and J. Yassin, "Modeling and Performance Prediction of a Solar Powered Rankin Cycle/Gas Turbine Cycle," *Challenges of Power Engineering and Environment*, pp. 103-107, 2007.

[93] J. Peterseim, S. White, A. Tadros and U. Hellwig, "Concentrated solar power hybrid plants, which technologies are best suited for hybridisation?," *Renewable Energy*, vol. 57, pp. 520-532, 2013.

[94] B. Kelly, U. Herrmann and M. Hale, "Optimization Studies for Integrated Solar Combined Cycle Systems," *Opus.bibliothek.fh-aachen.de*, 2015. [Online]. Available: http://opus.bibliothek.fh-aachen.de/frontdoor/index/index/docId/7086. [Accessed: 16- May- 2015].

[95] S. Hirasawa, R. Tsubota, T. Kawanami and K. Shirai, "Reduction of heat loss from solar thermal collector by diminishing natural convection with high-porosity porous medium," *Solar Energy*, vol. 97, pp. 305-313, 2013.

[96] R. Vasquez Padilla, "Simplified Methodology for Designing Parabolic Trough Solar Power Plants," Ph.D dissertation, Dept. of Chemical and Biomedical Eng., University of South Florida, Florida, 2011.

[97] H. Torio and D. Schmidt, "Framework for analysis of solar energy systems in the built environment from an exergy perspective," *Renewable Energy*, vol. 35, no. 12, pp. 2689-2697, 2010.

[98] A. Mousafarash and P. Ahmadi, "Exergy and Exergo-Economic Based Analysis of a Gas Turbine Power Generation System," *Progress in Sustainable Energy Technologies Vol II*, pp. 97-108, 2014.

[99] M. Sharma, "Thermodynamic Evaluation of WHRB for it's Optimum performance in Combined Cycle Power Plants," *International Organization of*

Scientific Research, vol. 2, no. 1, pp. 11-19, 2012.

[100] K. Horkeby, "Simulation of Heat Recovery Steam Generator in a Combined Cycle Power Plant," *Diva-portal.org*, 2012. [Online]. Available: http://www.diva-portal.org/smash/get/diva2:509097/FULLTEXT01.pdf. [Accessed: 16- May- 2015].

[101] P. Denholm, "An analysis of concentrating solar power with thermal energy storage in a California 33% renewable scenario," *Searchworks.stanford.edu*, 2015. [Online]. Available: http://searchworks.stanford.edu/view/10361042. [Accessed: 16- May- 2015].

[102] R. Sioshansi and P. Denholm, "The Value of Concentrating Solar Power and Thermal Energy Storage," *IEEE Transactions on Sustainable Energy*, vol. 1, no. 3, pp. 173-183, 2010.

[103] M. El Jai, "Holdings: A modified model for parabolic trough solar receiver," *Elibrary.pks.mpg.de*, 2015. [Online]. Available: http://elibrary.pks.mpg.de/Record/DOAJ025945807. [Accessed: 16- May- 2015].

[104] T. Kashima, "Cost Optimal Operation of Thermal Energy Storage System with Real-Time Prices," *Web.stanford.edu*, 2015. [Online]. Available: https://web.stanford.edu/~boyd/papers/thermal_energy_storage.html. [Accessed: 16- May- 2015].

[105] J. Heier, "Energy Efficiency through Thermal Energy Storage: Possibilities for the Swedish Building Stock," M.S. thesis, Dept. of Energy Technology, KTH School of Industrial Engineering and Management, Stockholm, 2013.

[106] A. Kotb, "Hourly Simulation of Parabolic Trough Solar Collector with Simultaneous Solar Radiation and Weather Conditions during Sunshine Period in Cairo-Egypt," *International Organization of Scientific Research*, vol. 03, no. 05, pp. 45-59, 2013.

[107] B. Hefni, "Dynamic Modeling of Concentrated Solar Power Plants with the ThermoSysPro Library (Parabolic Trough Collectors, Fresnel Reflector and Solar-Hybrid)," *Energy Procedia*, vol. 49, pp. 1127-1137, 2014.

[108] M. Baxter, "Health and Environmental Impacts of Electricity Generation

Systems: Procedures for Comparative Assessment," *Journal of Environmental Radioactivity*, vol. 53, no. 1, pp. 121-122, 2001.

[109] M. Goran Wall, "Life Cycle Exergy Analysis of Solar Energy Systems," *The Journal of Fundamentals of Renewable Energy and Applications* , vol. 05, no. 01, 2014.

[110] I. Visa, *Sustainable energy in the built environment-- steps towards nZEB.*, proceedings of the Conference for Sustainable Energy (CSE) Brasov, 2014

[111] S. Thomas, J. Walker and J. Pittman, "Overview of the Turbine Based Combined Cycle Discipline," *Ntrs.nasa.gov*, 2009. [Online]. Available: http://ntrs.nasa.gov/search.jsp?R=20110012002. [Accessed: 16- May- 2015].

[112] Solarintegrationworkshop.org, "Solar Integration Workshop - SIW 2015," 2015. [Online]. Available: http://www.solarintegrationworkshop.org/brussels2015/. [Accessed: 16- May- 2015].

[113] G. Kolb, "Economic evaluation of solar-only and hybrid power towers using molten-salt technology," *Solar Energy*, vol. 62, no. 1, pp. 51-61, 1998.

[114] D. Sen, "Investment Analysis of a New Solar Power Plant," *International Journal of Research in Science and Engineering*, vol. 2, no. 6, p. 229, 2013.

[115] Eia.gov, "U.S. Energy Information Administration (EIA)," 2015. [Online]. Available: http://www.eia.gov/. [Accessed: 16- May- 2015].

[116] A. Joshi, I. Dincer and B. Reddy, "Solar hydrogen production: A comparative performance assessment," *International Journal of Hydrogen Energy*, vol. 36, no. 17, pp. 11246-11257, 2011.

[117] J. Carrasco Portaspana, "High temperature thermal energy storage systems based on latent and thermo-chemical heat storage," M.S. thesis, Faculty of Mechanical and Industrial Engineering, Vienna University of Technology, 2010.

Appendix A

i. Mass

The HTF mass m_{HTF} is calculated from the following equations:

$$m_{HTF} = \rho_{HTF}.V_{HTF} \quad (1)$$

where:

ρ_{HTF} Density of the heat transfer fluid

V_{HTF} Volume of the heat transfer fluid

The HTF volume V_{HTF} is

$$V_{HTF} = V_{HTFperArea}.A_{SolarField} \quad (2)$$

where:

$V_{HTFperArea}$ Volume per area for heat transfer fluid

$A_{SolarField}$ Solar Field Area

The densities for the seven HTFs are a function of the temperature and are shown in Table A.1

Table A.1: Heat transfer fluid density

HTF Name	***Density equation***
Nitrates Salts	$\rho = -6.36x10^{-1}.T + 2.090x10^{3}$
Caloria HT 43	$\rho = -1.265x10^{-4}.T^{2} - 6.617X10^{-1}.T + 8.85x10^{2}$
Therminol VP-1	$\rho = -7.762x10^{-4}.T^{2} - 6.367x10^{-1}.T + 1.0740x10^{3}$
Hitec	$\rho = -7.33x10^{-1}.T + 2.080x10^{3}$
Dowtherm Q	$\rho = -7.57332x10^{-1}.T + 9.80787x10^{2}$
Dowtherm RP	$\rho = -1.86495x10^{-4}.T^{2} - 6.68337x10^{-1}.T^{2} - 6.68337x10^{-1}.T + 1.04211x10^{3}$
Hitec XL	$\rho = -8.266x10^{-1}T + 2.240x10^{3}$

ii. Enthalpy

The HTF enthalpy is also a function of temperature and it is used in some solar field calculations such as average solar field temperature, freeze protection energy,

warm-up energy and the HTF mass flow rate. The enthalpy values for the six HTFs are shown in Table A.2

Table A.2: Heat transfer fluid enthalpy

HTF Name	***Enthalpy equation***
Nitrates Salts	$H = 8.6x10^{-2}.T^2 + 1.443x10^3.T$
Caloria HT 43	$H = 1.94.T^2 + 1.6060x10^3.T$
Therminol VP-1	$H = 1.377.T^2 + 1.498x10^3.T - 1.8340x10^4$
Hitec	$H = 1.560x10^3.T$
Dowtherm Q	$H = 1.51461.T^2 + 1.58967x10^3.T - 2.50596$
Dowtherm RP	$H = 1.4879.T^2 + 1.5609x10^3.T - 2.4798$
Hitec XL	$H = -3.79667x10^{-5}T^3 - 1.312x10^{-1}T^2 + 1.536x10^3T$

iii. Specific heat

The HTF specific heat is used in the calculations of the delivered thermal energy and is a function of the fluid's temperature that can be expressed by the following equations in Table A.3

Table A.3: Heat transfer fluid specific heat

HTF Name	***Specific heat equation***
Nitrates Salts	$Cp = 1.72x10^{-1}.T + 1.443x10^3$
Caloria HT 43	$Cp = 3.88.T + 1.6060x10^3$
Therminol VP-1	$Cp = 7.888x10^{-4}.T^2 + 2.496.T + 1.509x10^3$
Hitec	$Cp = 1.560x10^3 - T$
Dowtherm Q	$Cp = -5.3943x10^{-4}.T^2 + 3.2028.T + 1.5892x10^3$
Dowtherm RP	$Cp = -3.1915x10^{-6}.T^2 + 2.977.T + 1.5608x10^3$
Hitec XL	$C_P = -1.139x10^{-4}T^2 - 2.624x10^{-1}T + 1.536x10^3$

Appendix B

```
% Matlab code to predict technical performance of the Integrated
Solar Combined Cycle
clear all
clc

% Design Parameters
T1=input('Ambient temperature');
rp=input('Compression ratio');
gamma_a=input('Ratio of specific heat for air');
gamma_g=input('Ratio of Specific heat for gas');
eff_c=input('Isentropic efficency for compressor');
eff_t=input('Isentropic efficiency of turbine');
eff_m=input('Mechanical efficiency for compressor');
T3=input('Gas Turbine inlet temperature');
LHV=input('Low Heating Value');
Cpf=input('Specific heat of fuel');
Tf=input('Temperature of the fuel');
h1f=input('heat loss factor');
BD=input('Blow Down factor');
mdot_g=input('Gas flow rate');
Tpp=input('Pinch point');
Tap=input('Approach point');
Ts=input('Saturation steam temperature at superheater pressure');
hsh=input('Enthalpy_sh');
hs=input('Enthalpy_s');
hw1f=input('Enthalpy_w1f');
hw2f=input('Enthalpy_w2f');
h6=input('Enthalpy_6');
h7=input('Enthalpy_7');
h8=input('Enthalpy_8');
h9=input('Enthalpy_9');
Qs=input('Solar Field Thermal Output');
%
**********************************************************************
****
% 1) *** Gas Turbine Model ***

% 1.1  Air Compressor
T2=T1*(1+((rp^((gamma_a -1)/gamma_a)-1)/eff_c)); % Outlet temperature
of the compressor
Ta=(T1+T2)/2;
Rpa= (rp^((gamma_a -1)/gamma_a)-1)/eff_c;
Cpa=1.4;
% Cpa=1.0189e3 - (0.13784*Ta) +((1.9843e-4)*(Ta^2)) + ((4.2399e-
7)*(Ta^3)) - ((3.7632e-10)*(Ta^4));
Wc=(Cpa*T1*Rpa)/eff_m; % Compressor Work

% 1.2  Combustion Champer
Rpg=(1-(1/(rp^((gamma_g -1)/gamma_g))));
% Cpg=1.8083 - (2.3127e-3*T3) + (4.045e-6*(T3^2)) - (1.7363e-
9*(T3^3));
Cpg=2.34;
mdot_f=(Cpg*T3)-(Cpa*T1*(1+Rpg));
mdot_a=LHV+(Cpf*Tf)-(Cpg*T3);
f=(mdot_f/mdot_a);
% 1.3  Gas Turbine Unit
 T4=T3*(1- (eff_t*(1-(1/(rp^((gamma_g -1)/gamma_g)))))); % Exhaust
gas temperature from gas turbine
```

```
 Wt=(Cpg*T3*eff_t*Rpg)/eff_m; % Shaft work of the turbine
 Wgnet=Wt-Wc; % Net work of the gas turbine
 SFC=(3600*f)/Wgnet; % Specif Fuel Consumption
 Qadd=f*LHV; % Heat supplied
 eff_gt=Wgnet/Qadd; % Gas turbine efficiency
 HR=3600/eff_gt; % Heat Rate

%
**********************************************************************
***
% 2) *** Heat Recovery Steam Generator Model ***

 Tg1=T4; % Inlet gas temperature to HRSG equlas exhaust gas
temperature from gas turbine
 Tg3=Ts+Tpp; % Gas temperature leaving the evaporator
 Tw2=Ts-Tap; % Water inlet temperature to evaporator
 Qav=h1f*mdot_g*Cpg*(Tg1-Tg3); % Heat available with exhaust gases
from gas turbine
 mdot_s=Qav/((hsh-hs)+ BD*(hs-hw2f));
 Tg2=Tg1-((mdot_s*(hsh-hs))/(h1f*mdot_g*Cpg));
 Qsh= mdot_g*Cpg*(Tg1-Tg2)*h1f; % Superheater duty
 mdot_w=mdot_s*BD; % Water flow rate
 Tg4=Tg1-((mdot_s*BD*(hw2f-hw1f))/(mdot_g*Cpg)); % Exhaust gas
temperature at exit of HRSG

%
**********************************************************************
***
% 3) *** Steam Turbine Model ***

Wst=mdot_s*(h6-h7); % Steam turbine work

% 3.1 Condenser
Qcond=mdot_w*(h7-h8); % Heat reject from condenser

% 3.2 Pump
Wp=mdot_w*(h9-h8);

Wsnet=Wst-Wp; % Steam turbine net work
eff_st=Wsnet/Qav; % Steam turbine efficiency
eff_cc=(eff_gt+eff_st-(eff_gt*eff_st)); % Combined Cycle Efficiency
HRt=3600/eff_cc; % Total heat rate for Combined Cycle

% The ISCC Efficiency
eff_iscc=(Wsnet+Wgnet-Wp)/(Qadd+Qs);

disp('Performance Analysis of an Integrated Solar Combined Cycle
Power Plant')
fprintf('\n *****Results***** \n')
fprintf(' \n Gas Turbine Efficiency = %f\n ',eff_gt)
fprintf('\n Steam Turbine Efficiency = %f\n ',eff_st)
fprintf('\n Combined Cycle Efficiency = %f\n ',eff_cc)
fprintf('\n Integrated Solar Combined Cycle Efficiency = %f\n
',eff_iscc)
% Matlab code to predict the economic and environmental performance
clear all
clc

Pc=input('Plant Capacity');
```

```
LF=input('Load Factor');
q=input('Amort.');
m=input('Loan of interest');
n=input('No. of years');
r=input('Inflation rate');
Csc=input('Capital Cost');
Fj=input('Fuel Price projection');
eff=input('Plant Efficiency');
CV=input('Fuel Net Caloric Value');
OMF=input('Fixed O&M');
OMV=input('Variable O&M');
FCC=input('Fuel Carbon Content');
X0=input('x0');
CostPerTon=input('Cost per ton');
disc=input('Discount rate');

for i=0:24
    i=i+1;
% Annual Energy Production (GWh)
Pj=(8760*Pc*LF(i))/1000;

% Annual Capital Cost (US$ Million)
Ccj=q*(1+m).^n(i) * (1+r).^(n(i)-1) * Pc *1000 * Csc/1000000;

% Fuel Cost (US$ Million)
Cfj=31536000*(((Fj(i)/1000)*Pc*LF(i))/(1000000*eff*CV));

% Fixed O&M Cost (US$ Million)
COMF=12*OMF*Pc*(1+r).^(n(i)-1) *1000/1000000;

% Variable O&M Cost (US$ Million)
COMV=8760*(1+r).^(n(i)-1)*Pc*LF(i)*OMV/1000000;

% Fuel Consumption Indicator
FCI=3600/(eff*CV*1000);

% CO2 Environment Indicator
CO2EI=440/(12*FCI*FCC*X0);

% Co2 Generated By Year
Co2GPY=CO2EI*Pj;

% Annual Co2 Cost
AnnualCo2Cost=Co2GPY*CostPerTon(i);

% Expenses
Expenses=Cfj+COMF+COMV+AnnualCo2Cost;

% Total O&M Cost
TotalOMCost=COMF+COMV;

Disc.factor=(1+disc).^n(i);


NUM=(Ccj+Cfj+COMF+COMV+AnnualCo2Cost)/Disc.factor;

DEN=(Pj/Disc.factor);
```

```
end


% Levalizes Cost of Electricity
LCOE=NUM/DEN
```

Vita

Ahmad Abd Elmahmoud M. Abd Elrahman was born on February 25, 1984, in Riyadh, Saudi Arabia. He started his education in Al Mostaqbal High School where he graduated in 2001. He then joined the department of mechanical engineering, University of Khartoum in Sudan, from which he graduated in 2006. His degree was a Bachelor of Science (BSc) in Mechanical Engineering. Afterwards, he was appointed as a Teaching Assistant at the engineering drawing lab at University of Khartoum where he was responsible for lecturing, tutoring and assisting students with their course works. In 2008, Mr. Abd Elrahman started a Master's degree in Business Administration (MBA) which he completed in 2010. During the period extending from 2008 and 2012, he pursued a career in mechanical engineering with several reputable engineering companies in Khartoum, Sudan. He then moved to the United Arab Emirates in 2012 to continue his post graduate studies at the American University of Sharjah (AUS). In 2012, Mr. Abd Elrahman began a Master's program in Mechanical Engineering. Mr. Abd Elrahman is a member of the Sudanese Engineering Council (SEC), Sudanese Engineering Society (SES) and the American Society of Mechanical Engineers at AUS (Student Section).